T H E U N I V E R S I T Y O F M I C H I G A N

COLLEGE OF ENGINEERING
High Altitude Engineering Laboratory
Department of Aerospace Engineering
Department of Atmospheric and Oceanic Sciences

Technical Report

ACOUSTICS OF METEORS—EFFECTS OF THE ATMOSPHERIC TEMPERATURE AND WIND STRUCTURE ON THE SOUNDS PRODUCED BY METEORS

Part 1. Meteors as Sound Producers

Douglas O. ReVelle

ORA Project 010816

supported by:

NATIONAL AERONAUTICS AND SPACE ADMINISTRATION
GRANT NO. NGR 23-005-540
WASHINGTON, D.C.

administered through:

OFFICE OF RESEARCH ADMINISTRATION ANN ARBOR

January 1973

TABLE OF CONTENTS

ACKNOWLEDGMENTS

I gratefully acknowledge the support, optimism, and guidance of my advisor Dr. F. L. Bartman. His perspective has greatly influenced me. It is my hope that this report will adequately reflect this influence.

My thanks also go to Dr. R. E. McCrosky of the Smithsonian and to all the others who took the time and had the patience to reflect on the nature of meteor sounds.

Lastly, I thank my wife Ann, for her patience, understanding, and for the idea underlying the usefulness of z'.

This research was supported in part by NASA Grant NGR 23-005-540.

LIST OF FIGURES

LIST OF TABLES

LIST OF SYMBOLS

A	meteor cross-sectional area
A_E	meteor cross-sectional area at z'
C	adiabatic sound speed
C_D	coefficient of drag
d_m	meteor diameter as a function of altitude
d_{mE}	meteor diameter at z'
$\overline{Ei}(x)$	exponential integral of x
f	reverse rocket effect parameter
g	acceleration due to gravity
H	scale height of the isothermal atmosphere
H_o	value of scale height at z = 0
$\bar{K}$	thermal conductivity of the meteor
Kn	Knudsen number for p^* constant
$\overline{Kn}$	Knudsen number for p^* decreasing exponentially
m	meteor mass
m_E	meteor mass at z'
M	mean molecular weight of dry air
p_o	hydrostatic pressure at z = 0
$p(z)$	hydrostatic pressure as a function of altitude
p^*	modified ballistic entry parameter
p^*_E	value of p^* at z'
Q	heat of ablation of the meteor

r_m	meteor radius
r_{mE}	meteor radius at z'
R	universal gas constant
t	time variable
T	gas kinetic temperature in degrees absolute
V(z)	meteor velocity as a function of altitude
V_E	meteor velocity at z'
V_m	meteor velocity at which ablation ceases
V_j	j^{th} value of meteor velocity
w	velocity of ablation products with respect to the meteor
z	altitude, increasing upward from the surface of the earth
z'	altitude at which the meteor deceleration is first zero
z''	altitude of maximum rate of energy deposition
z'''	altitude of maximum deceleration
z''''	altitude at which the meteor deceleration is again zero
α'	altitude scale height gradient
γ	ratio of the specific heat at constant pressure to that at constant volume
θ	entry elevation angle
λ	mean free path as a function of altitude
λ_o	mean free path at z = 0
ρ_o	air density at z = 0
ρ_m	meteor density

ρ_{mE} meteor density at z'

σ ablation parameter

FOREWORD

This report will be published in three sections. The present section is devoted to a brief historical introduction to the problem and to some of the theoretical aspects regarding meteors as sources of sound. Single body ballistic entry with and without ablation present is considered under several simplistic yet useful assumptions. The primary subjects of Parts 2 and 3 will be as follows.

Part 2. Temperature and Wind Refraction and Atmospheric Attenuation of Meteor Induced Cylindrical Blast Waves.

Part 3. Theoretical Analysis of Existing Data on Meteor Induced Infrasonic Pressure Waves and Estimates of the Probability of Occurrence of Sound Producing Meteors.

I. INTRODUCTION

A. HISTORICAL ASPECTS

Over the last hundred years many spectacular geophysical phenomena have attracted the attention of world scientists. Krakatoa and other volcanic eruptions, numerous notilucent cloud displays, brilliant meteor showers and aurora, and the Great Siberian Meteor of 1908 have created much discussion about the nature of our world and its place within the solar system.

Reports of the audible sounds produced by bright fireballs date back to 585 A.D. (Astapovich, 1951). The Great Siberian Meteor of 1908 was audible over hundreds of miles and its effects were measured on sensitive microbarographs as far away as Great Britain (Whipple, 1930). Apparently the Krakotoa eruption was so powerful that atmospheric pressure waves associated with it were detected after traveling around the globe more than once (Cook, 1969). These pressure waves are commonly called infrasound. They are pressure waves of very low frequency for which absorption of the signal is very small.

In the 1910-30 period, A. Wegener and F.J.W. Whipple reported on the audible sounds produced by bolides, i.e., exploding meteors and attempts were made to deduce information about the atmosphere from these observations (Wegener, 1917; Whipple, 1923). These observations suffered from the fact that meteor entry is a relatively short lived and unpredictable phenomena. The recollections of startled observers regarding the audible part of the phenomena which usually occurred several minutes after the visual sighting were generally unreliable.

In the 1940-60 period, the study of the effects of the atmosphere on the propagation of infrasound had begun (Craig, 1965). By the end of this period instruments capable of reliably recording atmospheric "events" were becoming available. Over the last ten years or so many infrasonic "events" have been recorded and cataloged and many of these have been studied extensively. To our knowledge, very little has been done, however, regarding a systematic study of the generation, propagation and the resulting detection of "sounds" produced by meteors. The recent research of Tsikulin (1970) is apparently the only major work to be found on this subject.

Since about 1965, the infrasonic observatory operated by NOAA in Boulder, Colorado has recorded at least three "events" which correlate well in time and direction with large meteor entry into our atmosphere (Goerke, 1971). The U.S. military bomb detection systems have recorded meteor "events" on very sensitive microbarographs but most of this information remains classified (Lowry, and Shoemaker, 1967; Gault, 1970). Other infrasonic signals from meteors have also been recorded (Wilson, 1972). The only known audible recording of a meteor was made by chance by Miss E. M. Brown in Northern Ireland in 1969 (Millman, 1970). This was associated with the Bovedy and Sprucefield Meteorites which were subsequently recovered. These observations are discussed in detail in Section VII (Part 3). In addition to these observations in the atmosphere, many reports exist of air-coupled Rayleigh Waves recorded on sensitive seismographs (LaPaz, 1958). These observations have been distinguished from the more coventional P and S waves which would result from ground impact of a large meteorite. While these observations have been noted on occasion by

seismologists the potential remains for indirectly studying the atmospheric disturbance which generated the crustal motion. Simply expressed this type of disturbance represents a wave traveling in the upper crustal layer of the earth at the speed of sound in air induced by the air pressure oscillations of the meteor shock wave. This slower speed of movement as compared to P and S waves is readily recognizable on a seismic recording.

Other than these observations only the memories of startled observers remain to relate to scientists their often confused recollections. It is hoped that motivation for further study of meteor "sounds" will be stimulated by the ideas expressed in this paper.

B. QUALITATIVE DESCRIPTION OF THE METEOR SOUND PHENOMENON

Before attempting to formulate the problem mathematically a few brief qualitative statements regarding the "sounds" from meteors should be considered. "Sounds" are defined here as the pressure wave effects produced by meteor entry into the atmosphere. The range of frequencies involved is from a few hundred Hertz down to about 10^{-3} Hertz (Millman, 1970; Whipple, 1930; Goerke, 1971). Thus the frequencies of interest include audible sound waves as well as the lower frequency infrasonic, acoustic gravity and gravity waves. See V (Part 2) for more precise definitions of these wave frequency regimes.

Meteor entry to the atmosphere at hypersonic velocities causes numerous visual phenomena. The conventional "shooting star" meteors are generally observed in a region of the atmosphere where the Knudsen number is large and are completely destroyed by ablation and slowed down to very small velocities

long before a distinct shock wave can form (Öpik, 1958). For those bright fireballs which are able to survive to regions of the atmosphere where the Knudsen number is small, a well-defined atmospheric shock wave is able to form ahead of the body. This has been generally termed a bow shock wave (Loh, 1968). The passage of the meteor at hypersonic velocities through a medium like the atmosphere produces many strongly nonlinear effects along and within a certain distance of the atmosphere trajectory. Ionization and dissociation, as well as rotational and vibrational excitations of atmospheric and meteoric species are produced and some of these effects are visible and/or instrumentally recordable at ground level (Millman, 1968). Via the drag interaction between the meteor and the atmosphere, energy is transferred into kinetic energy of the rapidly expanding shock front, the gas along the path is heated, and energy is transferred back from the very strong shock wave causing the body to ablate, fragment or totally break up (or "explode"). This interaction will be considered in detail in IVA (Part 2). Thus we are dealing with a very complex phenomena when a metor survives into the continuum flow regime of the gaseous envelope surrounding a planet. These phenomena are dealt with in great detail in Bronshten's work (1964) with the notable exception of the shock wave and subsequent sound wave propagation at large distances from the body. It is the purpose of this paper to help delineate this poorly known area of meteor research.

The following represents a brief summary of the observed audible sounds from meteors.

First of all there have been reports of swishing or clicking noises heard either slightly before or during the visual sighting of the meteor. These have been called ethaerial or electrophonic noise. Since the existence of these noises is speculative and explanations which have been put forth are of an electromagnetic nature (Barringer and Hart, 1949; Astapovich, 1951; Roming and Lamar, 1963; Roming and Lamar, 1965), no other mention will be made of them here.

Next a single sharp crack or multiple shocks may or may not arrive depending on where the observer is with respect to the trajectory and depending on the nature of the atmospheric temperature and wind structure aloft as well as upon whether the meteor is fragmenting, etc. Undoubtedly local topographic features causing reflections (i.e., echoes) to be set up at or near ground level also contribute to the many types of audible observations which exist (Wylie, 1932).

A rumbling effect is also commonly reported and is frequently compared with the sounds produced by lightning discharges in thunderstorms (Wylie, 1932; Nininger, 1952; McKinley, 1961). It is felt that these effects are related to dispersion, distortion, and attenuation of the propagating signal, as well as to the location of the observer with respect to the meteor, but their overall significance will be best understood after careful observations utilizing audible and infrasonic pressure sensors are carried out. It is the hope of the author that infrasonic detection systems can be set up in the prairies of the U.S. to be used with the existing Prairie Network (for photographing bright fireballs) to learn more about the atmosphere as well as about

large meteoroids. The recent work of Donn, et al., 1972 shows that many such stations could be utilized to probe the upper atmosphere. The use of these stations to study many different types of atmospheric phenomena which generate infrasound may someday be of great benefit to science.

Line source shock wave effects from meteors will be primarily considered in this analysis. Lyubarskiy (1951), using data from 1328 observations (of 959 meteors), determined that for only 19% of the observations were meteors reported to have displayed gross fragmentation effects. While these fragmentation effects are interesting and important to the overall problem of meteor acoustics, their theoretical treatment is complicated by such effects as: (1) accurately knowing how much energy was "released" (for the final bolide explosion this is the kinetic energy remaining at that altitude); (2) the non "point" source effects (if energy is deposited over a relatively short portion of the overall trajectory); and (3) the altitude range over which this occurs is a function of both the meteor (its composition, density, compressive strength, entry velocity, shape, etc.) as well as upon the atmosphere. For this reason further theoretical development on sounds from bolides is kept minimal in this analysis. Note that in the Russian papers on this subject the term bolide generally refers to bright fireballs and not specifically to point source type exploding meteors.

II. ATMOSPHERIC MODELS

A. FOR METEOR ENTRY DYNAMICS

In order to study meteors as a sound source, models of both the atmosphere and the meteor itself need to be developed. In this section models of the atmosphere for both the meteor entry dynamics as well as for the resulting atmospheric sound propagation are considered.

It is well known that in a hydrostatic isothermal atmosphere both density and pressure decrease with increasing altitude in an exponential manner (Craig, 1965):

$$\rho(z) = \rho_o \exp(-z/H)$$

$$p(z) = p_o \exp(-z/H) \qquad (1)$$

where

ρ_o = atmospheric density at the ground

p_o = atmospheric pressure at the ground

z = altitude above the ground

H = constant scale height of this isothermal atmosphere

p = pressure at an altitude z

ρ = density at an altitude z

These relations allow calculations of parameters such as the mean free path and the Knudsen number as a function of altitude; i.e., $Kn = \lambda/d_{mE}$; for

meteor Model 1

where

$\lambda = \lambda_o \exp[z/H]$ = mean free path of the isothermal hydrostatic model atmosphere

λ_o = value of λ at $z = o$ (ground level)

d_{mE} = meteor diameter at the altitude where the drag force balances the weight of the body

See Section III for more detail.

If, instead of assuming a constant temperature hydrostatic atmosphere, an atmosphere of constant scale height gradient is chosen, then the density and pressure are given by:

$$\rho(z) = \rho_o\left(1 + \frac{\alpha'}{H_o} z\right)^{-(1 + 1/\alpha')}$$

$$p(z) = p_o\left(1 + \frac{\alpha'}{H_o} z\right)^{-(1/\alpha')} \qquad (2)$$

where

$\alpha' = \frac{\partial H}{\partial z}$ = scale height gradient

H_o = ground value of the scale height

$H = H_o + \alpha' z$ = scale height as a function of altitude

(Note: in the limit as $\alpha' \to 0$, equation (2) reduces to equation (1).)

For the meteor entry dynamics the additional refinement of (2) has a very small effect on the results. From 100 km downward it is a reasonable approximation as far as entry dynamics is concerned to assume an isothermal hydrostatic atmosphere. It will be seen shortly that for the study of ducting

of meteor sounds it is primarily the nonuniformity in the temperature and wind structure which produces refractive multipath propagation. For that aspect of the problem the inhomogeneity of the medium must be known in great detail. See Table 1 for the model isothermal hydrostatic atmosphere used for the meteor entry dynamics. See Figure 1 for a comparison between this model and other nonisothermal models. The mean molecular weight, M, was assumed constant and equal to 28.97 g/mole at all altitudes for this model. At altitudes below about 160 km this is a reasonable approximation (Craig, 1965).

B. FOR SOUND PROPAGATION

When considering the effects of the inhomogeneity of the atmosphere on meteor sound propagation, the chief parameters of interest are the vertical variations of the temperature field and of the horizontal winds. Except for the initial very strong shock wave effects, what we basically consider is the sound propagation structure of the atmosphere.

For the mean or climatological temperature structure, the U.S. Standard Atmosphere Supplements (1966) were used to deduce the seasonal variations of the vertical temperature field. These have been converted to phase velocities using the relation $C = (\gamma RT/M)^{1/2}$ and are shown in Figure 2. In this expression, γ is the ratio of the specific heat at constant pressure to the specific heat at constant volume; R is the universal gas constant; T is the temperature of the gas (in degrees absolute); and M is the mean molecular weight of the gas. The climatological information on winds was taken from Batten (1961) and from the CIRA 1965 International Reference Atmosphere.

See Figure 3. There was no attempt to make a general study of vertical temperature and wind field changes as a function of time on a scale smaller than a month. In Section VII (Part 3), when specific fireball sounds are considered, attempts are made to consider the most realistic temperature and wind field information available for the time and day of the "event." If this information was not available climatological data was used as the next best approximation to what the actual temperature and wind profiles were. Throughout all of the analyses the atmosphere was considered to be horizontally stratified, i.e., horizontal temperature and wind gradients as well as vertical wind motions were assumed to be nonexistent.

The climatological information on temperature and wind was then tabulated in layers of 10 km in thickness. In IVC (Part 2), a simple approximate method of transferring between the isothermal model used for meteor entry dynamics to the climatological nonisothermal model is presented.

The assumption of a horizontally stratified atmosphere is often made for sound propagation studies. The troposphere is probably not well modeled by this assumption especially near the surface in the atmosphere boundary layer where the winds are not geostrophic and meteorological disturbances and storms are present. In the stratosphere and mesosphere the approximation is more justifiable since, generally, only small vertical winds are believed to exist. The temporal variations present in the troposphere as well as the spatial variations generally make this approximation a poor assumption except for short propagation distances. The general applicability of this model to the lower thermosphere is also assumed to be valid.

III. METEORS AS SOUND PRODUCERS

In this section meteors are considered as sound producers. Two models are developed. In the first model, ablation of the entering meteor is not considered. For the second model ablation is assumed to proceed at an exponential rate utilizing the σ parameter. It will be seen in IIIB, that the first model is just a special case of the second. For both models the range of the extremes of all important variables in the dynamical problem will be considered. These extremes are:

Meteor Entry Velocity: $11.2 \leq V_E \leq 73.2$ km/sec

Meteor Density: $0.30 \leq \rho_{mE} \leq 7.70$ g/cm^3

Meteor Radius: $0.05 \leq r_{mE} \leq 500$ cm

Entry Elevation Angle: $10° \leq \theta \leq 90°$ (vertical entry)

It was assumed throughout that C_D, the drag coefficient, is exactly unity. Variations of this parameter as a function of the flow regimes at the high meteor Mach numbers involved are small (Groves, 1957). Changing C_D by a factor of 2.0 changes the altitude of maximum deceleration by at most 3-4 km. The possible values of the σ parameter were discussed recently in a paper by McCrosky and Ceplecha (1970). For the relatively large sizes of meteors ultimately used for this study an upper limit of $5 \cdot 10^{-12}$ sec^2/cm^2 was chosen. It should be pointed out, however, that for similar body sizes a relatively large range of values has been reported (McIntosh, 1970). This fact is reflected in the effective model discussed in IIIC. While accuracies differ in obtaining σ from

luminosity data, the range of values reported may result from trying to apply a reasonably simple theory to this most complex phenomena. While in reality $\theta = f(V_E)$ prior to entry (Wood, 1961), it was assumed during the calculations that for any possible entry velocity, any value of θ was possible. In both models a single spherical body which entered the atmosphere on a ballistic trajectory was assumed; i.e., no forces are assumed to be acting normal to the meteors trajectory during entry. In addition for both models the plane parallel atmosphere approximation was utilized.

A. MODEL 1 - BALLISTIC ENTRY WITHOUT ABLATION

Following Allen and Eggers (1958) and Groves (1957), the velocity profiles of nonablating objects with ballistic trajectories in the earth's atmosphere were calculated. A hydrostatic isothermal atmosphere was assumed for the entry dynamics. The entering meteor is in effect considered as a blunt body in aerodynamic terms (Tsikulin, 1970).

$$\frac{mdV}{dt} = mg \sin\theta - \frac{1}{2}\rho V^2 C_D A \tag{3}$$

$$\frac{dz}{dt} = -V\sin\theta = \frac{dz}{dV}\frac{dV}{dt} \tag{4}$$

$$\frac{dm}{dt} \equiv 0 \tag{5}$$

where

m = meteor mass

V = meteor velocity

g = acceleration due to gravity

ρ = atmospheric density

$A = \pi r_m^2$ = meteor cross sectional area

z = altitude (increasing upward)

t = time variable

Since for this problem the range of entry velocities is known, Grove's technique utilizing the energy conservation principle prior to atmospheric entry was not needed. Accelerations will take place in the vicinity of the earth so that entry velocities will exceed slightly the range of velocities just given but this effect is quite small in general except for the slower meteors (Cosby and Lyle, 1965). Entry was assumed to take place at an altitude z' along the trajectory where the drag force balanced the weight of the body. This range of entry altitudes (calculated for the extremes of entry density, velocity, entry angle, and size of a single spherical body) was obtained by the use of the following relationship:

$$p(z') = p^* \left(\frac{2gH}{V_E^2} \right)$$

where

$$p^* = \frac{mg \sin \theta}{C_D A} = \frac{4 \rho_m r_m g \sin \theta}{3 C_D} \quad \text{(for a sphere)}$$

Following Groves (1957) two other altitudes of interest are also readily calculated assuming p^* is constant. These are:

$$p(z'') = \frac{2}{3} p^*$$

$$p(z''') = p^*$$

where z'' is the altitude at which the maximum rate of energy deposition occurs, and z''' is the altitude at which the maximum deceleration occurs.

There is one final altitude that serves to bound the straightline portion of the meteors trajectory. This has been termed z''''. It is readily calculated as the altitude at which the deceleration of the body is once again zero. Between z' and z'''' the trajectory is a straightline (to a first order approximation).

Using (3) and (4) and the assumption of a hydrostatic isothermal atmosphere for the altitude region below z' where the weight of the body (i.e., the effect of gravity) is small compared to the resistance forces the atmosphere offers against being compressed, (3) can be rewritten as (Allen and Eggers, 1958):

$$\frac{dV}{dz} V \sin\theta = \left[\frac{1}{2} \frac{C_D A}{m} \rho_o e^{-z/H}\right] V^2$$

Dividing by V^2 and rewriting ρ_o as p_o/Hg we get:

$$\frac{dV}{V} = \frac{1}{2}\left(\frac{C_D A}{mg \sin\theta}\right) \frac{p_o}{H} e^{-z/H} dz$$

but $p^* = mg \sin\theta / C_D A$

$$\therefore \frac{dV}{V} = \frac{1}{2}\left(\frac{p_o}{p^*}\right) \frac{1}{H} e^{-z/H} dz \qquad (6)$$

Above z' assume $V = V_E \cong$ constant

Below z' integrate (6) as follows

$$\int_{V_E}^{V} \frac{dV}{V} = \frac{1}{2}\frac{p_o}{p^*}\frac{1}{H}\int_{z=z'}^{z=z} e^{-z/H} dz \qquad (7)$$

$$\ell n \frac{V}{V_E} = -\frac{1}{2}\frac{p_o}{p^*}\left[e^{-z/H} - e^{-z'/H}\right]$$

therefore

$$V = V_E \exp\left[-\frac{1}{2}\frac{p_o}{p^*}\left[e^{-z/H} - e^{-z'/H}\right]\right]$$

Velocity profiles were then calculated using the above formula for a range of p* values and V_E values. See Figures 4-43.

The Knudsen number of the problem was considered next. For this model, with p* constant, the body size was considered constant and the mean free path (that of the ambient neutral gas was used here) was calculated for the isothermal atmosphere. See Figures 44-51 for z', z'', z''', z'''', and Kn = 0.05 versus r_{mE} for this model. At the altitude at which Kn = 0.05, the bow shock is detached from the meteor and slightly ahead of it. Following the reasoning of Grad (1959), this distance will be on the order of several mean free paths.

Note from these figures that for the larger bodies bow shock waves can be generated before the luminosity associated with the meteor entry (as seen at the ground) begins. Here we are assuming that significant luminosity begins near and below the altitude at which dV/dt is first zero, i.e., the work done against drag above z' is very small compared to the total energy associated with the meteor. Published luminosity data on meteor entry only involve

altitudes where the meteor was decelerating in the atmosphere (Jacchia, 1967). Thus this assumption appears to be reasonable. While we have not allowed for mass loss in this model (in a somewhat artificial manner), it has been shown by Riddell and Winkler (1962) that the larger the meteor is at entry, the better the approximation expressed in equation (5) becomes.

From these simple calculations certain conclusions can be drawn concerning meteors as line source sound producers. From the range of extremes used there is no situation where a single spherical body of $r_{mE} = 0.05$ cm and of relatively low density will ever penetrate to an altitude where Kn is small. In fact the $r_{mE} = 0.5$ cm case is still on the borderline. For this model then it seems that for the range of dynamical extremes considered a body must be at least as big as 1 cm in diameter in order to reach an altitude where Kn is small and still be moving fast enough to generate a distinct bow shock wave. It has been assumed throughout that at an altitude where Kn = 0.05 the pressure gradient developed across the bow shock is much larger than other pressure gradients that may exist in the flow. This assures that the shock wave is well developed (Groves, 1957). To be sure this is only an approximate criterion. The cases which have been removed from consideration using this model cover meteors whose initial kinetic energies range from $\sim 10^{8}$ - $4.2 \cdot 10^{12}$ ergs. See Tables 2 and 3 for all of the dynamical possibilities involved.

B. MODEL 2 - BALLISTIC ENTRY WITH EXPONENTIAL ABLATION

While Model 1 predicts the maximum penetration of a single spherical body, Model 2 attempts to predict the minimum penetration. Here the parameter p^* is replaced with $p_E^* \exp[-(\sigma/6)(V_E^2 - V^2)]$ (following Bronshten, 1964) and σ is determined from meteor photographic detection stations. The alternative of a generalized variable p^* presents itself, but the complications involved in applying the basic equilibrium thermodynamics as a function of the various flow regimes (and whether laminar or turbulent conditions prevail) seem very formidable. Such calculations have been carried out recently (Baldwin and Sheaffer, 1971), however, these calculations are not as generalized as might be desired.

While p^* has been observed to vary linearly, exponentially or to remain constant over portions of the trajectory, it may vary in a generally complicated manner (Allen and James, 1964). It is felt that an exponential decay of mass for a single spherical body will represent a reasonable upper bound (i.e., minimum penetration depth) to the ablation problem when considering meteors as sound producers. It is to be noted that for $\sigma \equiv 0$, this case reduces to that of Model 1 identically.

There is the question: At what velocity does ablation cease? McCrosky has suggested 3 km/sec as a reasonable value (McIntosh, 1970). For the ray theory refraction analysis in Sections IVB and C (Part 2), we have assumed a cylindrical blast wave line source model of the meteor-atmosphere interaction over a portion of the straightline meteor trajectory. For this analysis then we are considering line source meteor sound generation only at space flight velocities. See Section IVA (Part 2) for more details on this. We are thus

avoiding at the moment sound generation at the lower Mach numbers including the dark flight portion of the meteors trajectory (at and below the altitude region where ablation ceases). Not only do the present meteor models become less realistic at these lower velocities, (where external pressure on the frontal face of the meteor can become so excessive that gross fragmentation or total break-up effects can readily occur), but the "explosion" analogy eventually breaks down and the sonic boom output of a rapidly decelerating body (or bodies) must be considered. Note that sonic boom theory is a linear theory (with cumulative nonlinear correction terms) for propagation of initially weak acoustic disturbances (Hayes, 1971). The cylindrical blast wave model to be discussed in IVA (Part 2) is a nonlinear theory resulting in the case of entering meteors from the very large entry Mach numbers (Lin, 1954).

At and below z'''' the rapidly curving trajectory introduces more complications as the meteor rapidly approaches Mach 1 (for a given altitude of interest where $V(z) = c(z)$). Below the altitude region where equation (24) can no longer be satisfied (see IVA, Part 2), the "instantaneous" energy release approximation is no longer suitable and the nonsteady flight of possibly many bodies each with an attached Mach cone interacting in a complex fashion over a rapidly curving path must be considered. Thus while we are considering dynamics of meteor entry throughout the entire range of velocities as a function of altitude (including simple ablation theory), we are only using those portions of each meteor's entry for which the "explosion" analogy is realistic. See Section VIII (Part 3) for additional comments on the transition region where neither model is strictly applicable.

It is an observational fact that only very bright fireballs have been reported to generate audible sounds at altitudes where the meteor was still luminous (Wylie, 1932). It has been suggested that sonic booms generated during dark flight are an additional indicator that a given bright fireball has penetrated deeply enough so that survival of a meteorite is likely (McCrosky, 1970). It is hoped that continuing studies in this area of research may help predict just how frequently infrasound might be recordable by ground based pressure sensors from the many bright fireballs which have been photographed by the Prairie Network.

With the above paragraphs in mind, equation (3) is rewritten as (following McCrosky and Ceplecha, 1970):

$$m\frac{dV}{dt} = mg \sin\theta - \frac{1}{2}\rho V^2 C_D A - fw\frac{dm}{dt} \qquad (8)$$

where

w = velocity of the ablation products with respect to the meteor

$-1 \leq f \leq 1$ and for isotropic ablation $f \equiv 0$.

For the reverse rocket effect $f > 0$ (Levin, 1956)

For this analysis we have assumed f to be exactly zero.

Equation (4) remains the same as before and equation (5) becomes (following Bronshten, 1964):

$$\frac{dm}{dt} = -\bar{K}\frac{A\rho V^3}{2Q}\left(\frac{V^2 - V_m^2}{V^2}\right) \qquad (9)$$

where

Q = heat of ablation of the meteor

$\bar{K}$ = thermal conductivity of the meteor

V_m = velocity at which ablation ceases

$\sigma = \dfrac{\bar{K}}{C_D Q}$ = ablation parameter

Equation (7) is now rewritten as (with p* replaced by

$$p_E^* \exp\left[-\frac{\sigma}{6}\left(V_E^2 - V^2\right)\right] \text{ where } p_E^* = \left(\frac{mg \sin\theta}{C_D A}\right) \text{ evaluated at } z')$$

$$\int_{V_E}^{V} \exp(\sigma V^2/6)\frac{dV}{V} = \int_{z'}^{z} \frac{1}{2}\frac{p_o}{p_E^*} \exp\left[\frac{\sigma}{6} V_E^2\right] \frac{1}{H} e^{-z/H}\, dz$$

Again above z', it is assumed that $V = V_E \cong$ constant.

Therefore, for $z \leq z'$

$$\left[\frac{\overline{Ei}\left(\sigma V^2/6\right) - \overline{Ei}\left(\sigma V_E^2/6\right)}{2}\right] = -\frac{1}{2}\frac{p_o}{p_E^*} \exp\left(\frac{\sigma}{6} V_E^2\right)\left[\exp(-z/H) - \exp(-z'/H)\right]$$

This can be rewritten as:

$$z = -H\left\{\ell n\left[e^{-z'/H} + \frac{2p_E^*}{p_o} \exp\left(-\frac{\sigma}{6} V_E^2\right)\left(\frac{\overline{Ei}\,\frac{\sigma}{6} V_E^2 - \overline{Ei}\left(\frac{\sigma}{6} V^2\right)}{2}\right)\right]\right\} \qquad (10)$$

where $\overline{Ei}$ is the exponential integral (Erdelyi, 1953).

Note that the exponential ablation expressed in equation (10) comes directly from equation (9) after substituting for V^2 from equation (8).

For small values of the argument of $\overline{Ei}$, note that the following approximation becomes applicable (McIntosh, 1970), i.e., for $\sigma V_j^2/6 \lesssim 0.5$

$$\overline{Ei}(\sigma V_j^2/6) \simeq \ell n\, V_j^2 + \frac{\sigma}{6} V_j^2$$

Bronshten has utilized the velocity at which ablation ceases, V_m, explicitly in his equations. The alternative which we have used here is to assume V_m is zero but calculate V(z) for Model 2 only down to that velocity at which ablation is assumed to cease. For our calculations this velocity is assumed to be 3 km/sec. Below the altitude at which this occurs the dark flight trajectory is assumed to exist such that m/A remains constant as before in Model 1. Below z'''' a variable θ problem with m/A constant has to be considered. The rigorous inclusion of V_m = 3 km/sec in the above set of equations produces a correction factor to be applied to the results we have given here. For V_m = 3 km/sec this correction factor is generally quite small and has been neglected (see Bronshten, 1964).

Equation (10) is then solved for z as a function of V and velocity profiles are then constructed as before. This data is also plotted in Figures 4-43. See Figures 52-59 for z', z'', z''', z'''', and $\overline{Kn}$ = 0.05 versus r_{mE} for this model. Here $\overline{Kn} = \lambda/d_m$ where d_m decreases in an exponential manner. For these figures the various parameters are plotted versus the initial meteor radius, r_{mE} (at z'). See IIIC for additional comments on these figures.

Since $\sigma = \overline{K}/C_D Q$ and $\overline{K}$ and Q are hard to determine, it seems that if the meteor composition were known a priori that the overall problem would be simpler. The detailed calculations of Baldwin and Sheaffer (1971) were accomplished

assuming that the composition was known and consisted of a relatively high density object (~3 gm/cm^3). This assumption conflicts with the conclusions reached by McCrosky and Ceplecha (1970). Q is a function of the various flow regimes and also depends on the size and composition of the meteor in that the exact ablation mechanism must be known. For this reason and other reasons discussed earlier, only one value of σ was used in the computations. This value was considered a constant independent of velocity, composition or body size. It is felt with some degree of confidence that this case should represent the maximum allowed ablation for a single spherical body. Actual meteor observations can be interpreted as being reasonably well bounded by these two models. In general, however, real meteors in the size range we have considered have velocity and drag profiles which appear more similar to the Model 2 results than to those of Model 1 (Allen and James, 1964). Model 1 does represent a lower boundary of penetration, however. As stated before, the complete thermodynamic treatment of survivable body sizes in terms of a generalized variable p* is most formidable and due to the extreme nonlinearity of the problem the results at best are only very approximate.

It is an observational fact that most of the fireballs observed by the Prairie Network have entry velocities below about 20 km/sec (McCrosky, et al., 1968). Extreme high values of about 35 km/sec have been observed, however. There are at least two explanations of this fact. The first is that these brighter fireballs represent a different class of bodies than those which have been classically observed with the Super Schmidt cameras (the conventional so-called "shooting stars," McCrosky, 1970). Another explanation is that

ablation is so significant for velocities in excess of about 30 km/sec that deep penetration into the atmosphere of a large massive body is highly improbable (Martin, 1953). The predictions of simple ablation theory (equation (10)) are consistent with this explanation. In fact both of these explanations may be correct. Perhaps it is also true that the relatively small number of large bodies ($\gtrsim$ 10 m in diameter) present in the solar system which encounter the orbit of the earth in space do not frequently possess large (> 30 km/sec) relative velocities with respect to the earth. Such speculations appear endless. We have chosen then to have an arbitrary velocity cut off of 30 km/sec for the initial entry velocity for Model 2. We have also implicitly assumed that above z' the total mass loss is insignificant. Only near and below z' (where it is assumed that the body and its surroundings become luminous) is mass loss assumed to be of importance.

The velocity profiles generated (for both Models 1 and 2) provide much useful information about meteors as sound producers. First of all they bound the altitude regions from which acoustic rays are generated (via known Knudsen numbers and Mach numbers). See Tables 2 and 3 and Section IVC (Part 2). Secondly, they provide information regarding the distance scale of the strong shock wave region of the pressure pulse. This information is obtained in IVA (Part 2) using a cylindrical blast wave model of the meteor bow shock wave (following the numerical work of Lin, 1954, Plooster, 1968, and the observational work of Few, 1969).

Two other points should also be noted. $\overline{Kn}$ for Model 2 is similar to that used in Model 1 except that the meteor radius changes via the assumed known

changes in the meteors cross-sectional area A. The new value of A used at progressively lower and lower altitudes does not include the ablation products removed from the meteor. These products are assumed to be quickly transferred to the meteor's wake (whether they may be plasma, gaseous, liquid or solid). This variation of the meteor's cross-sectional area can be expressed as:

$$A = A_E \exp\left[-\frac{\sigma}{3}\left(V_E^2 - V^2\right)\right]$$

where

A_E = value of the meteor's cross-sectional area at z'

Similarly, the variation in r_m can be expressed as:

$$r_m = r_{mE} \exp\left[-\frac{\sigma}{6}\left(V_E^2 - V^2\right)\right]$$

The above expression comes directly from the variation:

$$p^* = p_E^* \exp\left[-\frac{\sigma}{6}\left(V_E^2 - V^2\right)\right]$$

expressed earlier.

This later expression reduces to the above $r_m(z)$ expression if $\rho_m = \rho_{mE}$ = constant, while p* is proportional to $\rho_m r_m$. See IIIC.

In classical meteor theory, shape factors have been included. Here, the specific choice of a spherical shape has been made. Using other reasonable shapes will not change the entry dynamics greatly (Baldwin and Sheaffer, 1971). The survival of a given meteor, however, does depend on the fraction of the energy deposited into the atmosphere which is able to cause ablation of the

body. This energy flow depends on many factors during entry (shape factors among them) and is presumably far more complex than any theoretical calculations which have yet been used to model it.

From a more general viewpoint, however, the audible observations of sounds from meteors at close range are likely to be greatly affected by the shape of the body (or many bodies). Many irregular shaped bodies produce wider Mach cones than are predicted by simple sonic boom theory. As a result a complex series of shock wave arrivals may occur (Chamberlin, 1968; Millman, 1970).

From the results of Model 2 the additional cases which have been removed from consideration cover meteors whose initial kinetic energies range from $4.2 \cdot 10^{12}$ to $7.3 \cdot 10^{14}$ ergs. See Tables 2 and 3 for additional comments on all the dynamical possibilities involved. Note that θ and ρ_{mE} must be specified in addition to entry kinetic energy values before a judgment can be made on the dynamical possibilities for bow shock generation. The term, removed from consideration, in the case of Model 1 is appropriate while Model 1 represents the maximum possible penetration. In the case of Model 2 it must be recalled that the value of σ was chosen as strictly an upper limit. Thus for $0 \leq \sigma \leq 5 \cdot 10^{-12}$ sec^2/cm^2 the entry kinetic energies which are not dynamically possible cover the range $\sim 10^9 - 10^{15}$ ergs. If a smaller upper limit had been chosen for σ, the largest entry kinetic energy given above, for which a distant bow shock is not possible, would be reduced.

C. EFFECTIVE METEOR LINE SOURCE MODEL

This effective meteor model thus allows for single body ablation with $0 \leq \sigma \leq 5 \cdot 10^{-12}$. The region of interest is between the upper and lower altitude bounds imposed by the velocity profiles of the two meteor models for the two assumed density extremes. It is within these bounds (with certain other restrictions to be seen in Part 2) that the "explosion" analogy will be used to study the sounds generated by the meteor atmosphere interaction. See Figures 4-43. It now remains to test the allowed dynamical possibilities to see under what conditions pressure waves can reach ground level, at measurable intensities. This will be discussed in IVC and V (Part 2).

There are two interesting interpretation problems which arise when using the simple ablation theory which should be noted at this point. In the formulation of Model 1, p^* has been held constant (i.e., $\sigma \equiv 0$). While p^* is proportional to $\rho_m r_m$ primarily (the variations in g, sin θ, and C_D being small between z' and z''''), a constant p^* value can be interpreted as:

(1) ρ_m = constant, r_m = constant

(2) ρ_m decreasing, r_m increasing

(3) ρ_m increasing, r_m decreasing

Within certain limits, including a detailed knowledge of the inner structure of the meteor, all three of the above may be dynamically possible. Further, the large range of ρ_m used causes an interpretation problem when specifically considering the velocity-altitude profiles. The altitudes z', z'', z''', and z'''' all depend on p^*. In addition, z' and z'''' depend on V_E. Thus, analysis of the velocity altitude profile will enable us to determine only the

product $\rho_m r_m$. $\rho_m r_m$ always appears as an inseparable product in the dynamical equations. If the density and radius of an entering meteoroid can change during entry (such as in (2) and (3)), the interpretation of r_m is difficult even if p* is constant. Thus, for the factor of twenty-five density variation allowed, a subsequent factor of twenty-five is allowed for r_m when interpretations using p* are made. Thus, as can readily be seen in Figures 44-59, a low-density, high-velocity meteor can have nearly the same value of z' as a high-density, low-velocity meteor. All of these arguments neglect the possible gross fragmentation or total break-up phenomena which fall into the category of an n body physical theory of meteors. Throughout this analysis only single body theory has been considered.

The other interpretation problem involves the case where $\sigma \neq 0$. In this situation the mass variation with altitude of the entering meteor can be expressed as:

$$m = m_E \exp\left[-\frac{\sigma}{2}\left(V_E^2 - V^2\right)\right]$$

where

m_E = meteor mass at z'

Note that for Model 2 ($\sigma \neq 0$) this, and the other similar expressions relating an exponentially decreasing variation for A, r_m, and p* are valid only until V(z) = 3 km/sec. Below this velocity a constant m/A problem is again encountered (with $\sigma \equiv 0$), but with a rapidly changing θ due to the ever increasing effects of gravity (below z'''').

While this exponentially decreasing variation is proportional to σV_E^2, the range of σ and V_E values used again produces an interpretation problem. If a z(V) curve is interpretated in terms of $\sigma \neq 0$, only if V_E is known can the value of σ be determined with any degree of confidence.

The rate of ablation then using single body simple ablation theory is determined by the inseparable product $\frac{\sigma}{6}(V_E^2 - V^2)$. While this rate depends on V_E^2 the interpretation problem is not as difficult as it was for the constant p* situation. The fact that an upper limit of 30 km/sec has been set on V_E limits the possible σ values that can be reasonably used, however. Again we are limited to a single body interpretation of the phenomena. This interpretation is probably optimum for denser meteors and large body sizes at moderately low altitudes (before total break-up occurs due to the tremendous pressures imposed on the frontal face of the meteor).

Overall it appears that if the magnitude range of ρ_{mE} could be decreased or the composition or internal structure of the meteor were known, the interpretation difficulty could be considerably reduced. In Section VII (Part 3), m will be estimated (at least for one region of each fireball's entry) after assuming the body's shape, density, and velocity at that point. With further ray tracing effort in the future we hope to reduce the velocity uncertainty so that primarily only the shape and density need be known in order to estimate the meteor's mass. Thus well documented meteor sound observations will be shown to be potentially very useful.

One additional subject should be clarified. This involves the definition of the Knudsen number for the effective model considered. At the lower bound

of penetration there is no problem since d_m has been considered constant (as has ρ_m) throughout the entry. Once Kn = 0.05 has been reached, Kn continues to become smaller as λ decreases with decreasing altitude. In addition certain ρ_{mE}, r_{mE}, and θ combinations are not dynamically possible in terms of hypersonic velocity remaining with Kn = 0.05. See Table 2. For $\sigma \neq 0$ problems begin to arise, however. First of all λ has been calculated (for both models) for a neutral gas as if the meteor were not present. The neutral gas heating must increase λ. This increase is limited, however, by the fact that the density ratio across the shock front can (theoretically) never exceed six for a diatomic gas (Plooster, 1968). It is assumed, in general, that the local plasma effects have a very short relaxation time. Hence they do not greatly influence the shock wave formation and subsequent propagation beyond certain scaled distances from the trajectory. See IVA (Part 2). The success of the classical blast wave theory (as applied primarily to point explosions) in describing explosive phenomena supports the latter assumption. However, we have used d_m as the characteristic length to define Kn and $\overline{\text{Kn}}$. Perhaps once the shock has been well established a different length scale should be used. In the case of $\sigma = 0$ this may be an effective distance across the bow shock at a few body diameters behind the meteor. In the case of $\sigma \neq 0$ the ablation products in combination with the primary body (with both still traveling at hypersonic velocities) may produce a new effective length scale. These remarks are made in an attempt to understand the Knudsen number variation in the case $\sigma \neq 0$. While for this case d_m is proportional to $\exp\left[-\frac{\sigma}{6}(V_E^2 - V^2)\right]$, the rate at which d_m decreases can under certain circumstances exceed the rate at which λ

decreases (with decreasing altitude). For $0 < \sigma \leq 5.10^{-12}$ sec^2/cm^2 and for $15 \lesssim V_E \leq 30$ km/sec, $\overline{Kn}$ can actually increase with continually decreasing altitude before or even after $\overline{Kn} = 0.05$ has been reached. Whether or not this can actually physically occur depends on many factors as has been discussed. Fortunately as will be seen the larger r_{mE} is, the less important this increasing $\overline{Kn}$ is, while the turn around altitude region occurs at very small values of $\overline{Kn}$ ($\sim 10^{-3}$ or less). Only for $r_{mE} \lesssim 5.0$ cm is this phenomena even possible (for $\overline{Kn}$ to become greater than one to ten after it has reached 0.05). See Table 2 for more comments on this. As will be seen in V (Part 2), when considering ground based measurement of these signals only for $r_{mE} \gtrsim 5.0$ cm will measurement be likely (at certain distances and altitudes from the meteor) in terms of acoustic energy output and wave frequency absorption. Thus the problem of more precisely defining $\overline{Kn}$ for a body whose size is decreasing exponentially is no longer as vital to the overall problem as it may have seemed.

BIBLIOGRAPHY

1. Allen, H. J. and A. J. Eggers, Jr., A Study of the Motion and Aerodynamic Heating of Ballistic Missiles Entering the Earth's Atmosphere at High Supersonic Speeds, NACA Report 1381, pp. 1125-1140, 1958.

2. Allen, H. J. and N. A. James, Prospects For Obtaining Aerodynamic Heating Results From Analysis of Meteor Flight Data, NASA TN D 2069, July, 1964.

3. Astapovich, I. S., Sound Phenomena Simultaneous with the Flight of Bolides, Meteoritika, Vol. 9, pp. 71-101, 1951.

4. Baker, R.M.L., Jr., The Transitional Aerodynamic Drag of Meteorites, Astrophys. J , Vol. 129, pp. 826-841, 1959.

5. Baldwin B. and Y. Sheaffer, Ablation and Breakup of Large Meteoroids during Atmospheric Entry, J. Geophys. Res., Vol. 76, No. 19, pp. 4653-4668, July 1, 1971.

6. Barringer, B. and H. Hart, The Mechanism of the Sounds from Meteors, Cont. of the Meteor. Soc., pp. 507-518, December, 1949.

7. Batten, E. S., Wind Systems in the Mesosphere and Lower Thermosphere, J. Meteorology, Vol. 18, pp. 283-291, 1961.

8. Bronshten, V. A., Problems of the Movement of Large Meteoric Bodies in the Atmosphere, NASA TT-F-247, November, 1964.

9. Chamberlin, Von Del, Meteorites of Michigan, Bulletin No. 5 of the Beological Survey of Michigan, Lansing, Michigan, 1968.

10. Cook, R. K., Atmospheric Sound Propagation, Atmospheric Exploration By Remote Probes, Proc. of the Scientific Meetings of the Panel on Remote Atmos. Probing to the Comm. on Atmos. Science, National Academy of Sciences, and the National Research Council, Vol. 2, pp. 633-69, January, 1969.

11. Cosby, W. A. and R. G. Lyle, The Meteoroid Environment and Its Effects on Materials and Equipment, NASA SP-78, 1965.

12. Cospar International Reference Atmosphere 1965, North-Holland Publishing Company, Amsterdam, 1965.

13. Craig, R. A., The Upper Atmosphere-Meteorology and Physics, Academic Press, New York, 1965.

BIBLIOGRAPHY (Continued)

14. Donn, W. L. and D. Rind, Microbaroms and the Temperature and Wind of the Upper Atmosphere, J. Atmos. Sci., Vol. 29, pp. 156-172, January, 1972.

15. Erdelyi, A., Editor, Higher Transcendental Functions, H. Bateman Manuscript Project, Vol. II., 396 pp., McGraw-Hill Book Co., Inc., 1953.

16. Fay, J. A., W. C. Moffatt, and R. F. Probstein, An Analytical Study of Meteor Entry, AIAA Journal, Vol. 2, No. 5, pp. 845-854, May, 1964.

17. Few, A. A., Jr., Thunder, Ph.D. Thesis, Rice University, November, 1968.

18. Few. A. A., Jr., Power Spectrum of Thunder, J.G.R., Vol. 74, No. 28, pp. 6926-6934, 1969.

19. Gault, D., Saturation and Equilibrium Conditions for Impact Cratering on the Lunar Surface: Criteria and Implications, Radio Science, Vol. 5, No. 2, pp. 273-291, February, 1970.

20. Gazley, Carl, Jr., Meteoric Interaction With the Atmosphere; Theory of Drag and Heating and Comparison with Observations, The Rand Corporation, Report R-339, 6-1, 1959.

21. Goerke, V. H., Infrasonic Observations of a Fireball, Sky and Telescope, p. 313, November, 1966.

22. Goerke, V. H., Private Communication, July, 1971.

23. Grad, H., Equations of Flow in a Rarefied Atmosphere, The Rand Corporation, Report R-339, 11-1, 1959.

24. Groves, G. V., Velocity of a Body Falling Through the Atmosphere and the Propagation of its Shock Wave to Earth, J. Atmos. Terrestrial Physics, Vol. 10, pp. 73-83, 1957.

25. Hayes, W. D., Sonic Boom, Annual Review of Fluid Mechanics, M. VanDyke, W. G. Vincenti and T. V. Wehausen (Editors), Vol. 3, Annual Review, Inc., Palo Alto, Calif., pp. 269-290, 1971.

26. Jacchia, L. G., On Two Parameters Used In the Physical Theory of Meteors, Smithsonian contributions to Astrophysics, Vol. 2, No. 9, Washington, D.C., 1958.

27. Jacchia, L. G., et al., An Analysis of the Atmospheric Trajectories of 413 Precisely Reduced Photographic Meteors, Smithsonian contributions to Astrophysics, Vol. 10, No. 1, 1967.

28. Krinov, E. L., Principles of Meteoritics, Pergamon Press, New York, pp. 63-83, 1960.

29. Kushner, S. S. and J. W. Wescott, Propagation of Sound in Air (A Bibliography with Abstracts), The University of Michigan, College of Engineering, June, 1965.

30. LaPaz, L., Effects of Meteorites Upon the Earth, Advances in Geophysics, Vol. 4, pp. 219-350, 1958.

31. Levin, B. J., The Physical Theory of Meteors and Meteoric Matter in the Solar System, Izd. Akad. Nauk. SSSR, Moscow, 293 pp., 1956.

32. Lin, S. C., Cylindrical Shock Waves Produced by Instantaneous Energy Release, J. of App. Phys., Vol. 25, No. 1, pp. 54-57, January, 1954.

33. Loh, W.H.T., Re-Entry and Planetary Entry Physics and Technology, Volumes I and II, Springer-Verlag, New York, Inc., 1968.

34. Lowery, C. J. and E. M. Shoemaker, Airwaves Associated with Large Fireballs and the Frequency Distribution of Energy of Large Meteoroids, J. Meteoritical Soc., Vol. 3, No. 3, pp. 123-4, April, 1967.

35. Lyubarskiy, K. A., A Statistical Study of Bolides, Meteoritika, Vol. 11, pp. 153-164, 1952.

36. Martin, G. R., Recent Studies on Iron Meteorites. IV. The Origin of Meteorites, Geochimica et Cosmochimica Acta, Vol. 3, pp. 288-309, 1953.

37. McCrosky, R. E., The Lost City Meteorite Fall, Sky and Telescope, pp. 154-158, March, 1970.

38. McCrosky, R. E. and Z. Ceplecha, Fireballs and the Physical Theory of Meteors, Bull. Astron. Inst. Czechoslovakia, Vol. 21, No. 5, pp. 271-296, 1970.

39. McCrosky, R. E., and A. Posen, Prarie Network Meteor Data, Smithsonian Astrophysical Observatory, Special Report 273, May 10, 1968.

40. McIntosh, B. A., On the End Point of Fireballs, J. Roy. Astron. Soc. Canada, Vol. 64, pp. 267-281, October, 1970.

41. McKinley, D.W.R., Meteor Science and Engineering, McGraw-Hill Book Co., Inc., New York, 1961.

BIBLIOGRAPHY (Continued)

42. Millman, P. M., A Brief Survey of Upper Air Spectra, Physics and Dynamics of Meteors, Editors Kresak and Millman, D. Reidel Publishing Co., pp. 84-90, 1968.

43. Millman, P. M., A Tape Recording of the Belfast Meteorite, J. Roy. Astron. Soc. Canada, Vol. 64, No. 1, pp. 57-59, 1970.

44. Nininger H. H., Out of the Sky - An Introduction to Meteoritics, Dover Publications, Inc., New York, 1952.

45. Officer, C. B., Introduction to the Theory of Sound Transmission - With Application to the Ocean, McGraw-Hill Book Co. Inc., New York, 1958.

46. Öpik, E., Physics of Meteor Flight in the Atmosphere, Interscience Publishers, Inc., New York, 1958.

47. Plooster, M. N., Shock Waves from Line Sources, NCAR-TN-37, 83 pp., National Center for Atmospheric Research, Boulder, Colorado, 1968.

48. Riddell, F. R. and H. B. Winkler, Meteorites and Re-Entry of Space Vehicles at Meteor Velocities, ARS Journal, pp. 1523-1530, October, 1962.

49. Romig, M. F., The Physics of Meteor Entry, The Rand Corporation, 39 pp., AD 438437, April, 1964.

50. Romig, M. F. and D. L. Lamar, Anomalous Sounds and Electromagnetic Effects Associated with Fireball Entry, Rand Corporation Memorandum RM-3724-ARPA, July, 1963.

51. Romig, M. F. and D. L. Lamar, Electromagnetic Effects Associated with the San Francisco Fireball of November 7, 1963, Meteoritics, Vol. 2, No. 4, pp. 301-310, June, 1965.

52. Tsikulin, M. A., Shock Waves During the Movement of Large Meteorites in the Atmosphere, Translation Division of the U.S. Naval Intelligence Command, Alexandria, Virginia, available from the National Technical Information Service, Springfield, Virginia as AD 715-537, 1970.

53. U.S. Standard Atmosphere Supplements, U.S. Government Printing Office, Washington, D.C., 1966.

54. Wegener, A., Das detonierende Meteor vom 3 April 1916, 3 1/2 uhr nachmittags in Kurhessen, Schriften der Gesellshaft zur Beforderung der gesamten Naturwissenschaften zu Marburg, Band 14, Erstes Heft, pp. 1-83, 1917.

BIBLIOGRAPHY (Concluded)

55. Whipple, F.J.W., The High Temperature of the Upper Atmosphere as an Explanation of Zones of Audibility, Nature, Vol. 111, No. 2780, p. 187, February 10, 1923.

56. Whipple, F.J.W., Determination of the Temperature of the Upper Atmosphere by Meteor Observations, Nature, Vol. 112, No. 2821, p. 759, November 24, 1923.

57. Whipple, F.J.W., The Great Siberian Meteor and the Waves, Seismic and Aerial, Which it Produced, Quart. J. Roy. Meteor. Soc., Vol. 56, pp. 287-304, 1930.

58. Wilson, C. R., Private Communication, June, 1972.

59. Wood, J. A., Monthly Notices Royal Astronomical Society, Vol. 129, p. 79, 1961.

60. Wylie, C. C., Sounds From Meteors, Popular Astronomy, Vol. 40, No. 5, Whole No. 395, pp. 289-94, May, 1932.

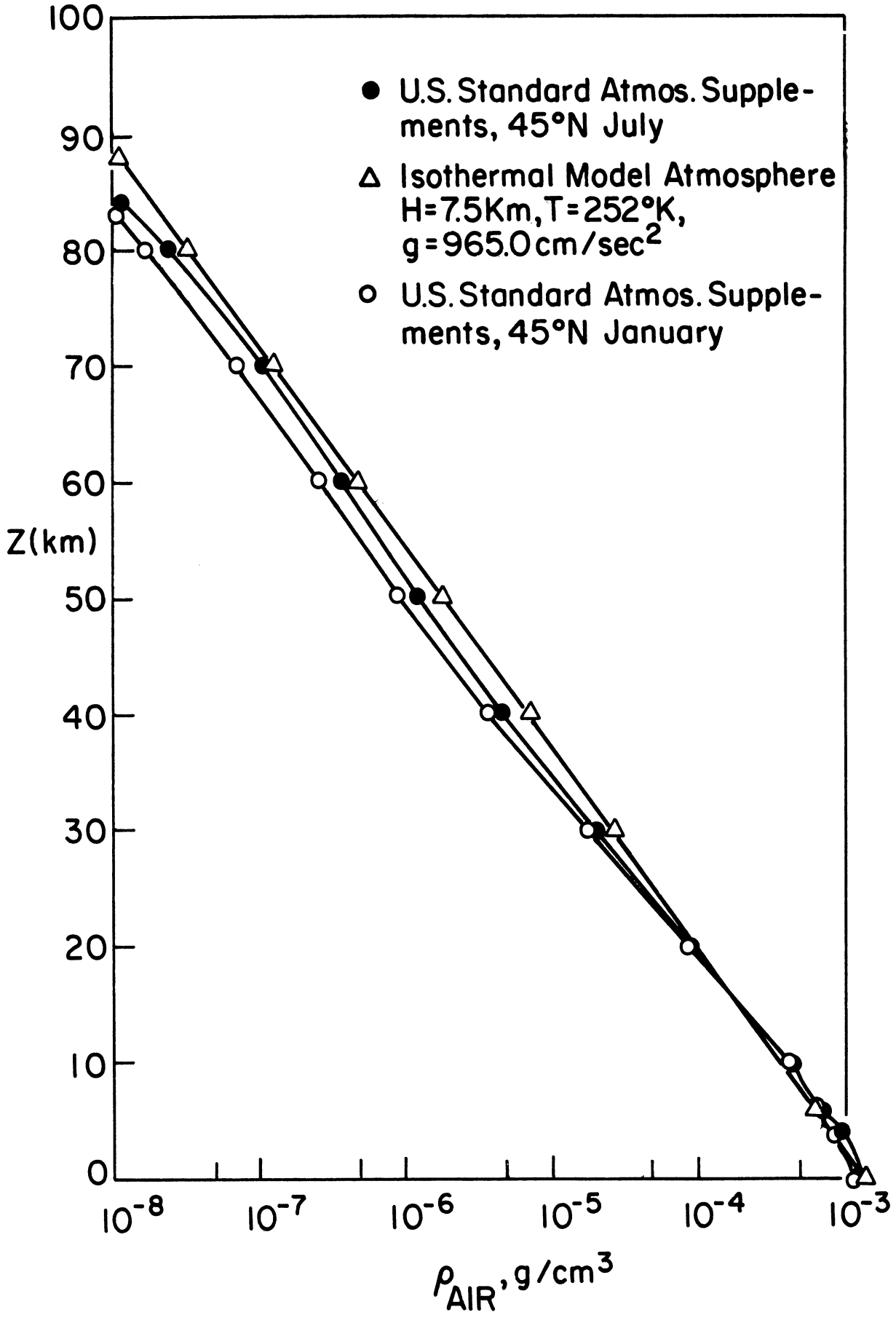

Figure 1. Atmospheric density as a function of altitude.

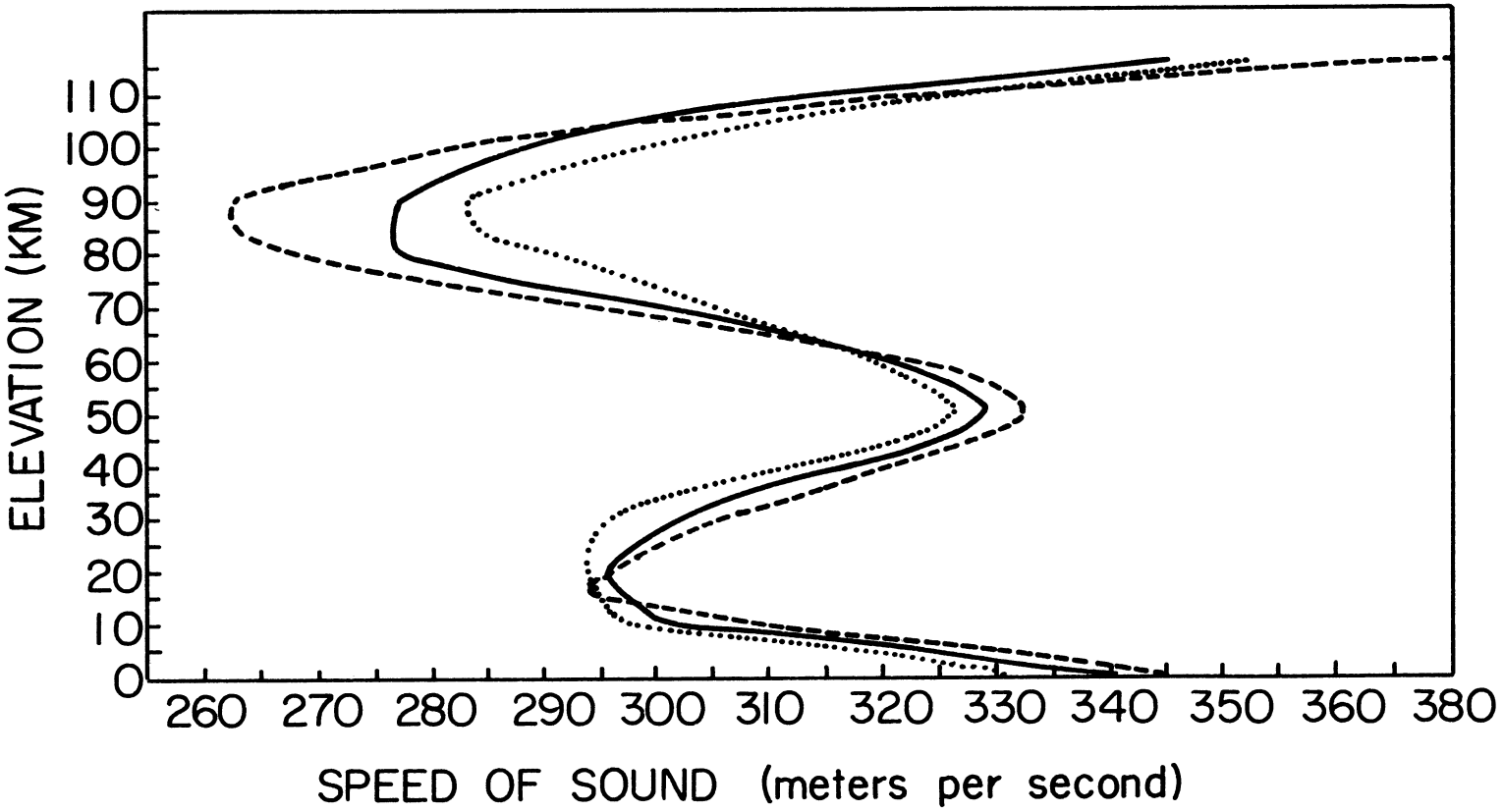

Figure 2. Speed of sound as a function of altitude and season for 45°N latitude, after Donn and Rind, 1972 (for winter, dotted line; for summer, dashed line; for spring-fall, solid line).

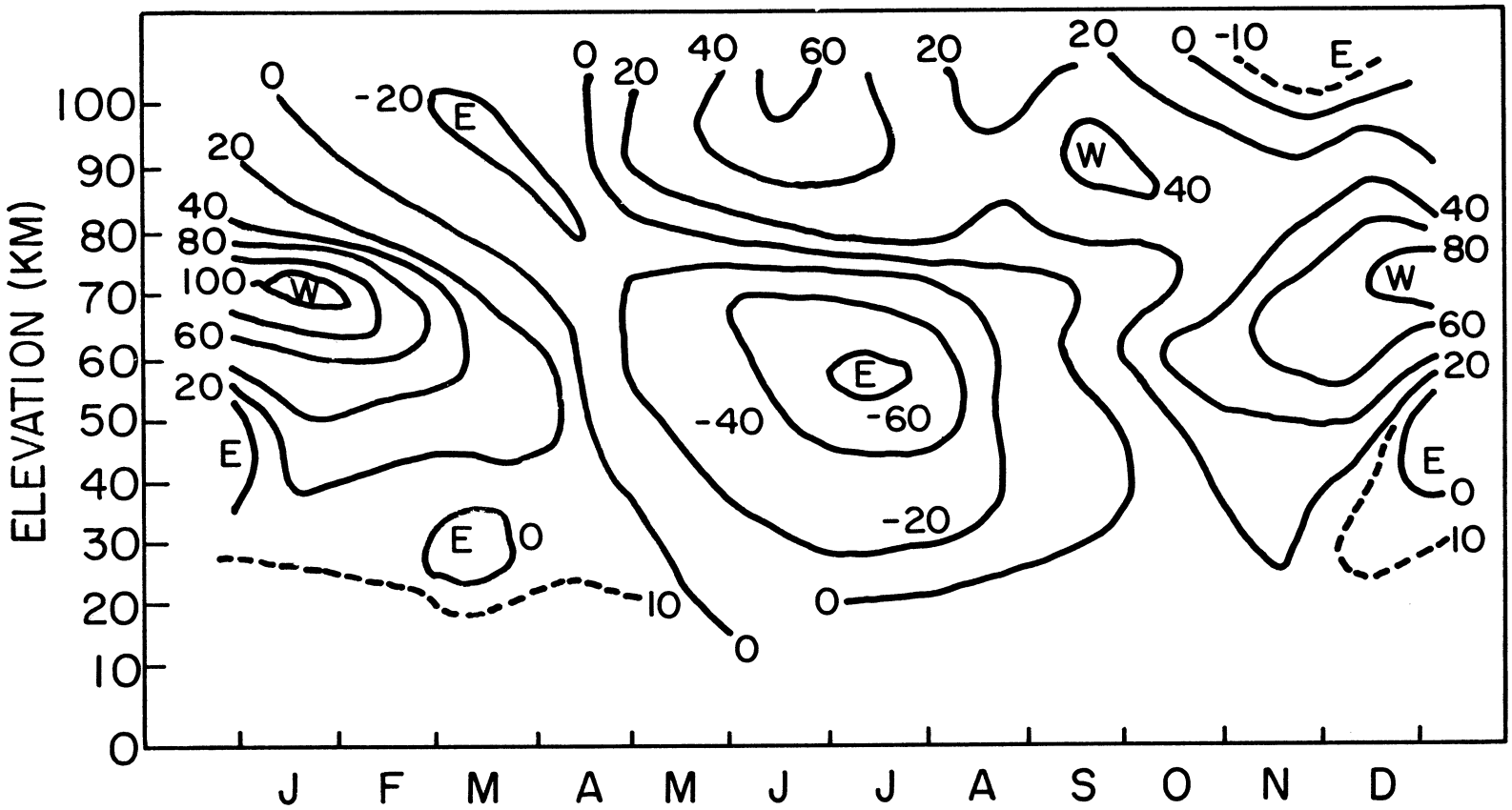

Figure 3. Middle latitude zonal wind field as a function of altitude and time of year, after Batten, 1961 (speeds in m/sec).

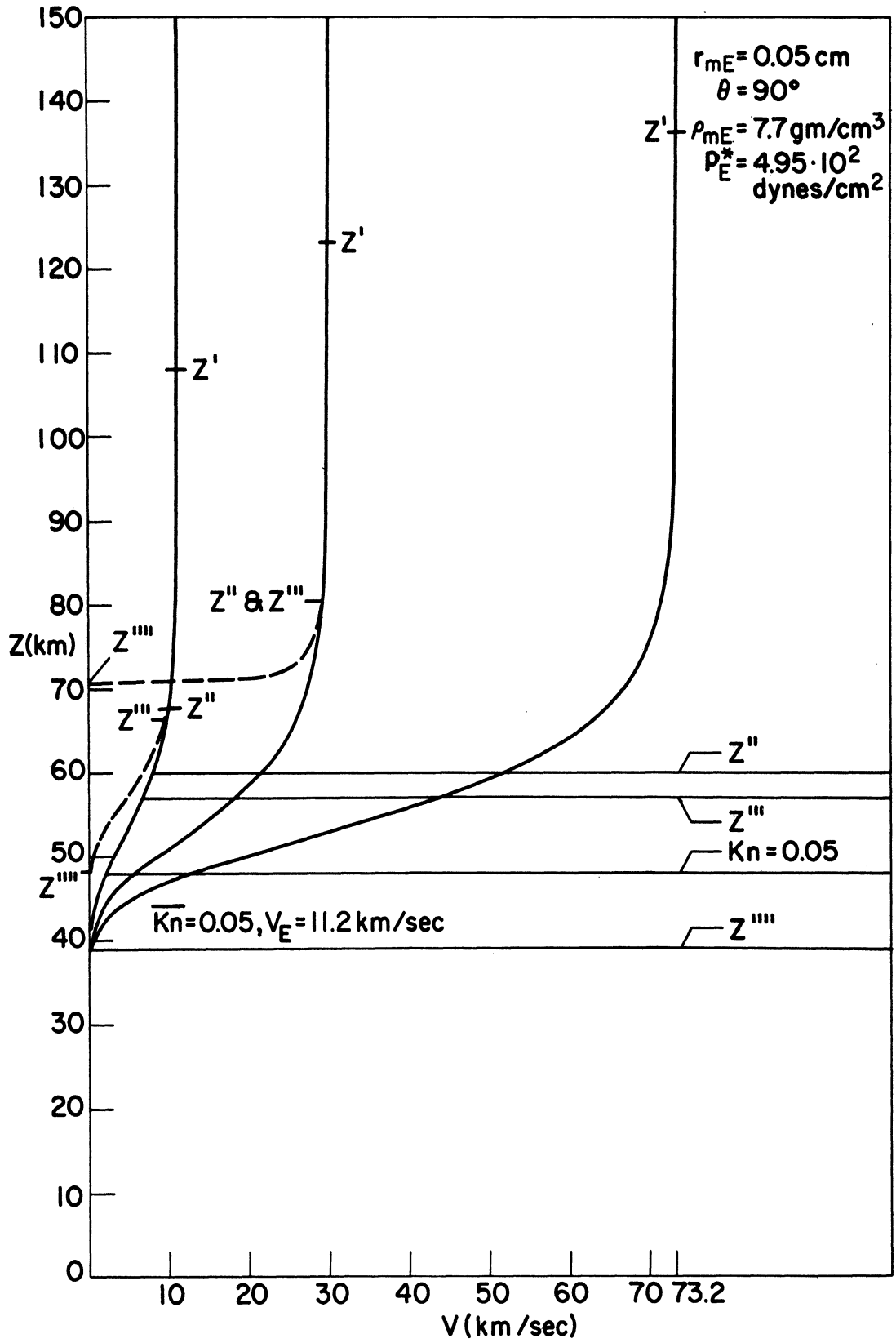

Figure 4. Meteor velocity as a function of altitude (σ = 0, solid curve; $\sigma = 5 \cdot 10^{-12}$ sec^2/cm^2, dashed curve), r_{mE} = 0.05 cm, θ = 90°, ρ_m = 7.7 g/cm^3.

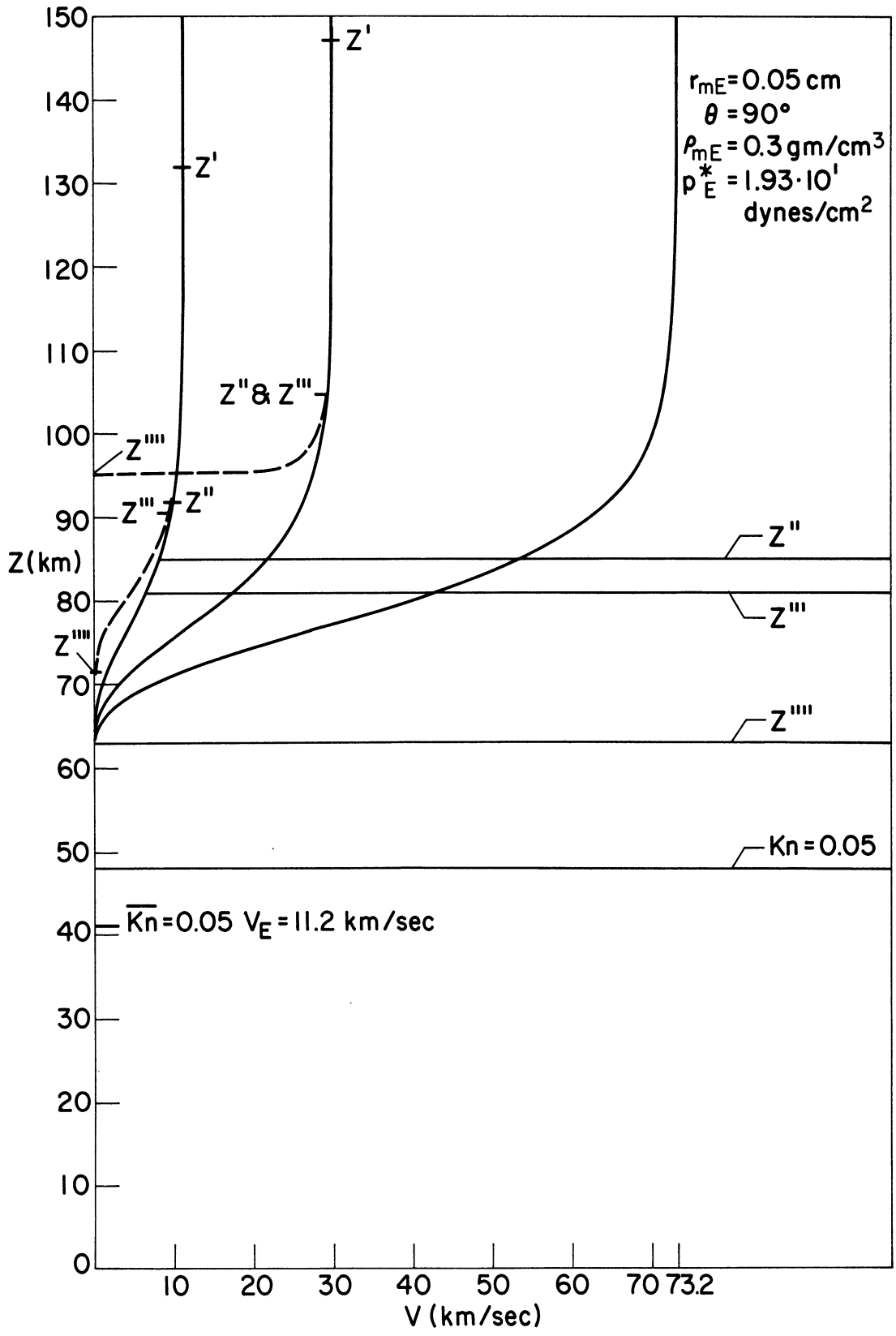

Figure 5. Meteor velocity as a function of altitude (σ = 0, solid curve; $\sigma = 5 \cdot 10^{-12}$ sec^2/cm^2, dashed curve), r_{mE} = 0.05 cm, θ = 90°, ρ_m = 0.3 g/cm^3.

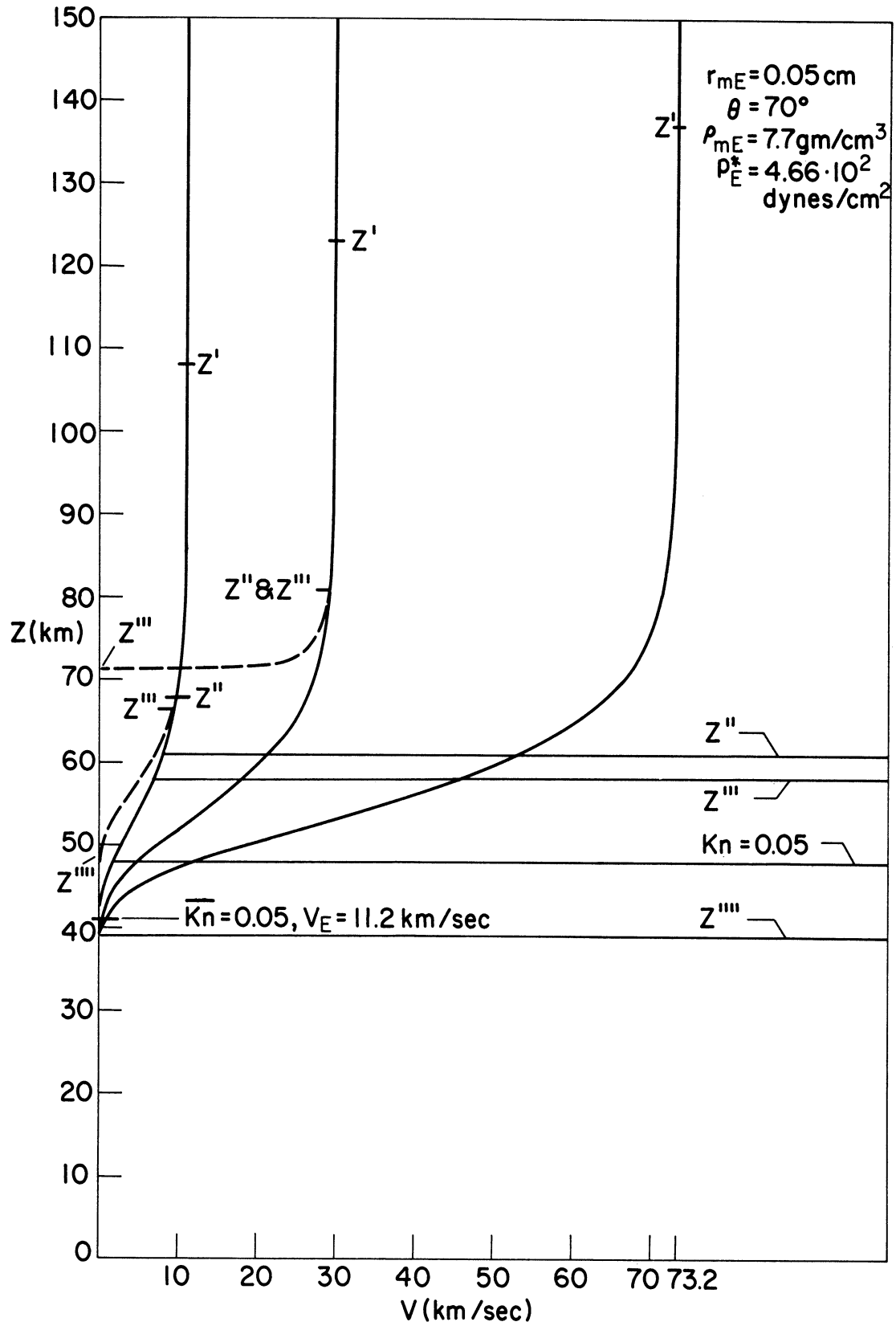

Figure 6. Meteor velocity as a function of altitude (σ = 0, solid curve; $\sigma = 5 \cdot 10^{-12}$ sec^2/cm^2, dashed curve), r_{mE} = 0.05 cm, θ = 70°, ρ_m = 7.7 g/cm^3.

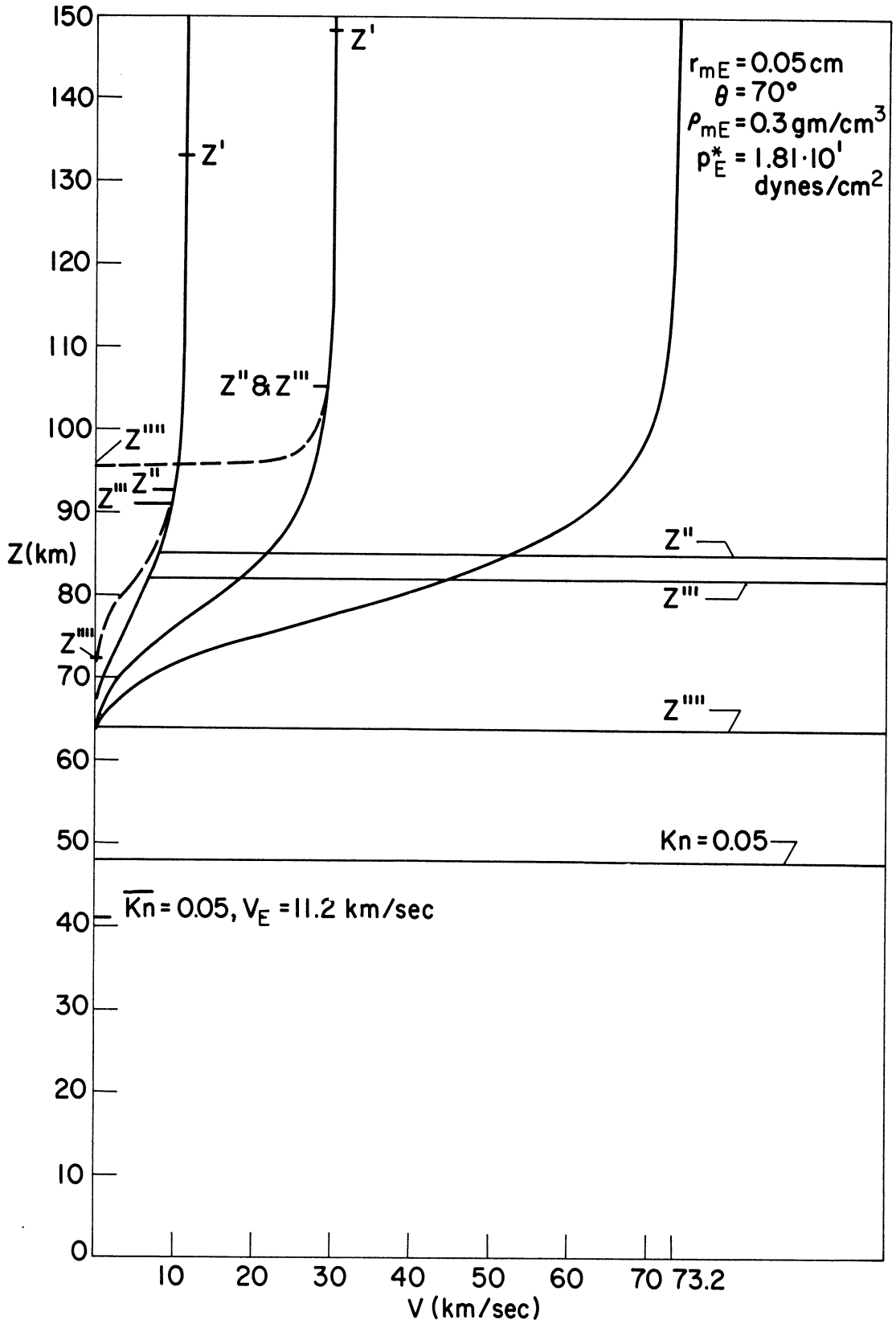

Figure 7. Meteor velocity as a function of altitude (σ = 0, solid curve; $\sigma = 5 \cdot 10^{-12}$ sec^2/cm^2, dashed curve), r_{mE} = 0.05 cm, θ = 70°, ρ_m = 0.3 g/cm^3.

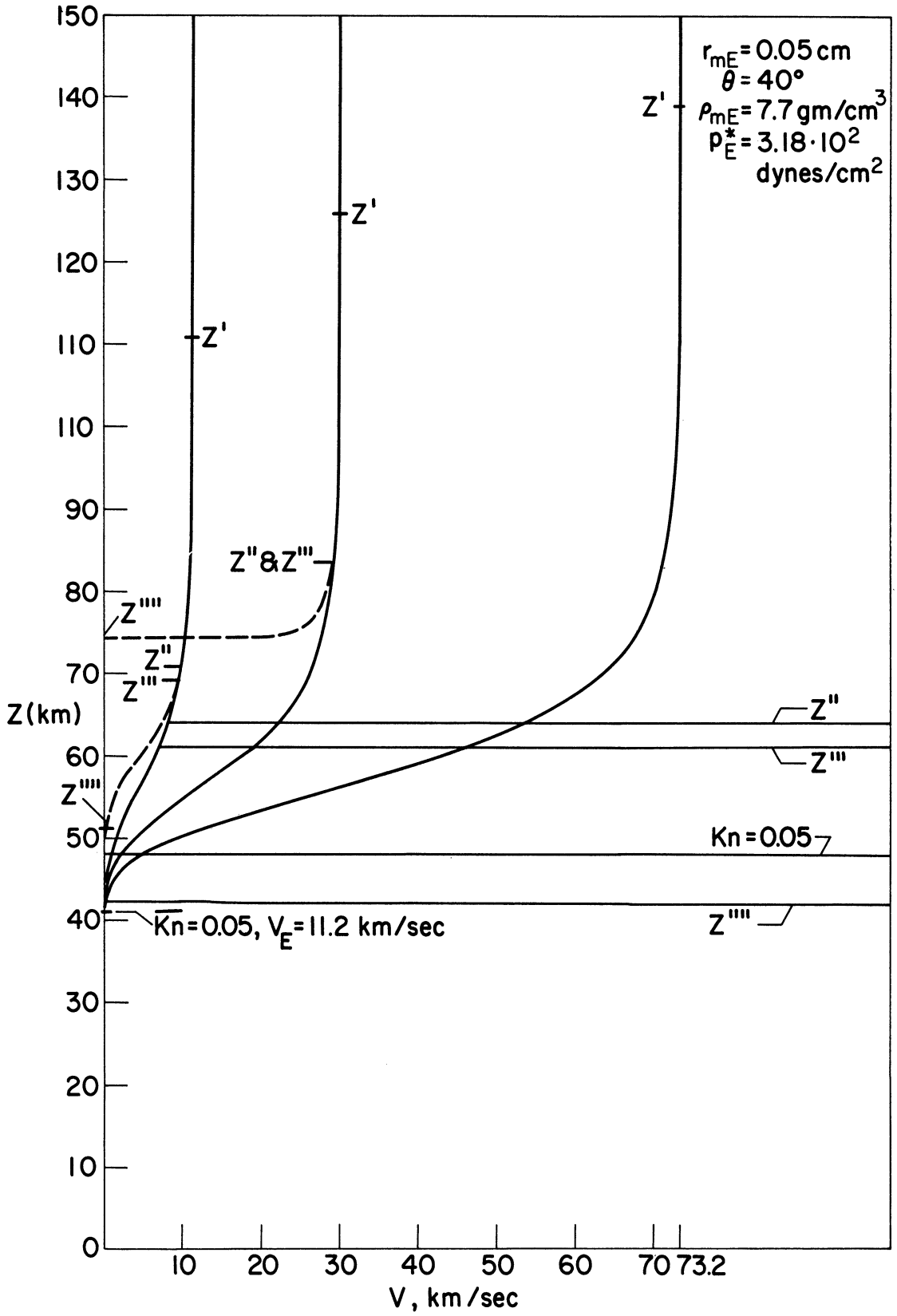

Figure 8. Meteor velocity as a function of altitude (σ = 0, solid curve; $\sigma = 5 \cdot 10^{-12}$ sec^2/cm^2, dashed curve), r_{mE} = 0.05 cm, θ = 40°, ρ_m = 7.7 g/cm^3.

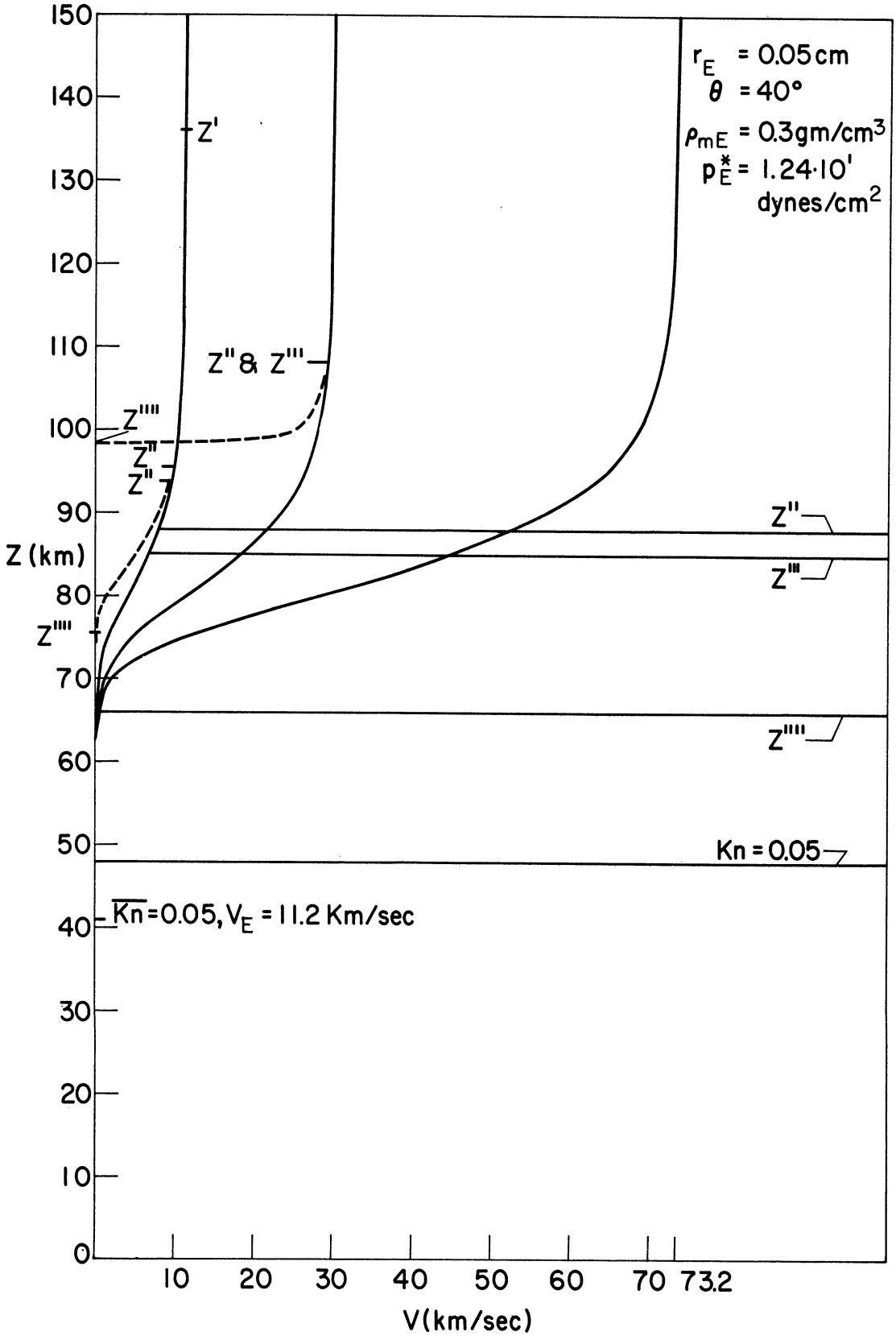

Figure 9. Meteor velocity as a function of altitude (σ = 0, solid curve; $\sigma = 5 \cdot 10^{-12}$ sec^2/cm^2, dashed curve), r_{mE} = 0.05 cm, θ = 40°, ρ_m = 0.3 g/cm^3.

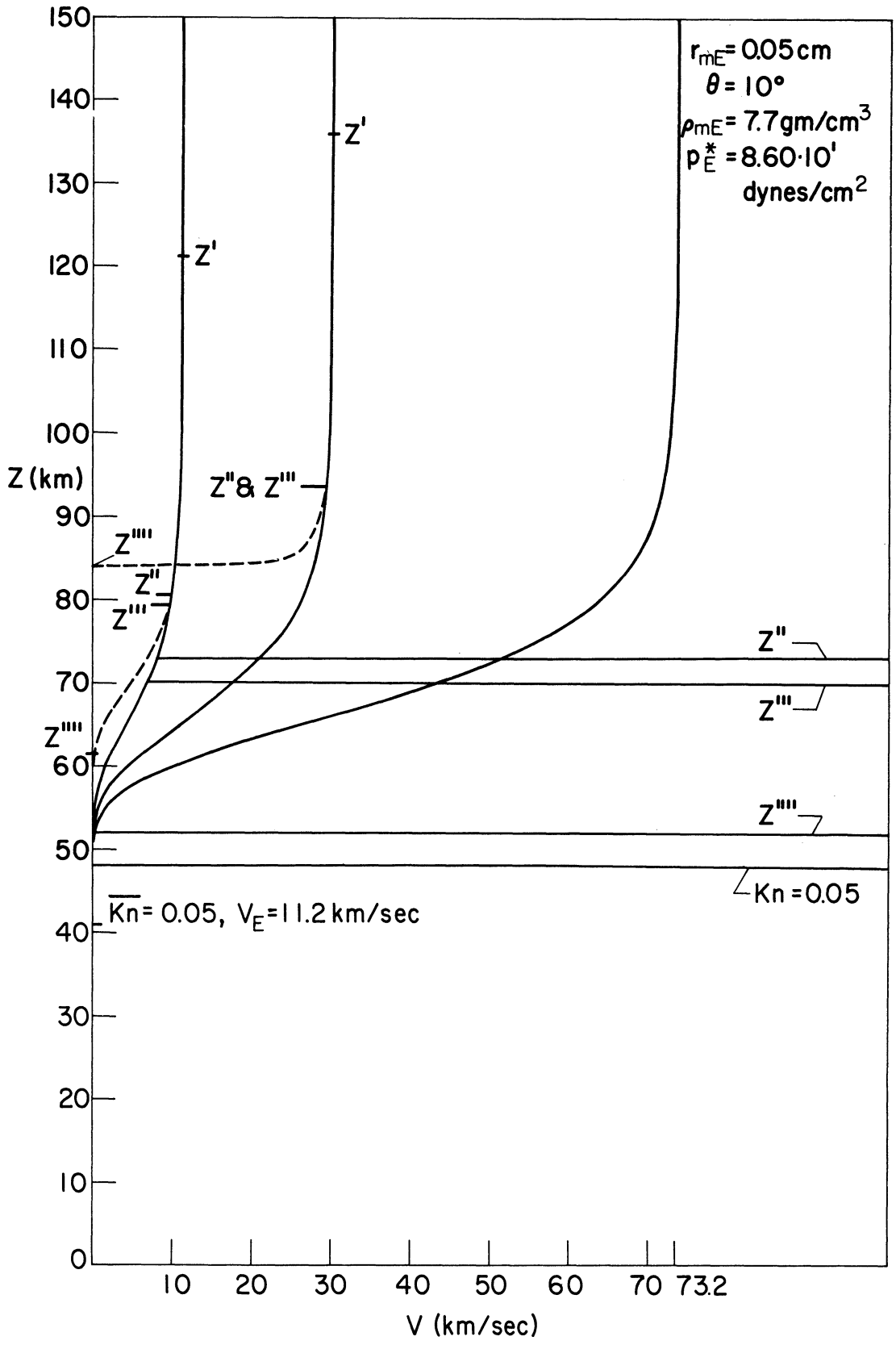

Figure 10. Meteor velocity as a function of altitude (σ = 0, solid curve; $\sigma = 5 \cdot 10^{-12}$ sec^2/cm^2, dashed curve), r_{mE} = 0.05 cm, θ = 10°, ρ_m = 7.7 g/cm^3.

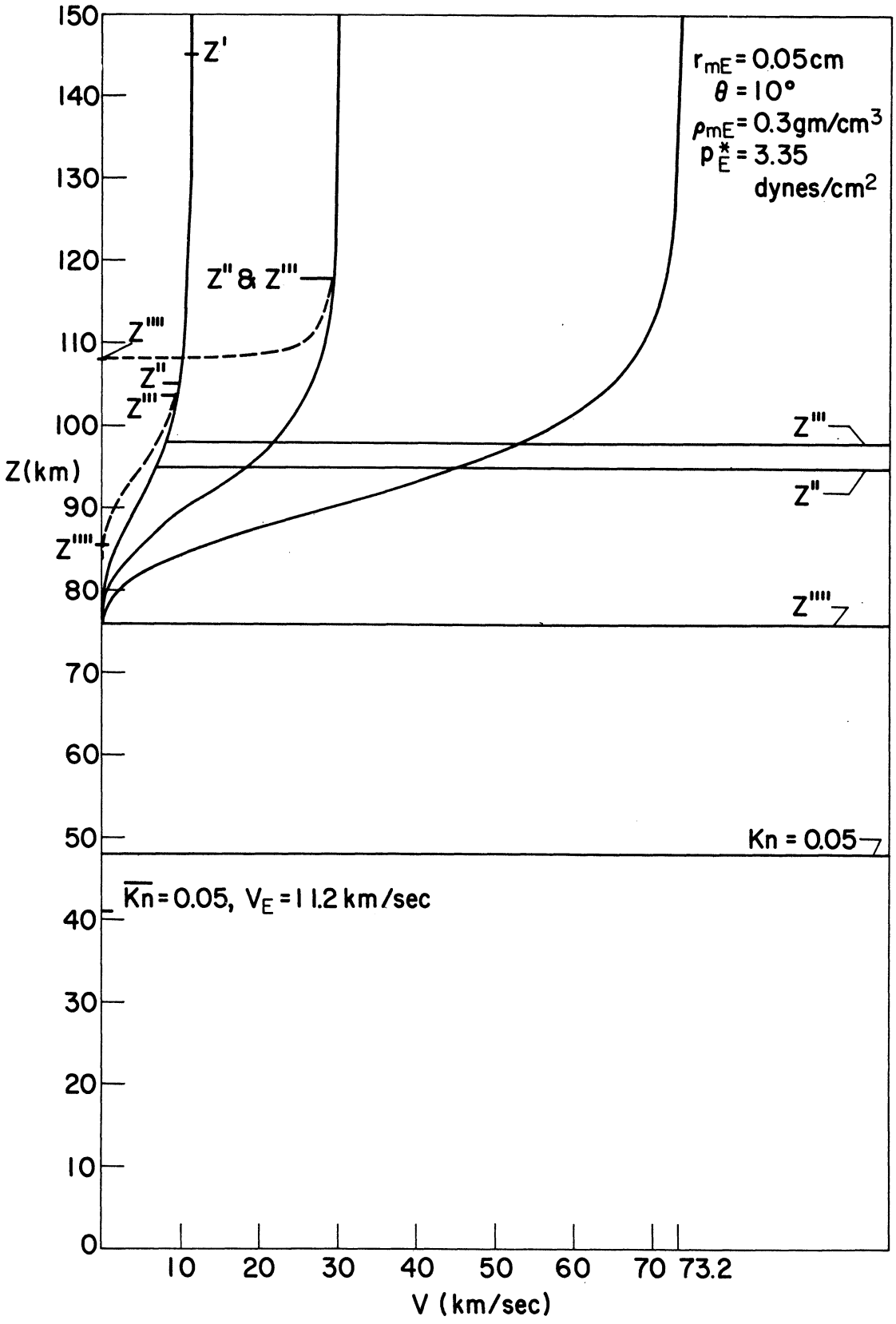

Figure 11. Meteor velocity as a function of altitude (σ = 0, solid curve; $\sigma = 5 \cdot 10^{-12}$ sec^2/cm^2, dashed curve), r_{mE} = 0.05 cm, θ = 10°, ρ_m = 0.3 g/cm^3.

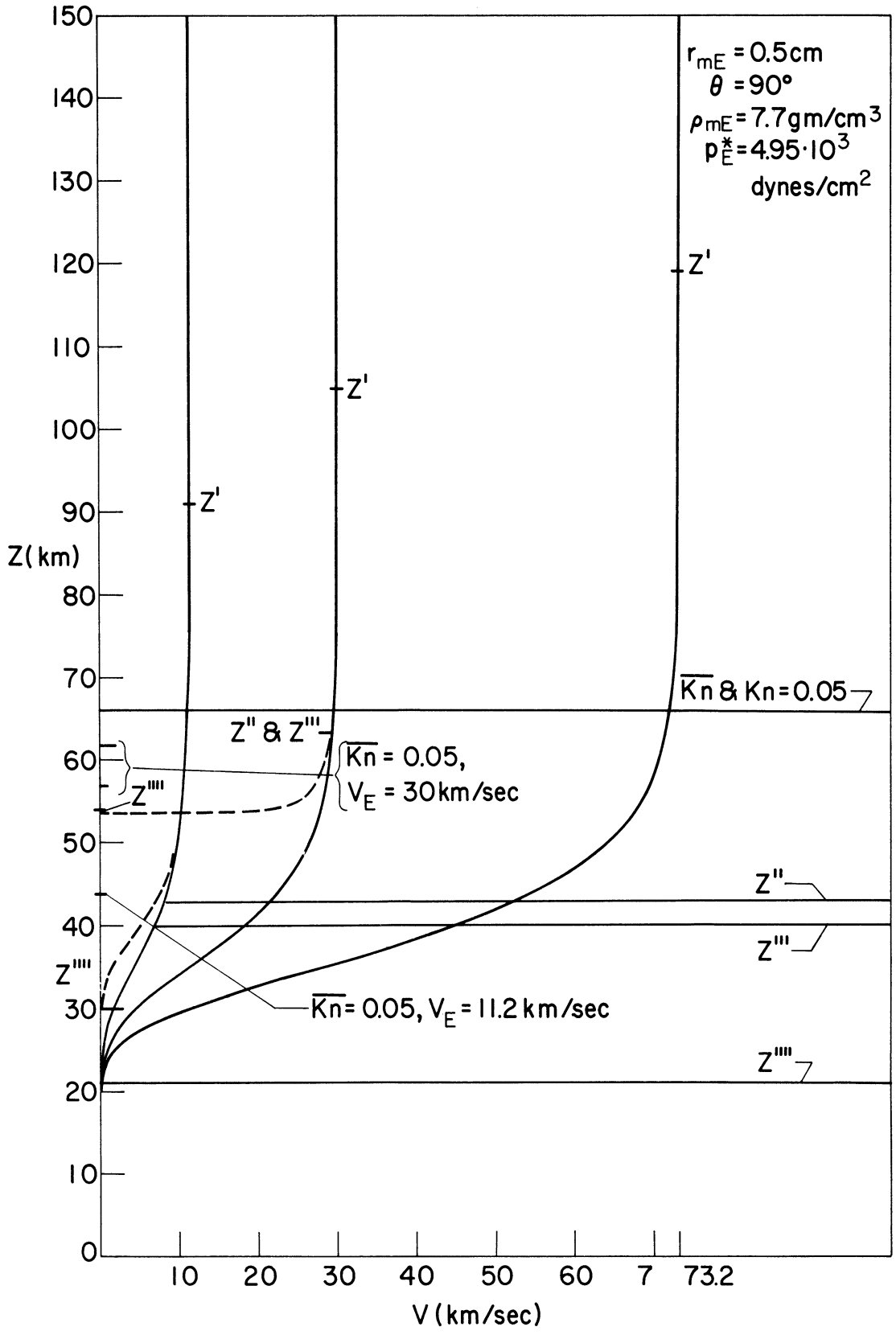

Figure 12. Meteor velocity as a function of altitude (σ = 0, solid curve; $\sigma = 5 \cdot 10^{-12}$ sec^2/cm^2, dashed curve), r_{mE} = 0.5 cm, θ = 90°, ρ_m = 7.7 g/cm^3.

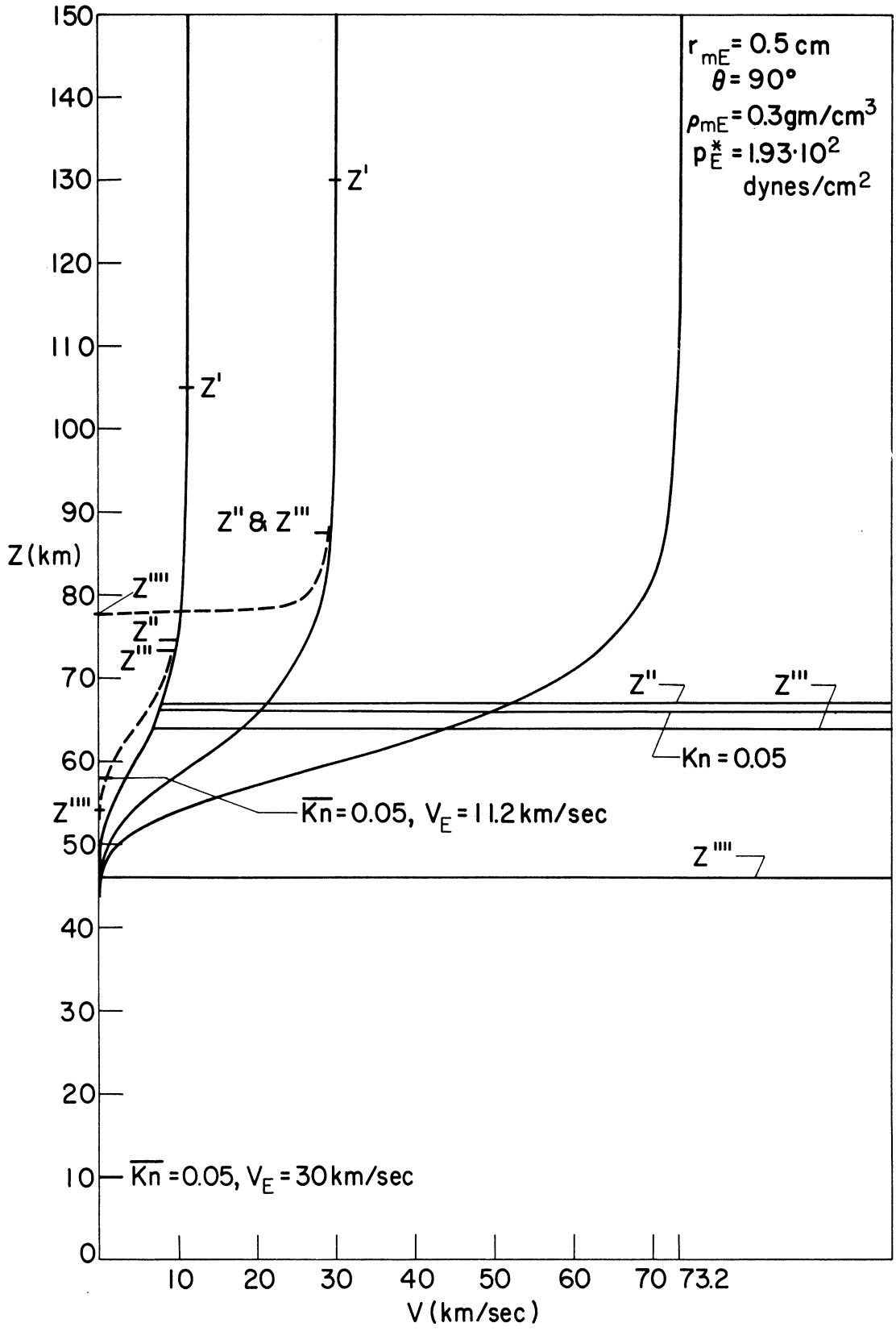

Figure 13. Meteor velocity as a function of altitude (σ = 0, solid curve; $\sigma = 5 \cdot 10^{-12}$ sec^2/cm^2, dashed curve), r_{mE} = 0.5 cm, θ = 90°, ρ_m = 0.3 g/cm^3.

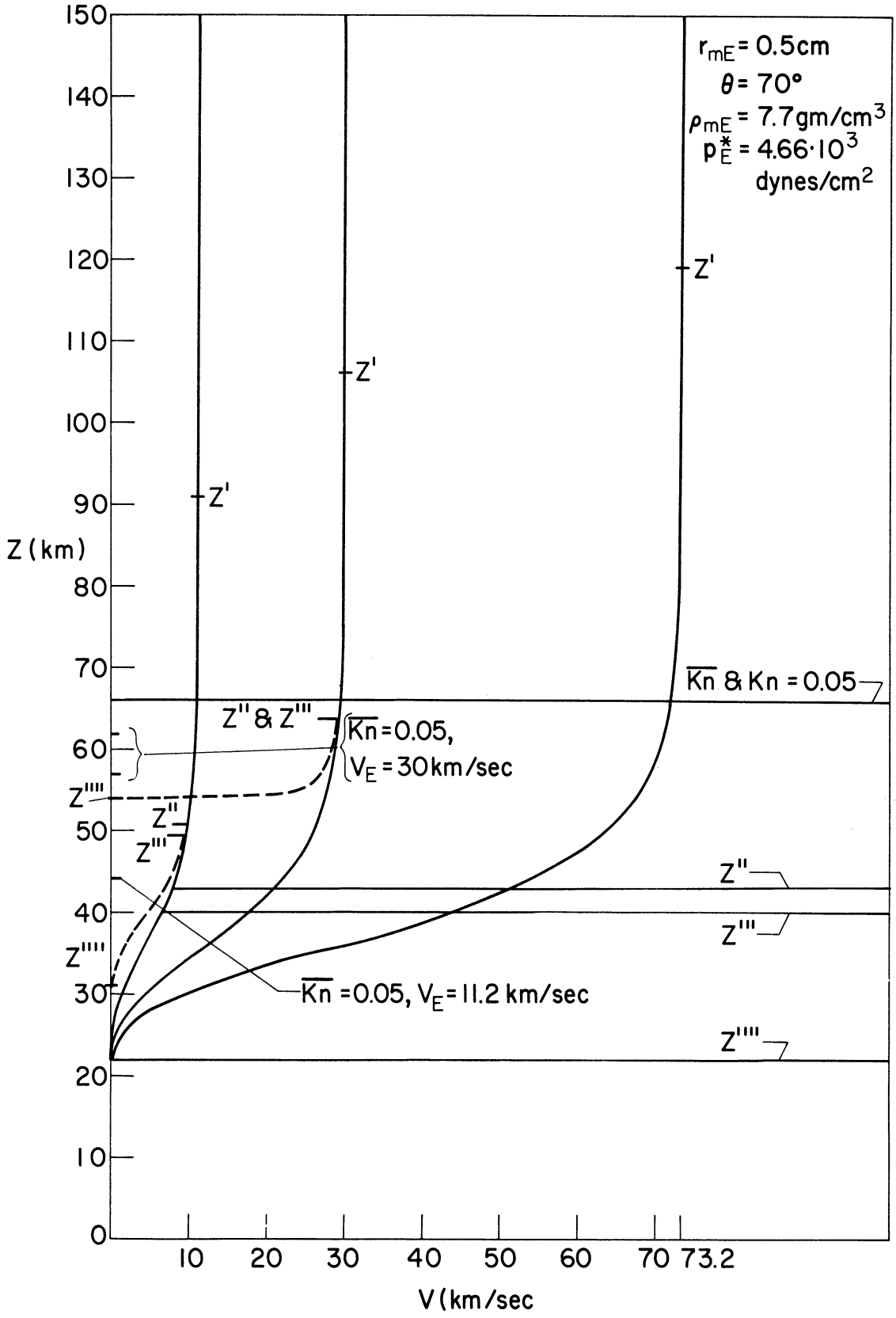

Figure 14. Meteor velocity as a function of altitude (σ = 0, solid curve; $\sigma = 5 \cdot 10^{-12}$ sec^2/cm^2, dashed curve), r_{mE} = 0.5 cm, θ = 70°, ρ_m = 7.7 g/cm^3.

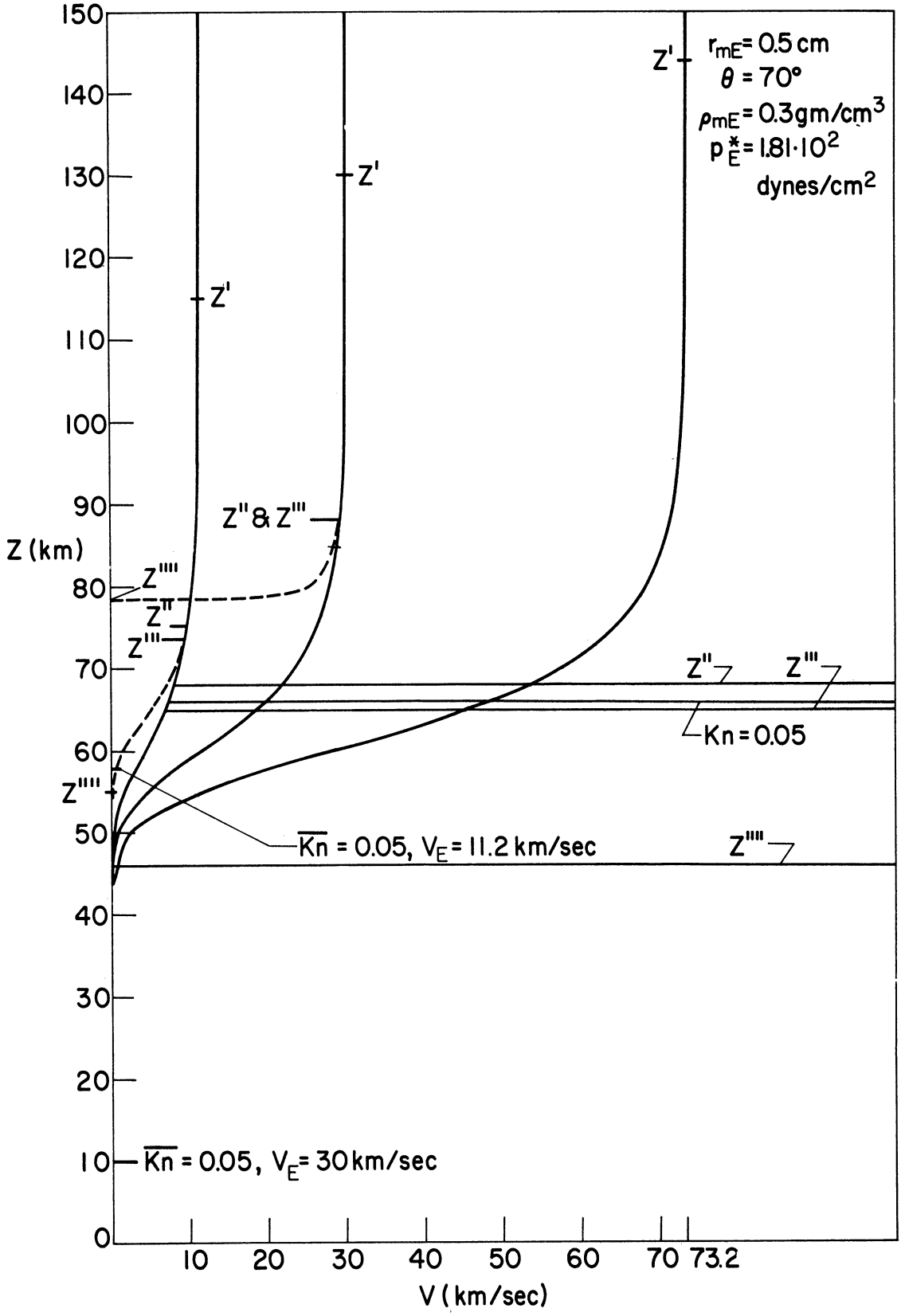

Figure 15. Meteor velocity as a function of altitude (σ = 0, solid curve; $\sigma = 5 \cdot 10^{-12}$ sec^2/cm^2, dashed curve), r_{mE} = 0.5 cm, Θ = 70°, ρ_m = 0.3 g/cm^3.

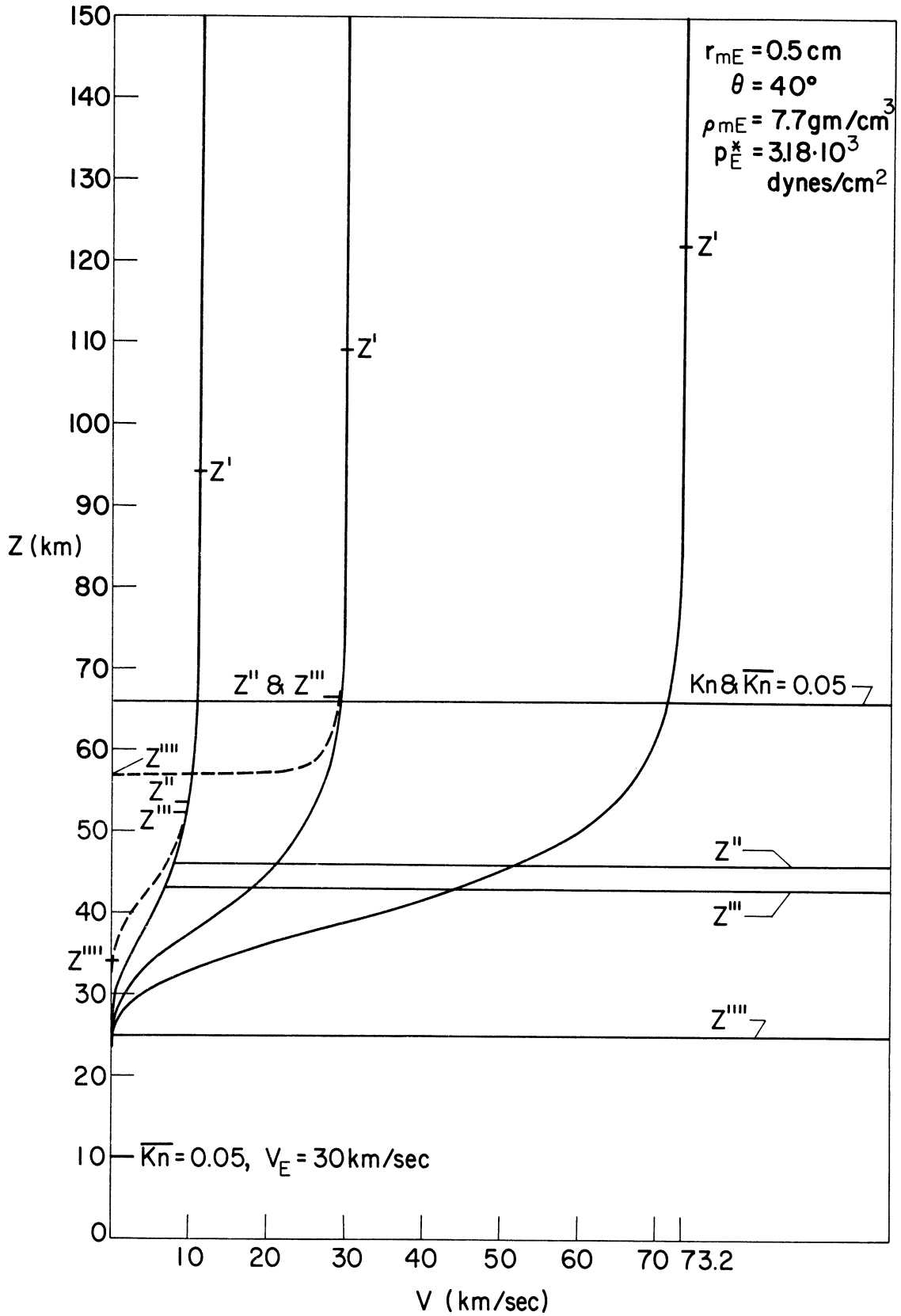

Figure 16. Meteor velocity as a function of altitude (σ = 0, solid curve; $\sigma = 5 \cdot 10^{-12}$ sec^2/cm^2, dashed curve), r_{mE} = 0.5 cm, θ = 40°, ρ_m = 7.7 g/cm^3.

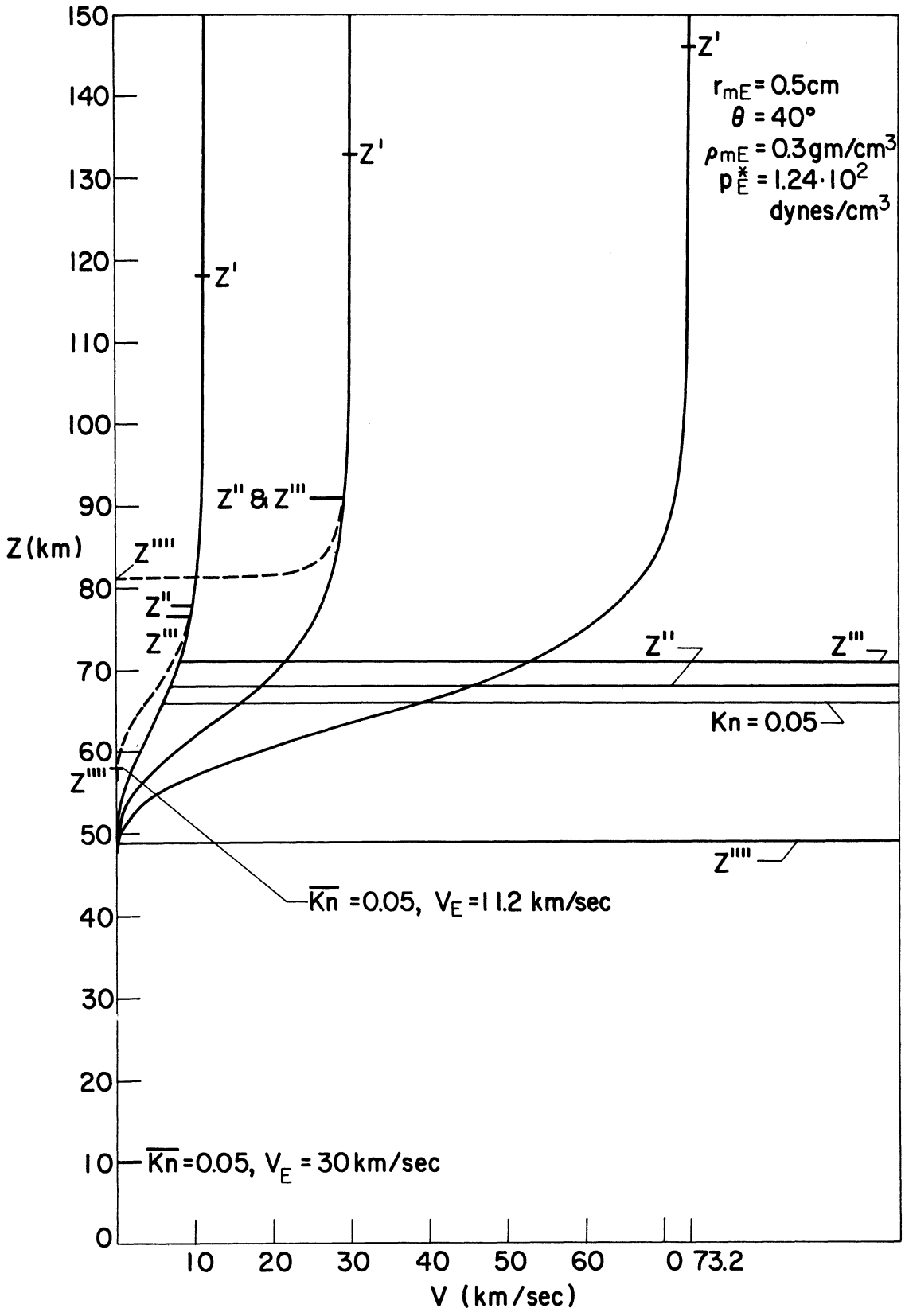

Figure 17. Meteor velocity as a function of altitude (σ = 0, solid curve; $\sigma = 5 \cdot 10^{-12}$ sec^2/cm^2, dashed curve), r_{mE} = 0.5 cm, θ = 40°, ρ_m = 0.3 g/cm^3.

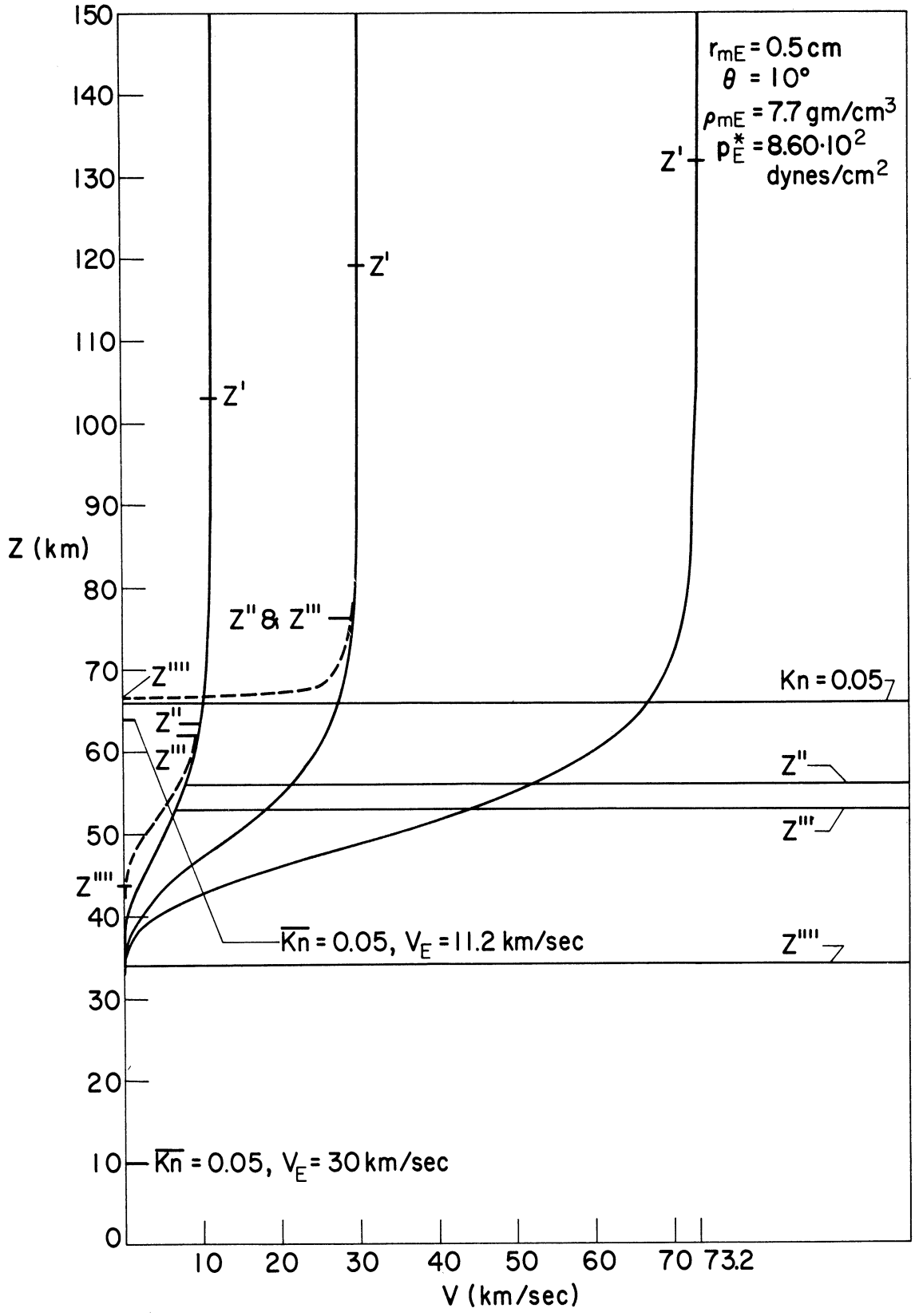

Figure 18. Meteor velocity as a function of altitude (σ = 0, solid curve; $\sigma = 5 \cdot 10^{-12}$ sec²/cm², dashed curve), r_{mE} = 0.5 cm, θ = 10°, ρ_m = 7.7 g/cm³.

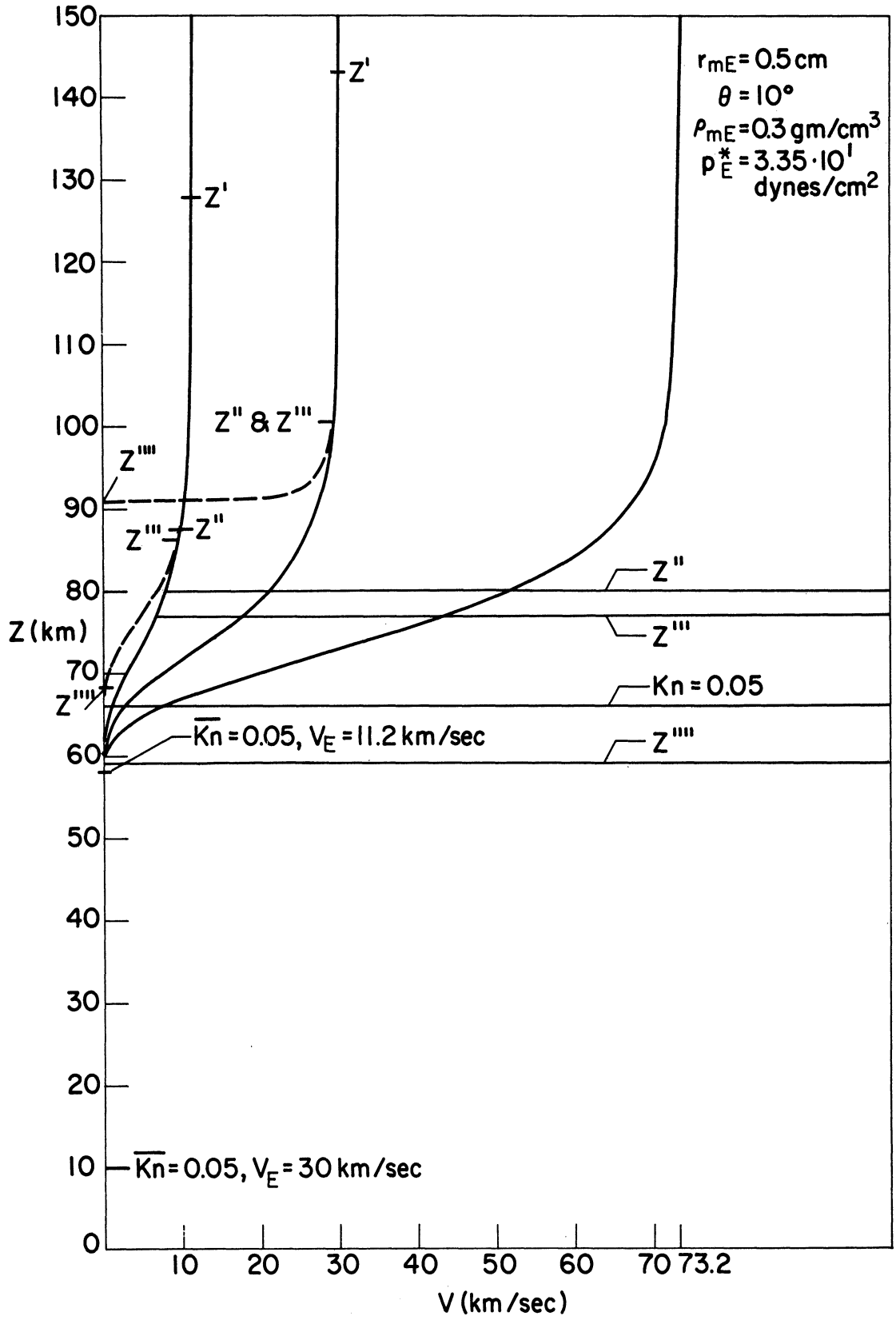

Figure 19. Meteor velocity as a function of altitude (σ = 0, solid curve; $\sigma = 5 \cdot 10^{-12}$ sec^2/cm^2, dashed curve), r_{mE} = 0.5 cm, θ = 10°, ρ_m = 0.3 g/cm^3.

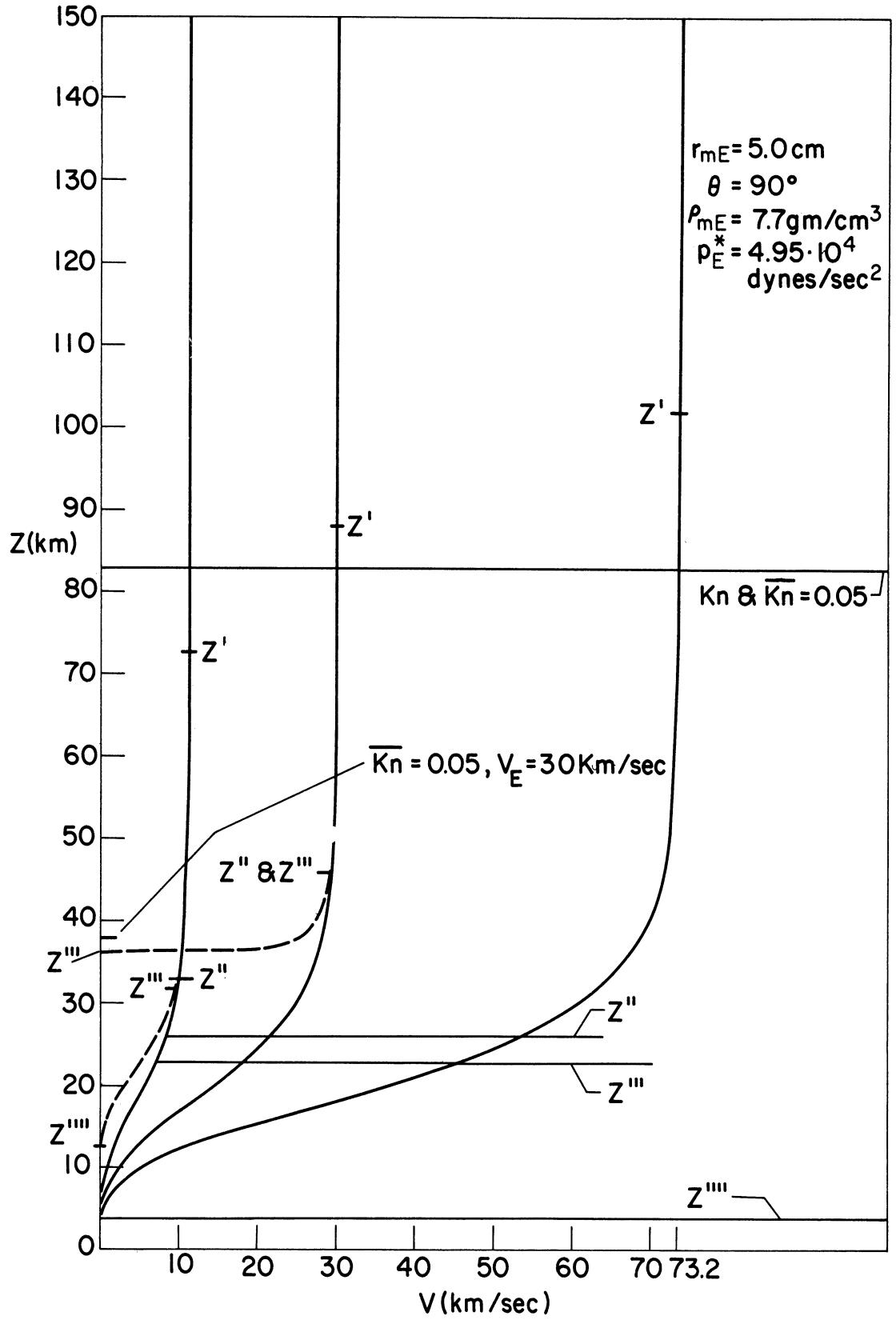

Figure 20. Meteor velocity as a function of altitude (σ = 0, solid curve; $\sigma = 5 \cdot 10^{-12}$ sec^2/cm^2, dashed curve), r_{mE} = 5.0 cm, θ = 90°, ρ_m = 7.7 g/cm^3.

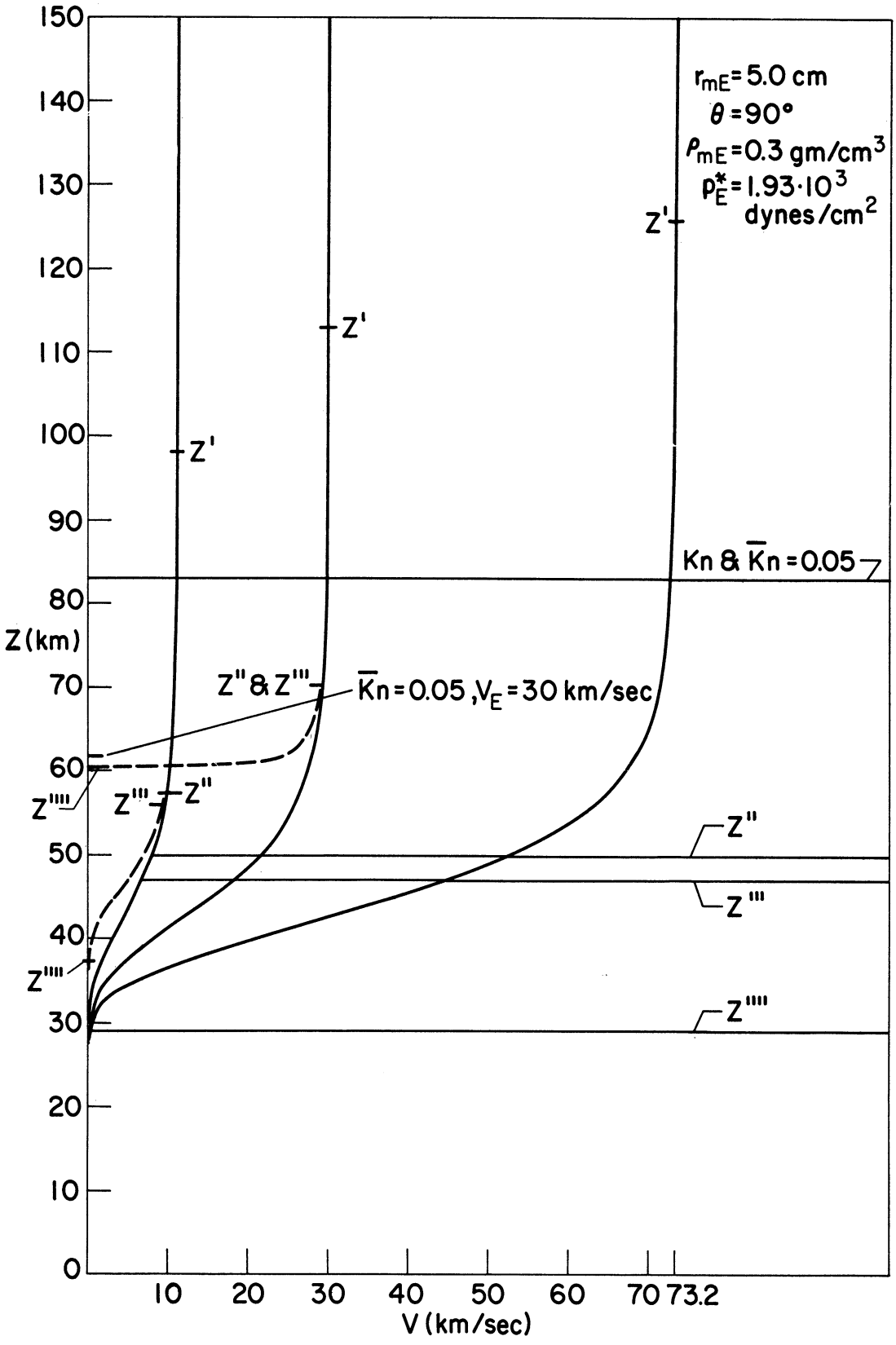

Figure 21. Meteor velocity as a function of altitude (σ = 0, solid curve; $\sigma = 5 \cdot 10^{-12}$ sec^2/cm^2, dashed curve), r_{mE} = 5.0 cm, θ = 90°, ρ_m = 0.3 g/cm^3.

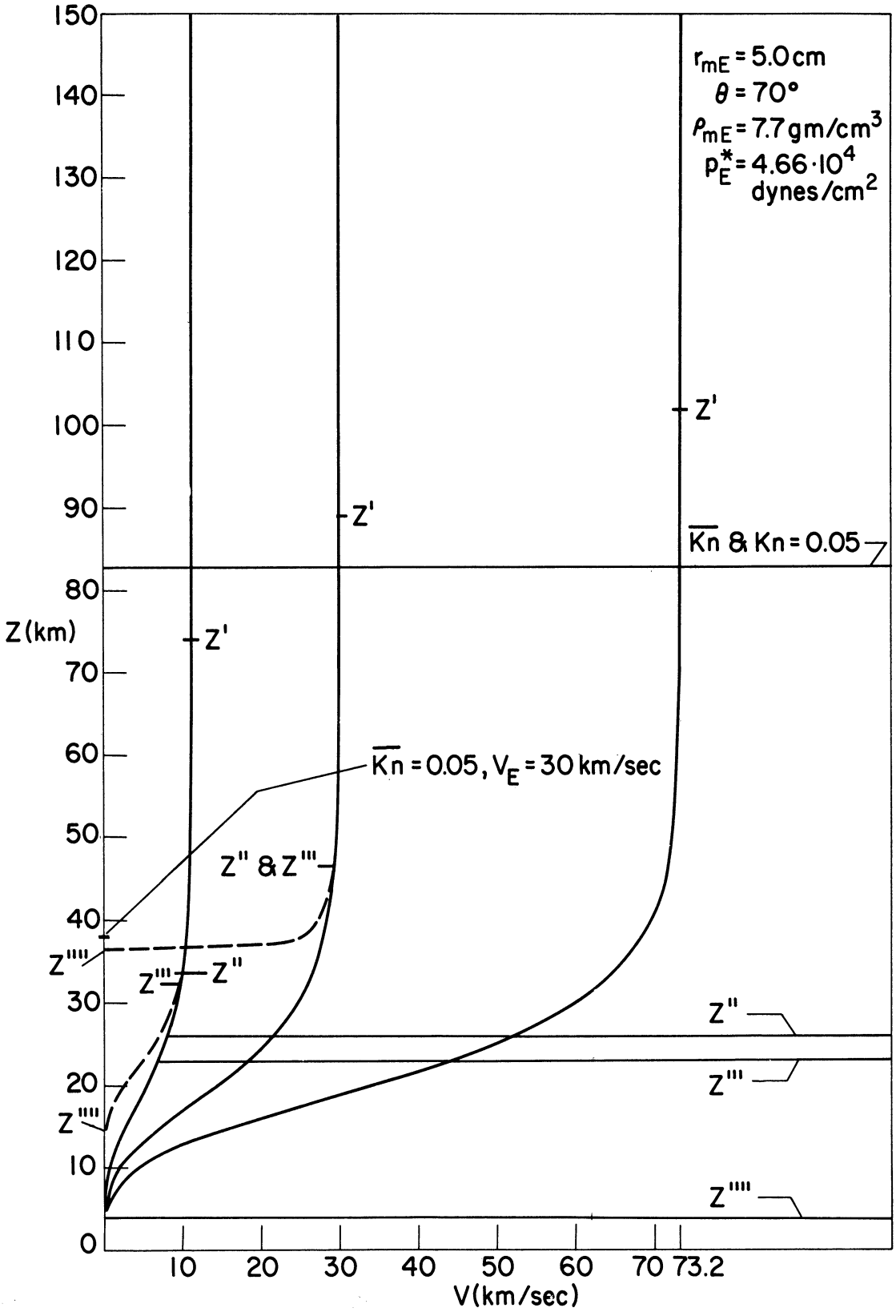

Figure 22. Meteor velocity as a function of altitude (σ = 0, solid curve; $\sigma = 5 \cdot 10^{-12}$ sec^2/cm^2, dashed curve), r_{mE} = 5.0 cm, θ = 70°, ρ_m = 7.7 g/cm^3.

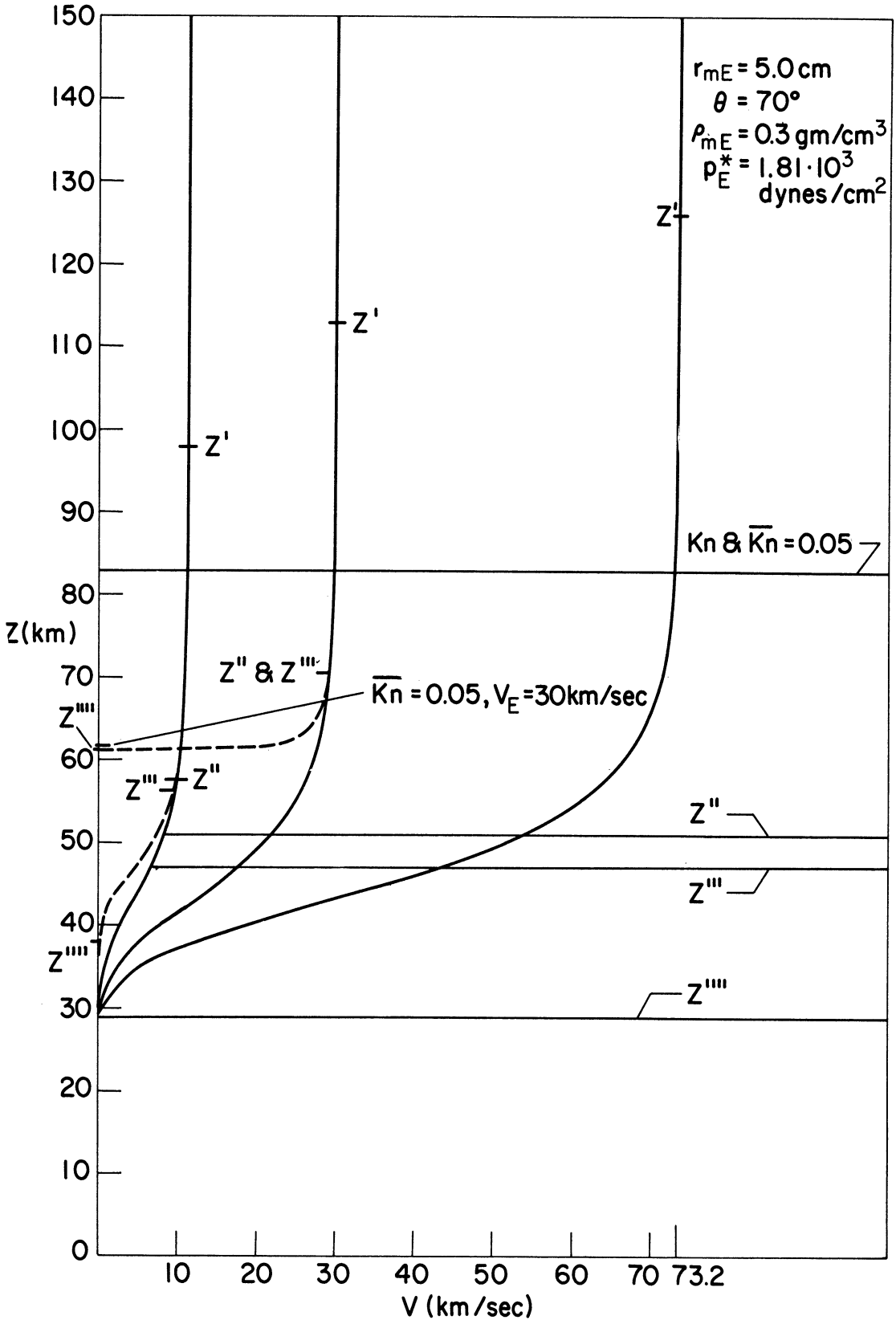

Figure 23. Meteor velocity as a function of altitude (σ = 0, solid curve; $\sigma = 5 \cdot 10^{-12}$ sec^2/cm^2, dashed curve), r_{mE} = 5.0 cm, $\theta = 70^\circ$, ρ_m = 0.3 g/cm^3.

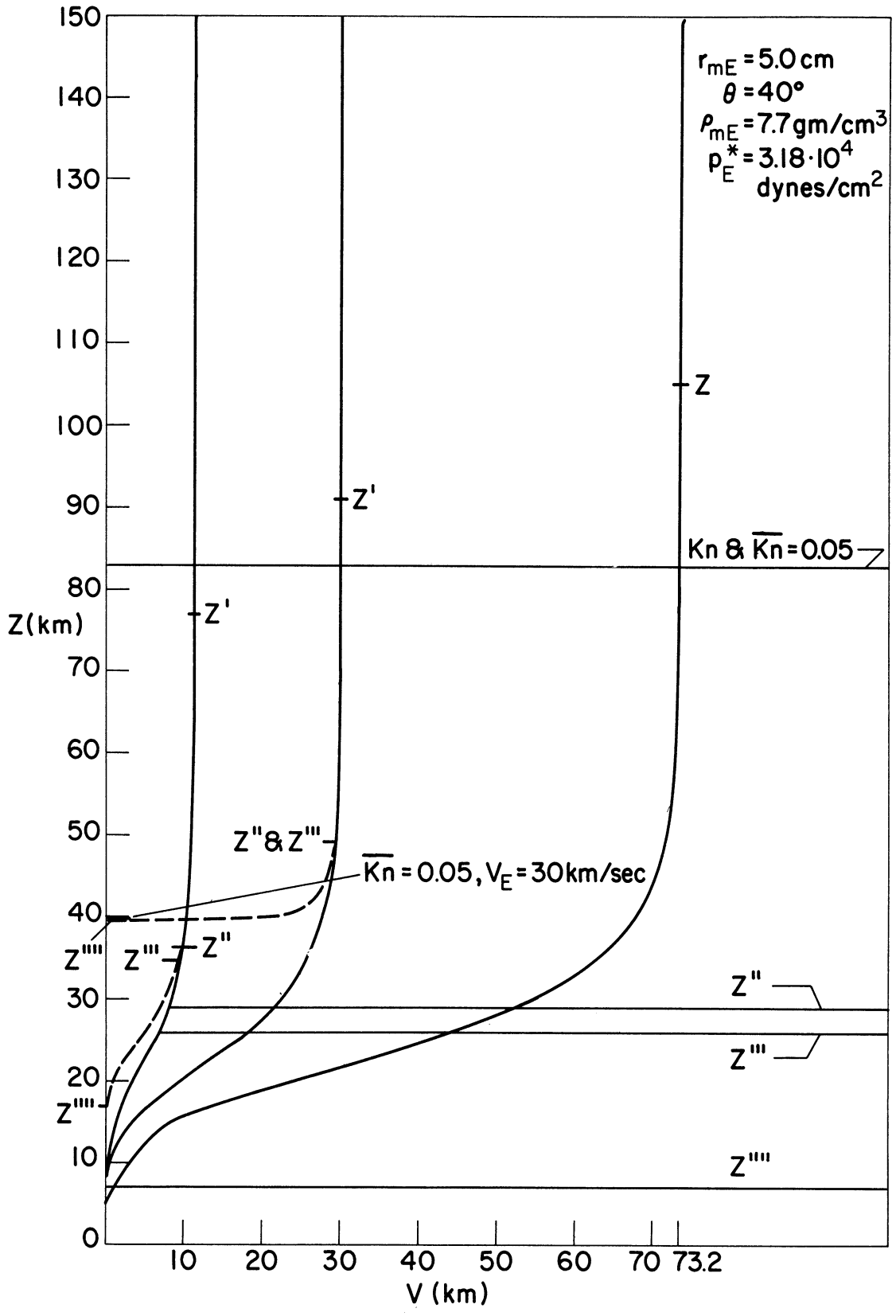

Figure 24. Meteor velocity as a function of altitude (σ = 0, solid curve; $\sigma = 5 \cdot 10^{-12}$ sec^2/cm^2, dashed curve), r_{mE} = 5.0 cm, θ = 40°, ρ_m = 7.7 g/cm^3.

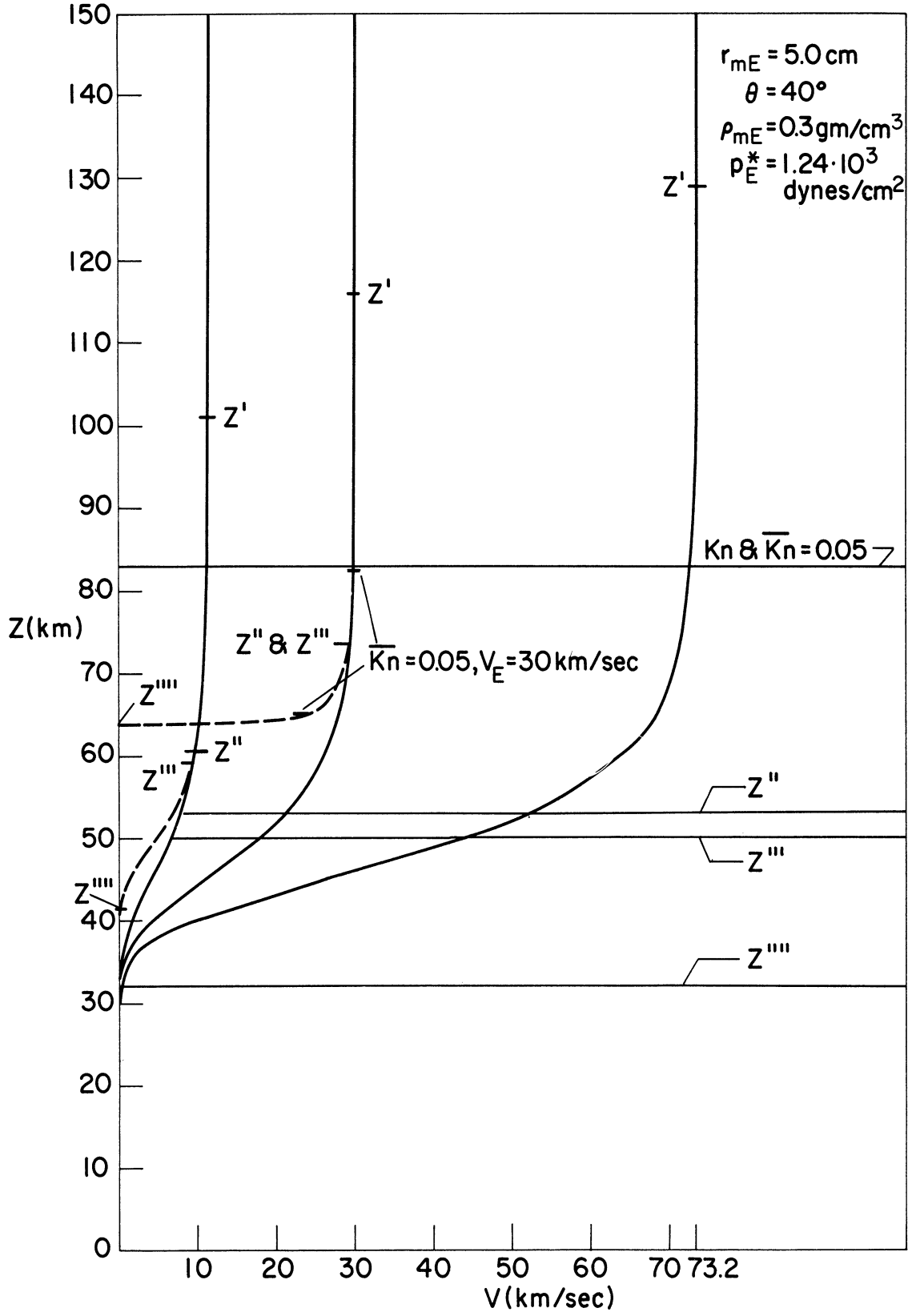

Figure 25. Meteor velocity as a function of altitude (σ = 0, solid curve; $\sigma = 5 \cdot 10^{-12}$ sec^2/cm^2, dashed curve), r_{mE} = 5.0 cm, θ = 40°, ρ_m = 0.3 g/cm^3.

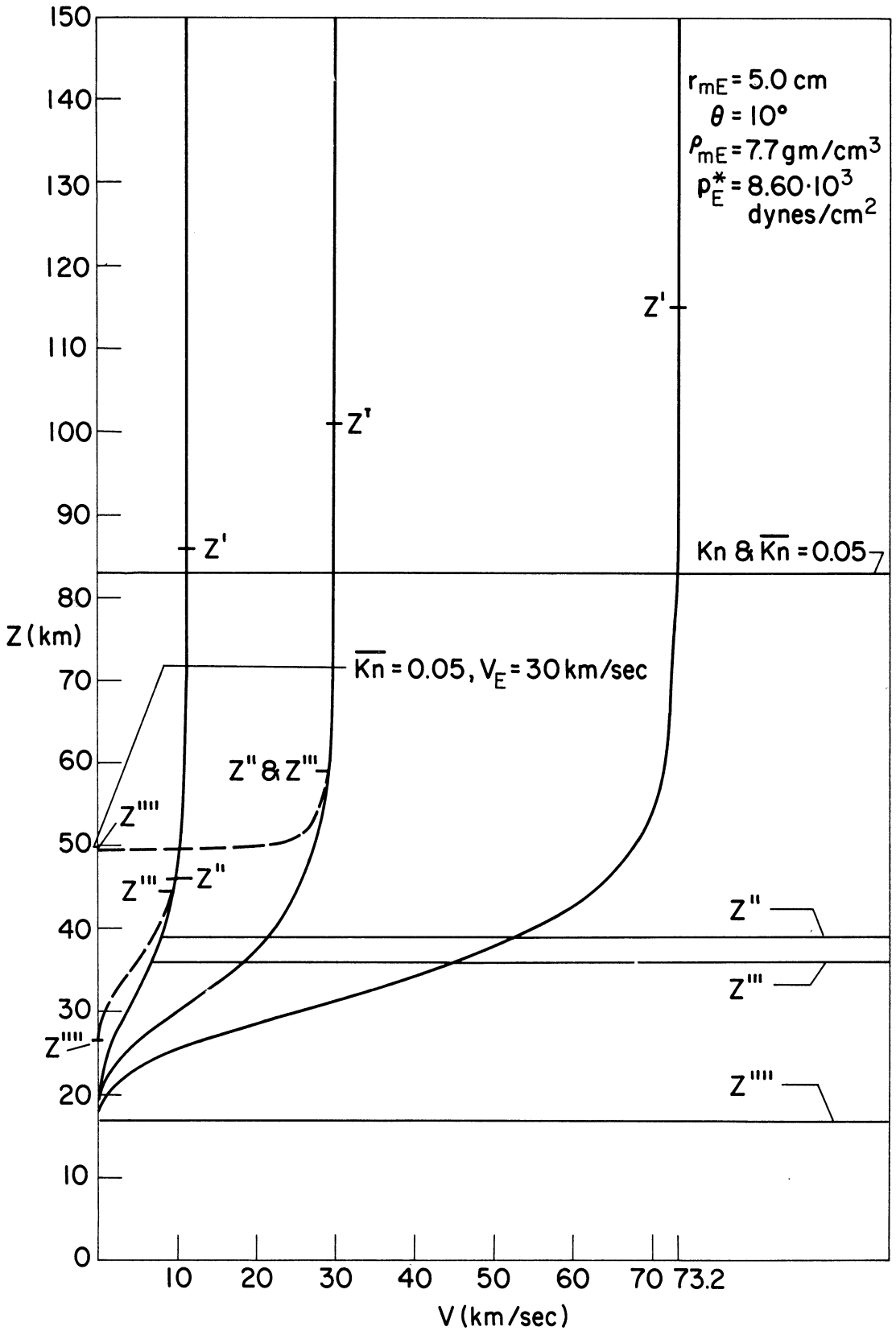

Figure 26. Meteor velocity as a function of altitude (σ = 0, solid curve; $\sigma = 5 \cdot 10^{-12}$ sec^2/cm^2, dashed curve), r_{mE} = 5.0 cm, θ = 10°, ρ_m = 7.7 g/cm^3.

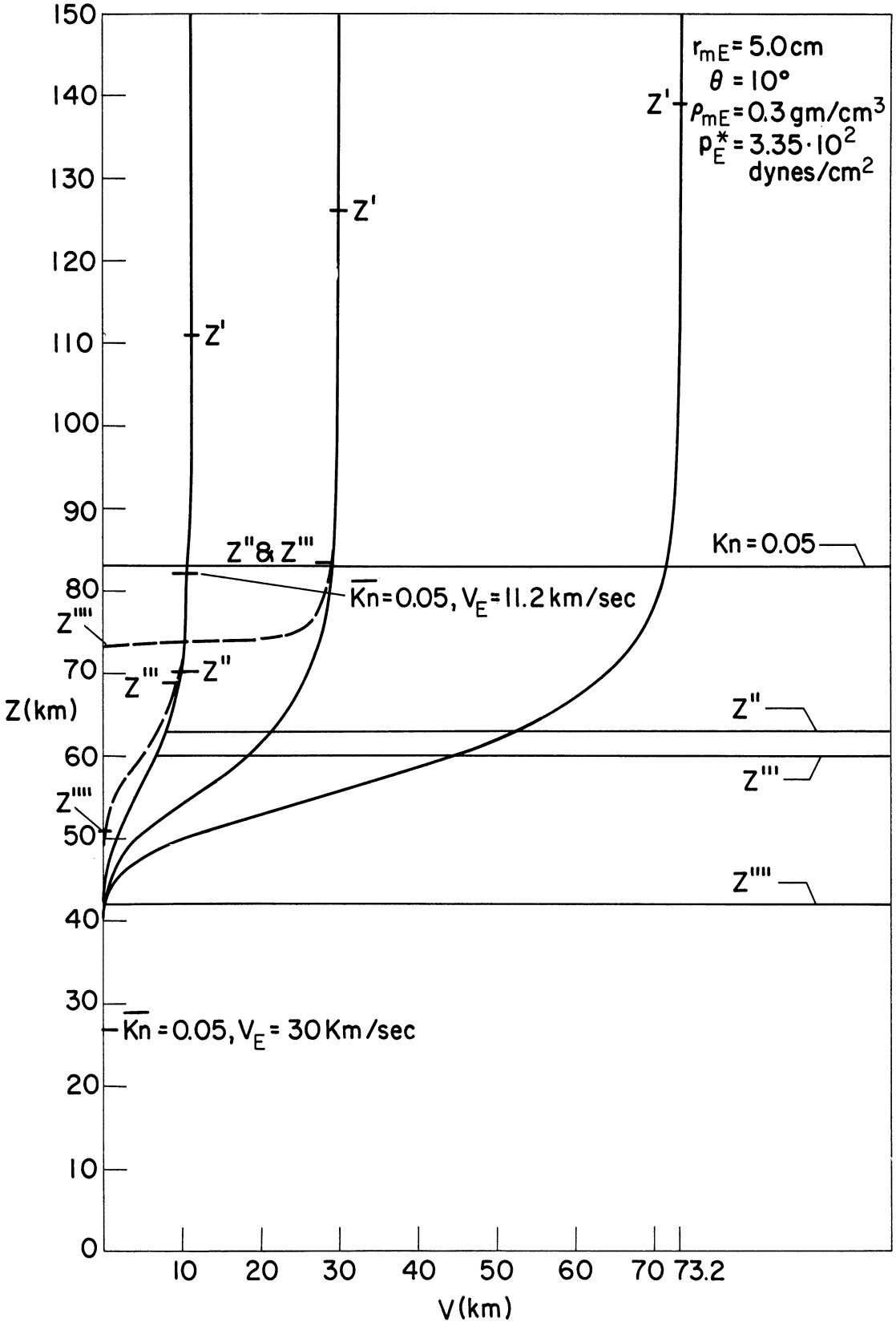

Figure 27. Meteor velocity as a function of altitude (σ = 0, solid curve; $\sigma = 5 \cdot 10^{-12}$ sec^2/cm^2, dashed curve), r_{mE} = 5.0 cm, θ = 10°, ρ_m = 0.3 g/cm^3.

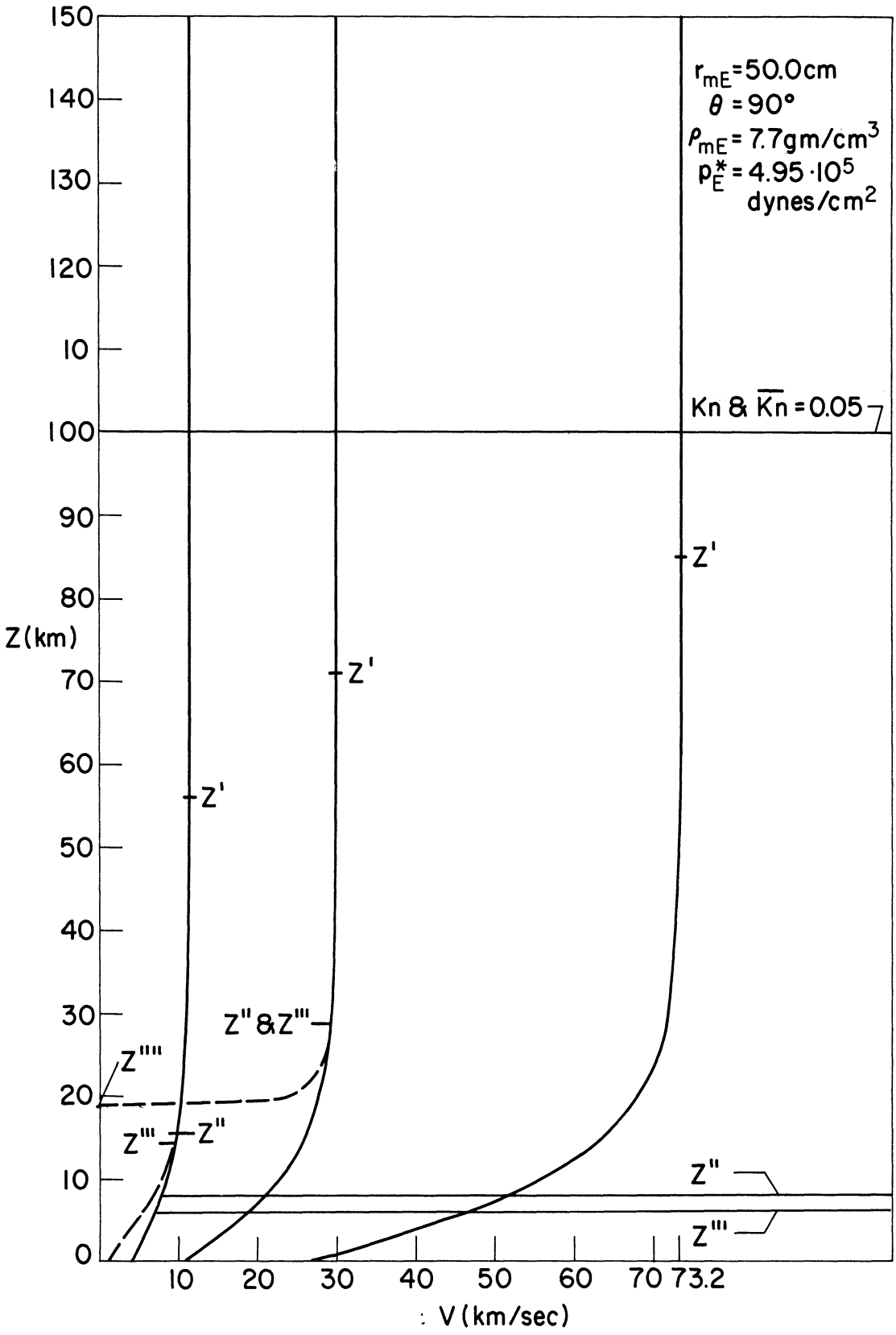

Figure 28. Meteor velocity as a function of altitude (σ = 0, solid curve; $\sigma = 5 \cdot 10^{-12}$ sec^2/cm^2, dashed curve), r_{mE} = 50.0 cm, θ = 90°, ρ_m = 7.7 g/cm^3.

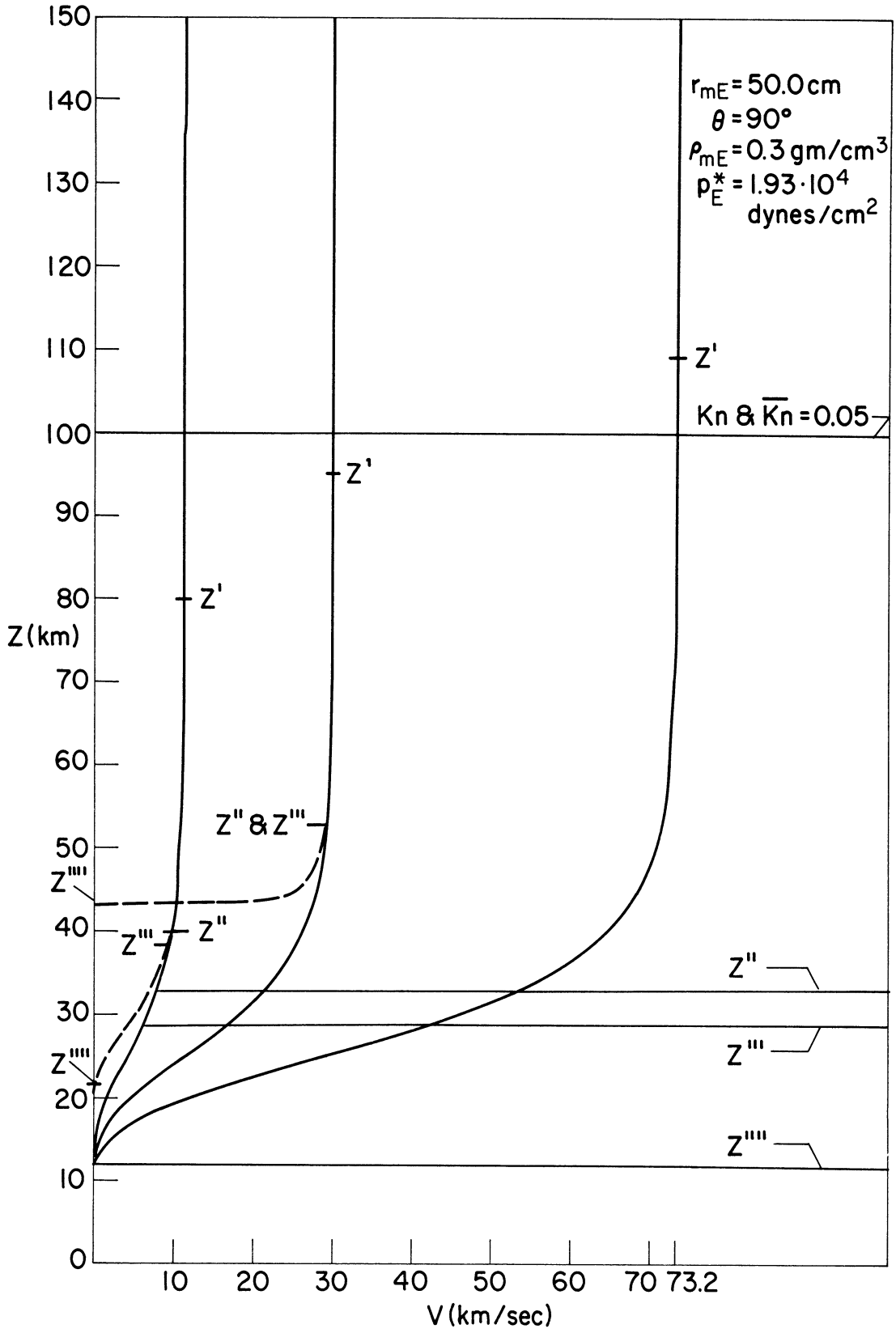

Figure 29. Meteor velocity as a function of altitude (σ = 0, solid curve; $\sigma = 5 \cdot 10^{-12}$ sec^2/cm^2, dashed curve), r_{mE} = 50.0 cm, θ = 90°, ρ_m = 0.3 g/cm^3.

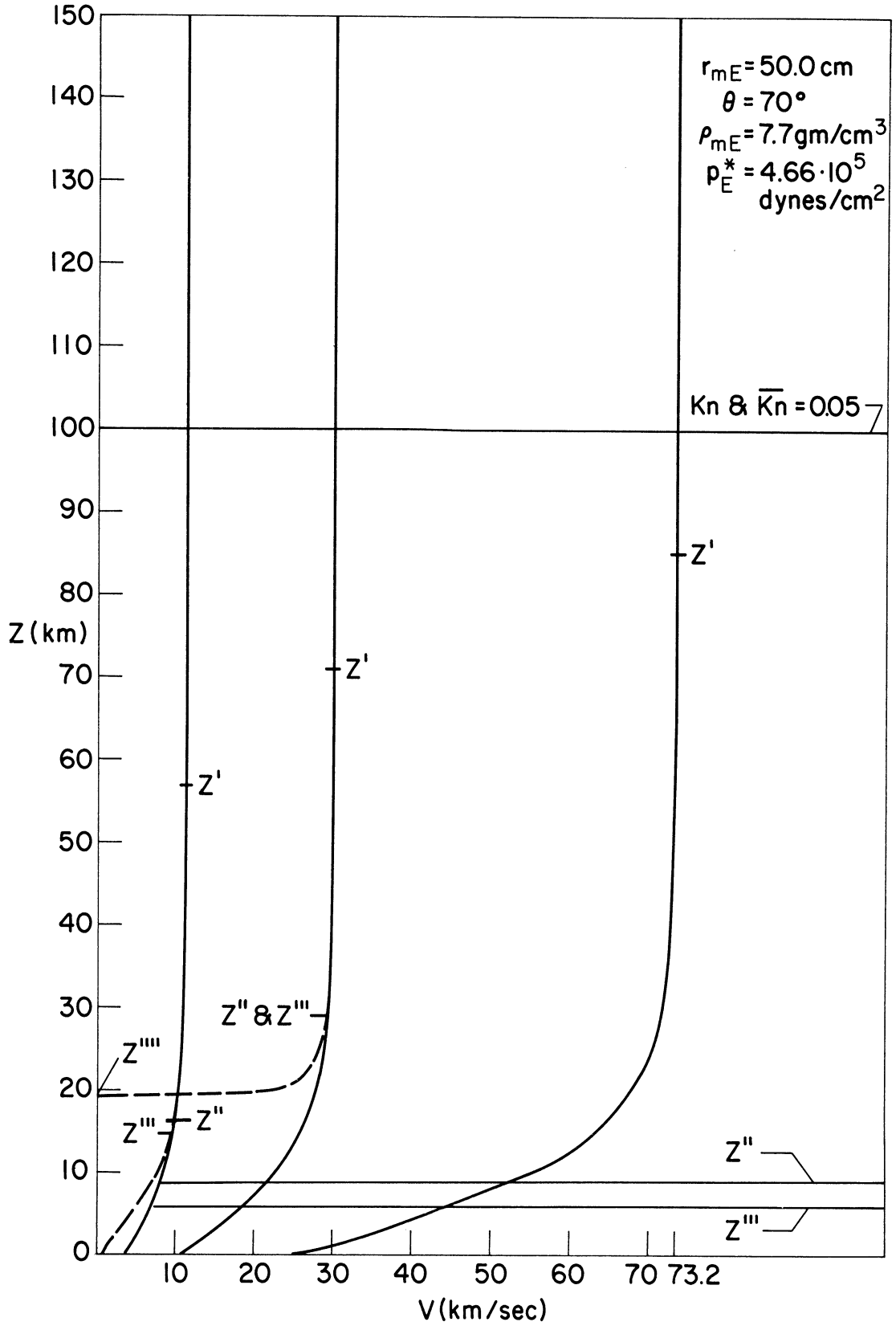

Figure 30. Meteor velocity as a function of altitude (σ = 0, solid curve; $\sigma = 5 \cdot 10^{-12}$ sec^2/cm^2, dashed curve), r_{mE} = 50.0 cm, θ = 70°, ρ_m = 7.7 g/cm^3.

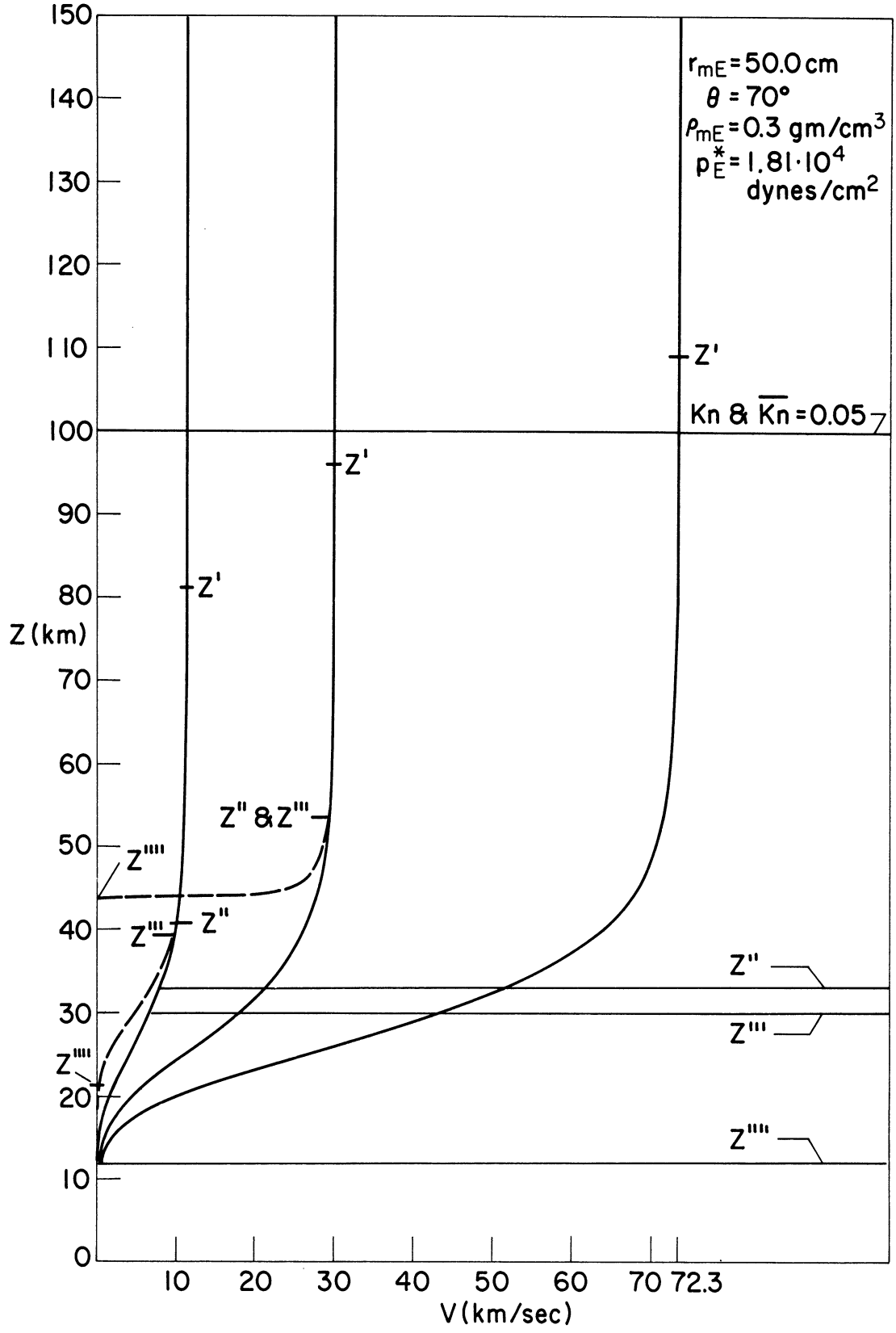

Figure 31. Meteor velocity as a function of altitude (σ = 0, solid curve; $\sigma = 5 \cdot 10^{-12}$ sec^2/cm^2, dashed curve), r_{mE} = 50.0 cm, θ = 70°, ρ_m = 0.3 g/cm^3.

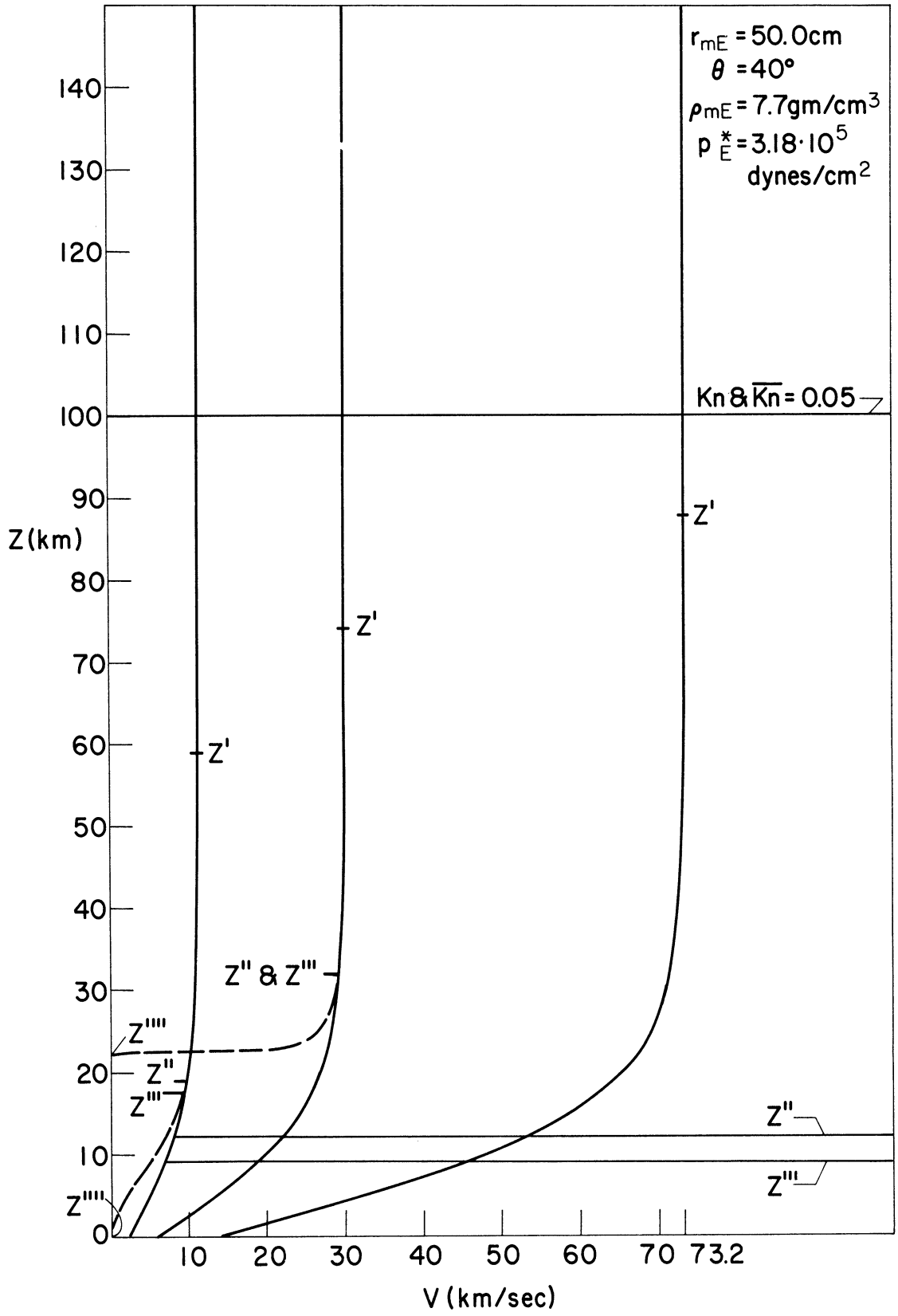

Figure 32. Meteor velocity as a function of altitude (σ = 0, solid curve; $\sigma = 5 \cdot 10^{-12}$ sec^2/cm^2, dashed curve), r_{mE} = 50.0 cm, θ = 40°, ρ_m = 7.7 g/cm^3.

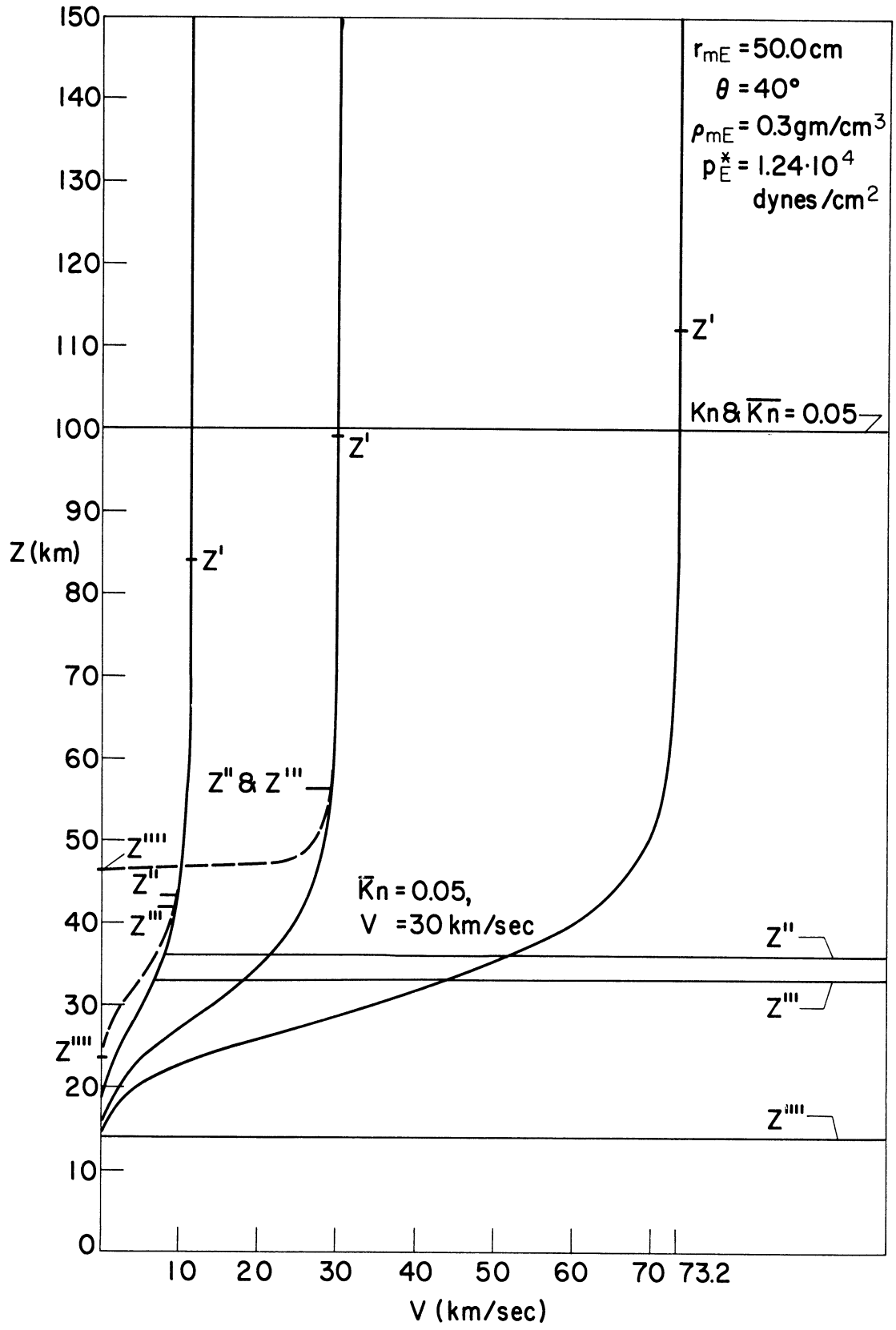

Figure 33. Meteor velocity as a function of altitude (σ = 0, solid curve; $\sigma = 5 \cdot 10^{-12}$ sec^2/cm^2, dashed curve), r_{mE} = 50.0 cm, θ = 40°, ρ_m = 0.3 g/cm^3.

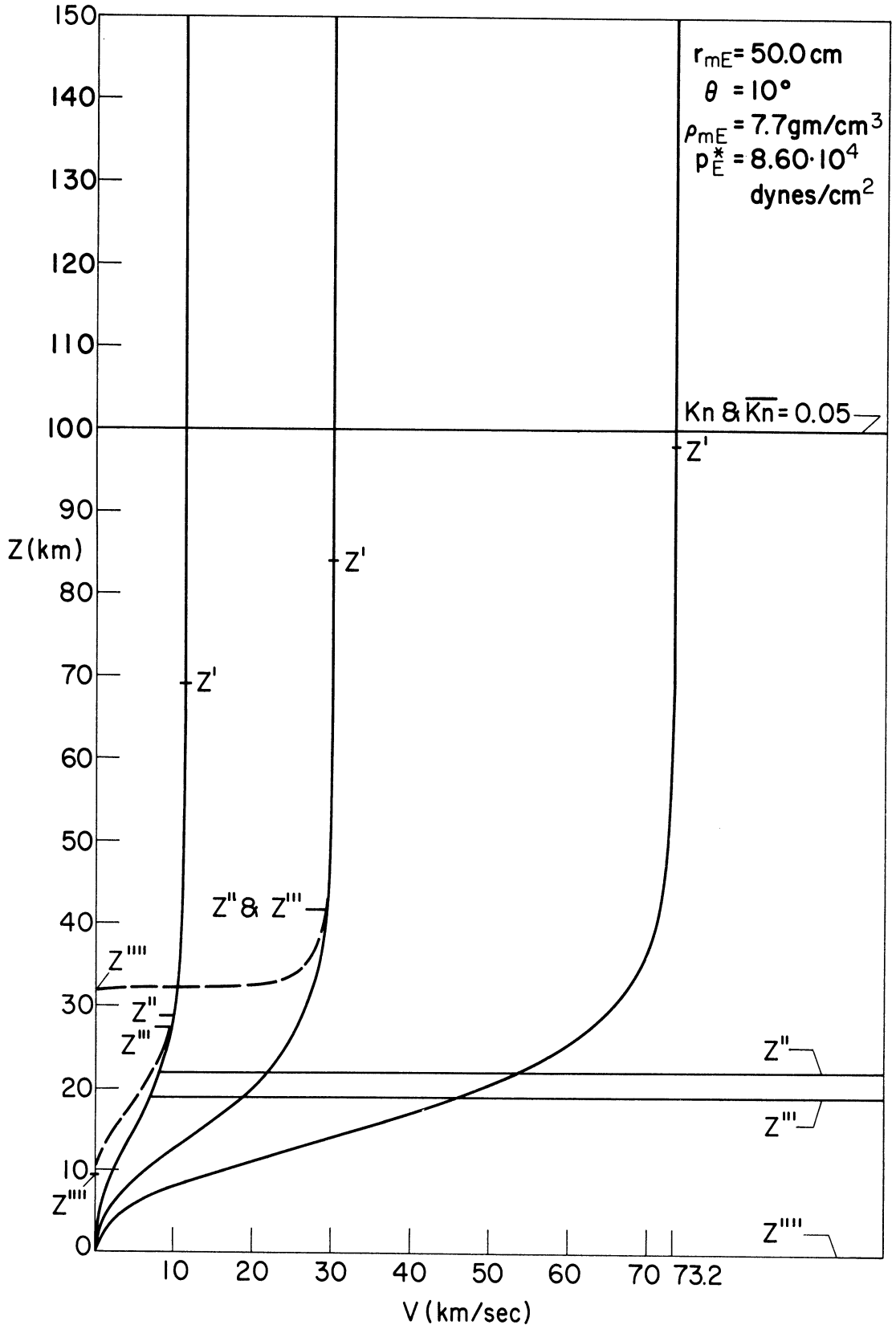

Figure 34. Meteor velocity as a function of altitude (σ = 0, solid curve; $\sigma = 5 \cdot 10^{-12}$ sec^2/cm^2, dashed curve), r_{mE} = 50.0 cm, θ = 10°, ρ_m = 7.7 g/cm^3.

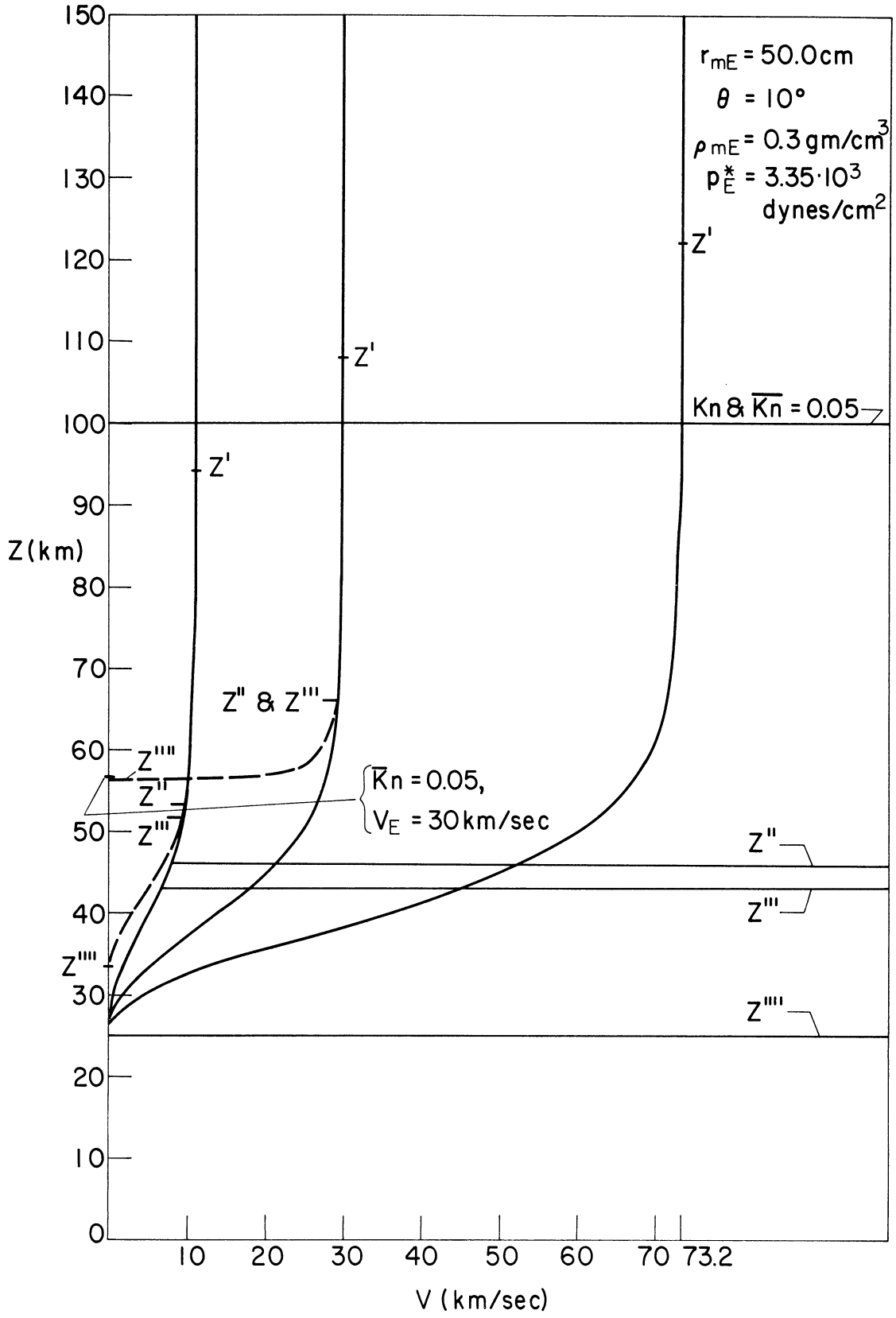

Figure 35. Meteor velocity as a function of altitude ($\sigma = 0$, solid curve; $\sigma = 5 \cdot 10^{-12}$ sec^2/cm^2, dashed curve), r_{mE} = 50.0 cm, $\theta = 10°$, ρ_m = 0.3 g/cm^3.

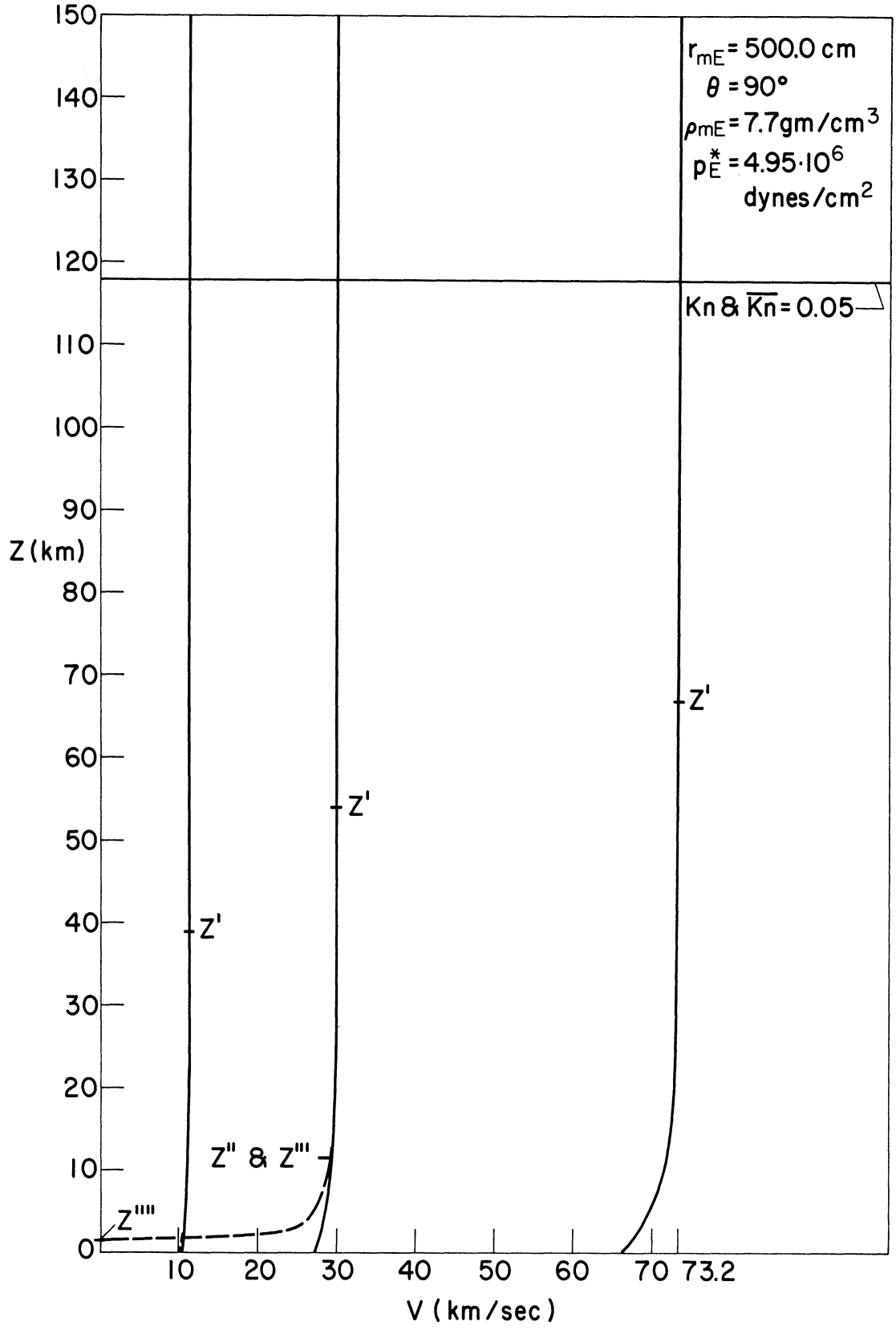

Figure 36. Meteor velocity as a function of altitude (σ = 0, solid curve; $\sigma = 5 \cdot 10^{-12}$ sec^2/cm^2, dashed curve), r_{mE} = 500.0 cm, θ = 90°, ρ_m = 7.7 g/cm^3.

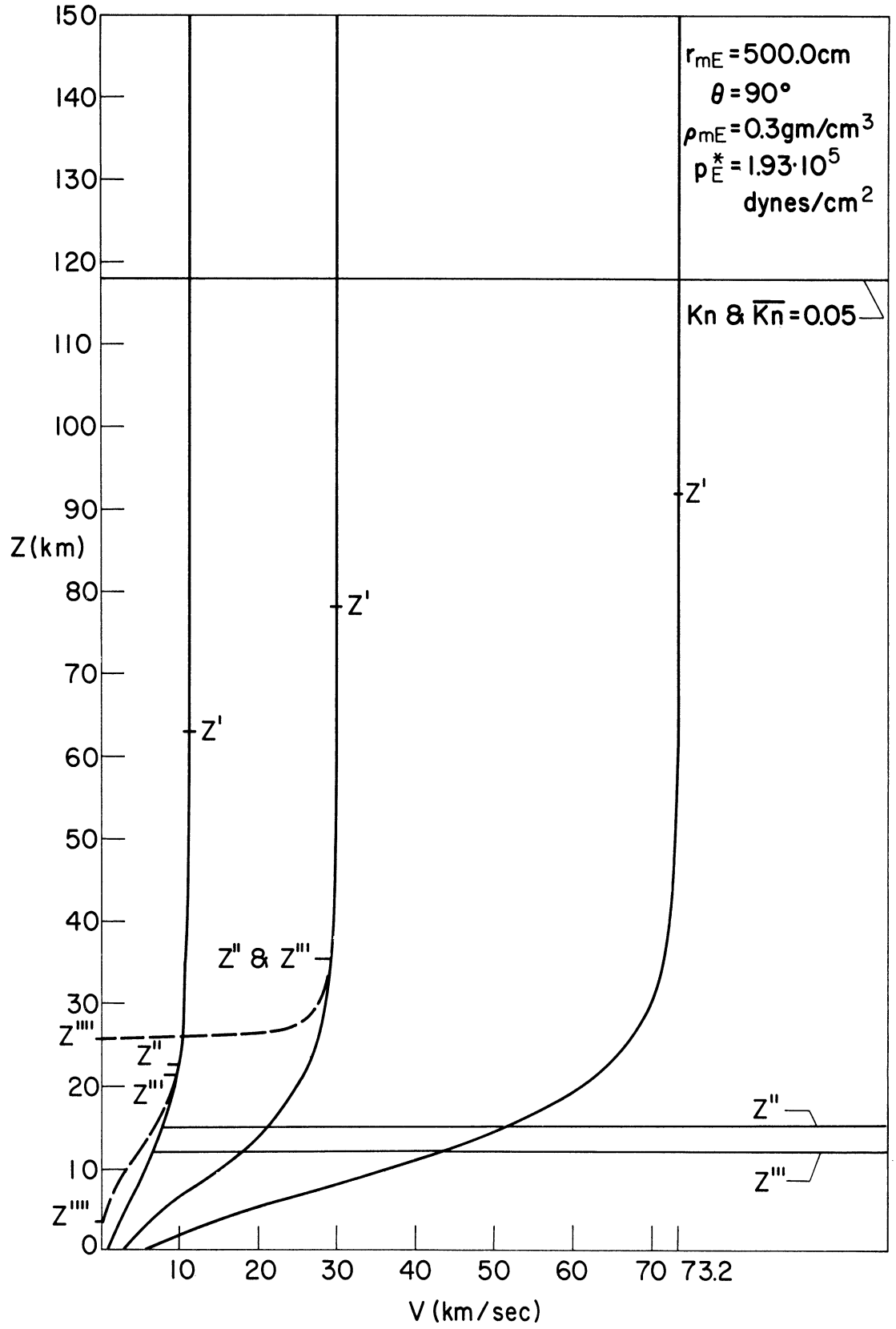

Figure 37. Meteor velocity as a function of altitude (σ = 0, solid curve; $\sigma = 5 \cdot 10^{-12}$ sec^2/cm^2, dashed curve), r_{mE} = 500.0 cm, θ = 90°, ρ_m = 0.3 g/cm^3.

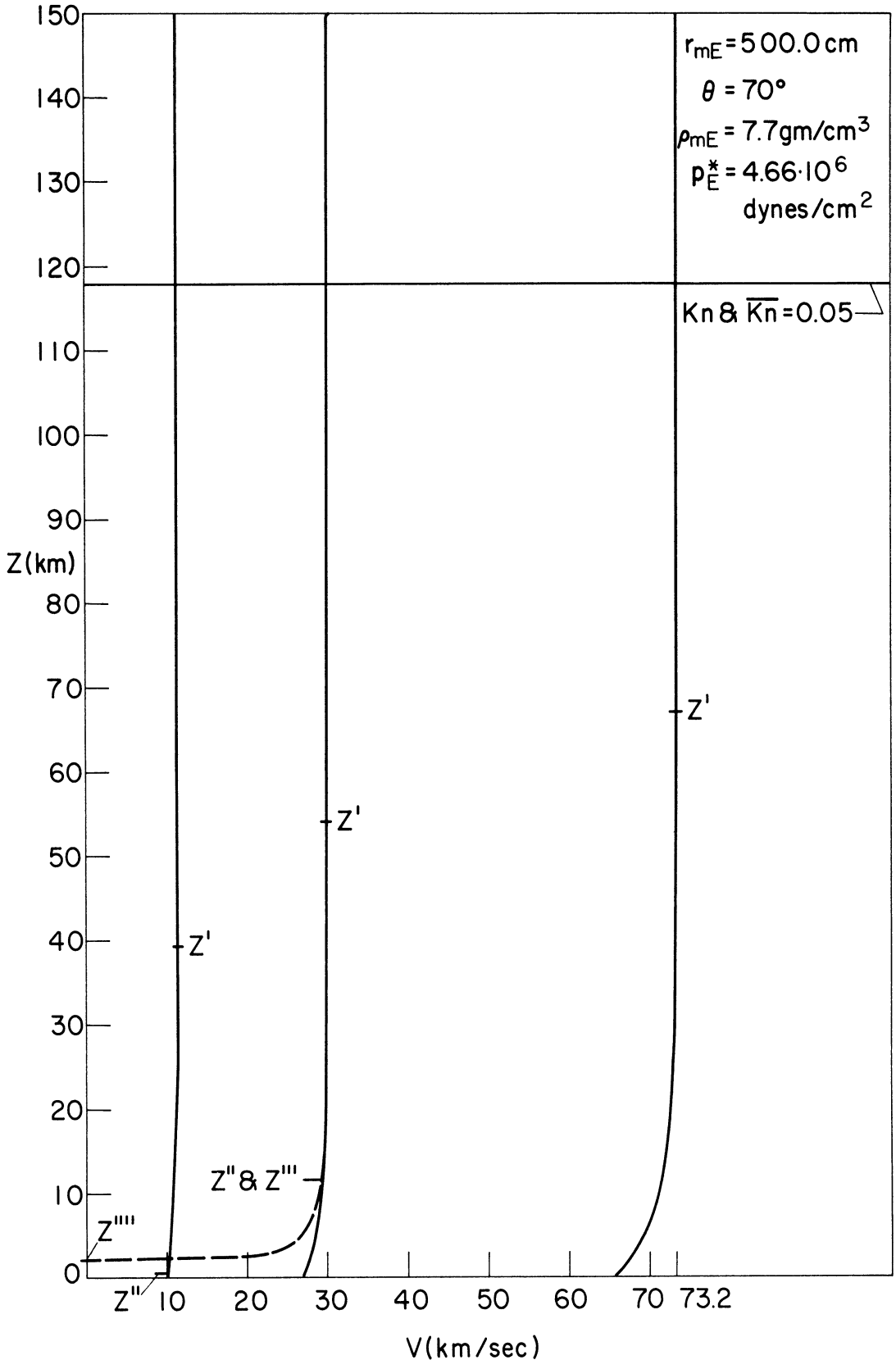

Figure 38. Meteor velocity as a function of altitude (σ = 0, solid curve; $\sigma = 5 \cdot 10^{-12}$ sec^2/cm^2, dashed curve), r_{mE} = 500.0 cm, θ = 70°, ρ_m = 7.7 g/cm^3.

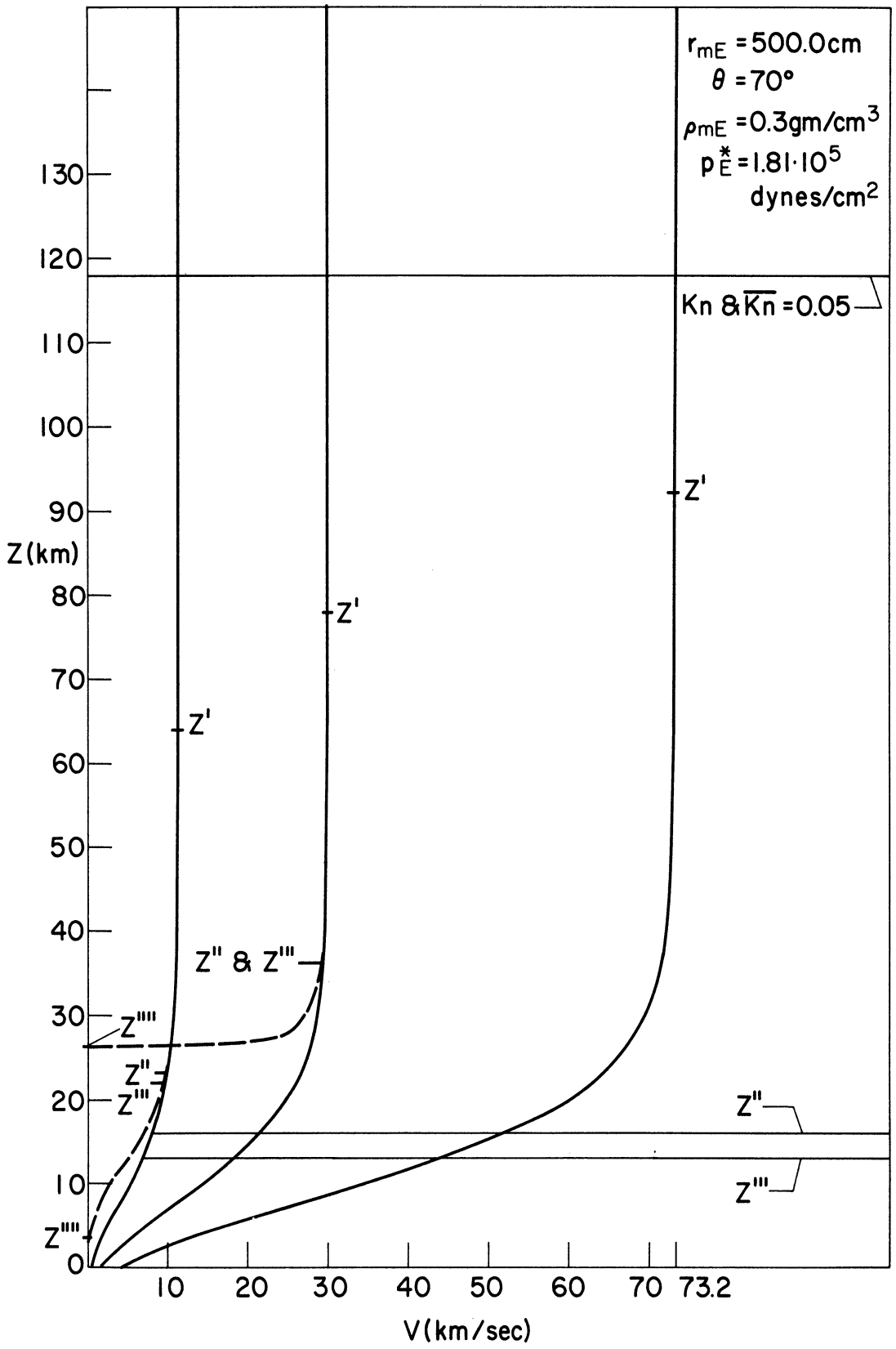

Figure 39. Meteor velocity as a function of altitude (σ = 0, solid curve; $\sigma = 5 \cdot 10^{-12}$ sec^2/cm^2, dashed curve), r_{mE} = 500.0 cm, θ = 70°, ρ_m = 0.3 g/cm^3.

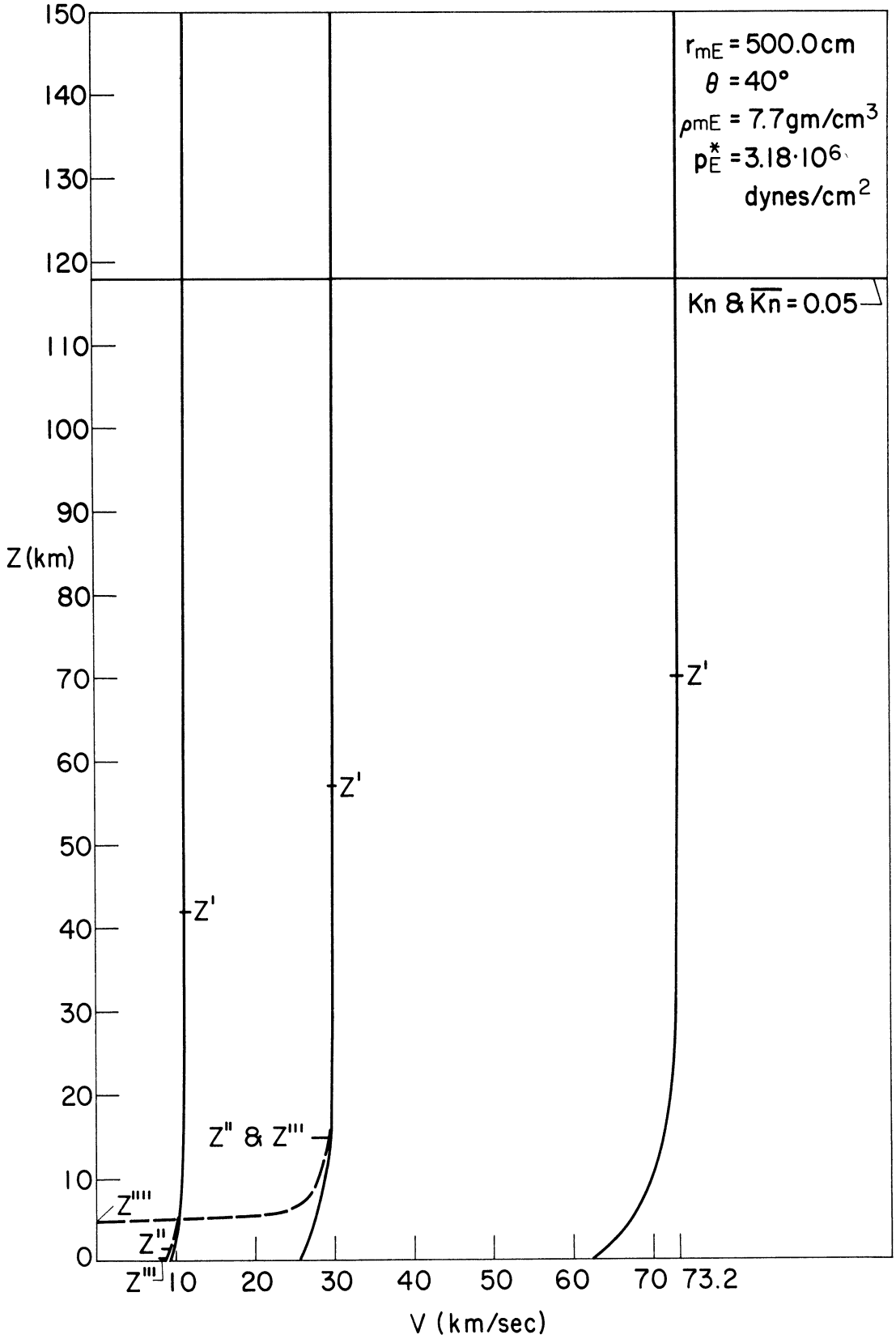

Figure 40. Meteor velocity as a function of altitude (σ = 0, solid curve; $\sigma = 5 \cdot 10^{-12}$ sec^2/cm^2, dashed curve), r_{mE} = 500.0 cm, θ = 40°, ρ_m = 7.7 g/cm^3.

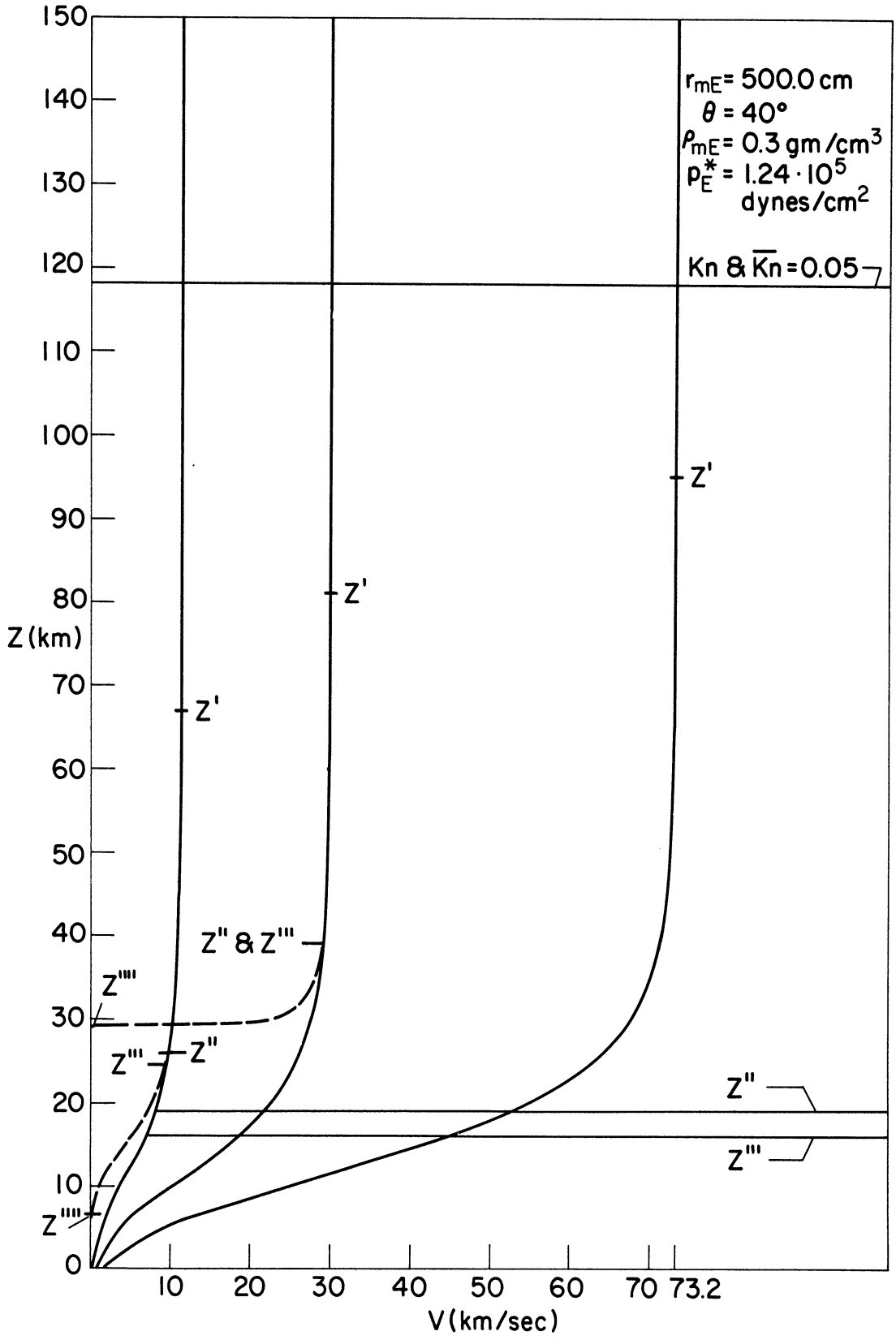

Figure 41. Meteor velocity as a function of altitude (σ = 0, solid curve; $\sigma = 5 \cdot 10^{-12}$ sec^2/cm^2, dashed curve), r_{mE} = 500.0 cm, θ = 40°, ρ_m = 0.3 g/cm^3.

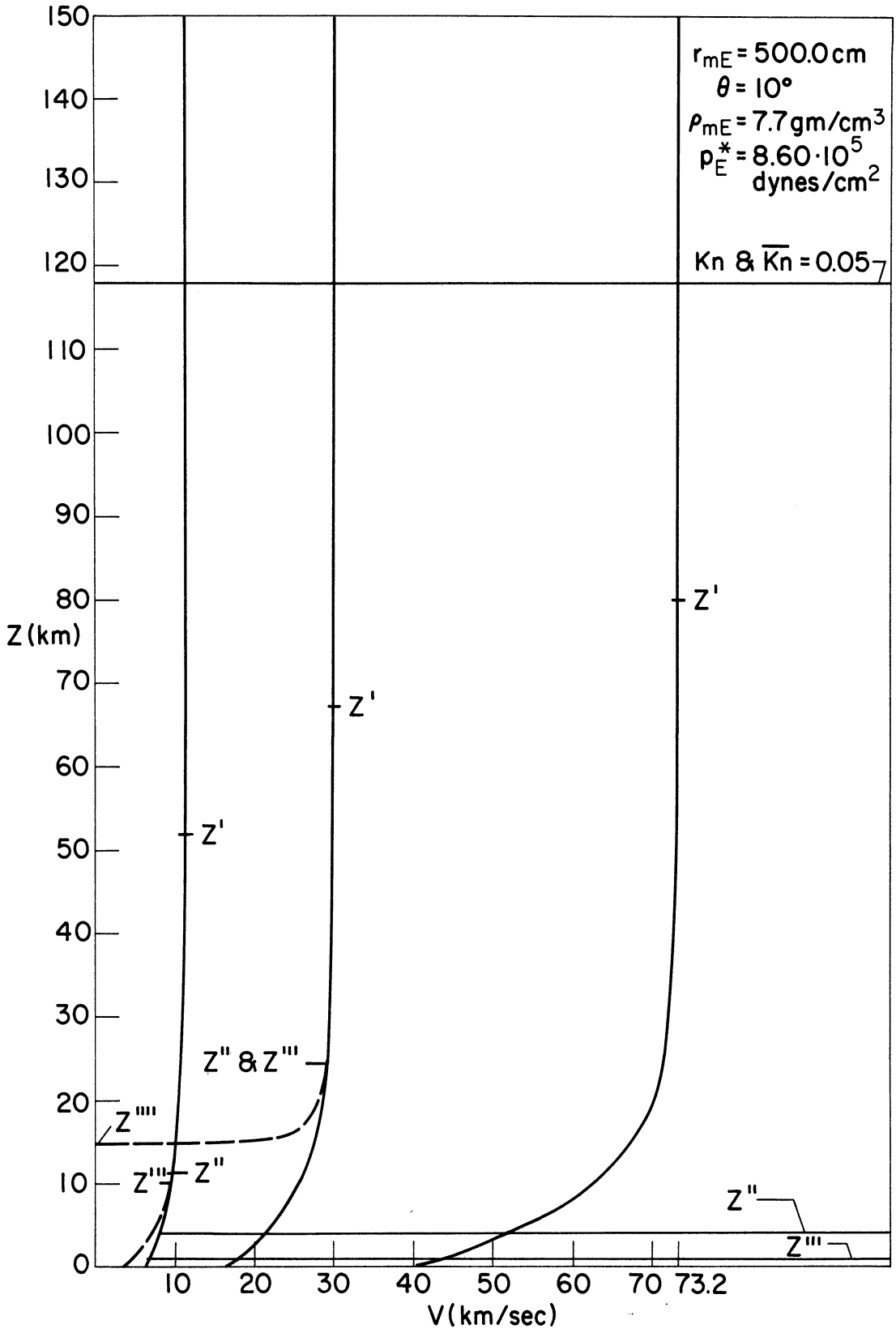

Figure 42. Meteor velocity as a function of altitude (σ = 0, solid curve; $\sigma = 5 \cdot 10^{-12}$ sec^2/cm^2, dashed curve), r_{mE} = 500.0 cm, θ = 10°, ρ_m = 7.7 g/cm^3.

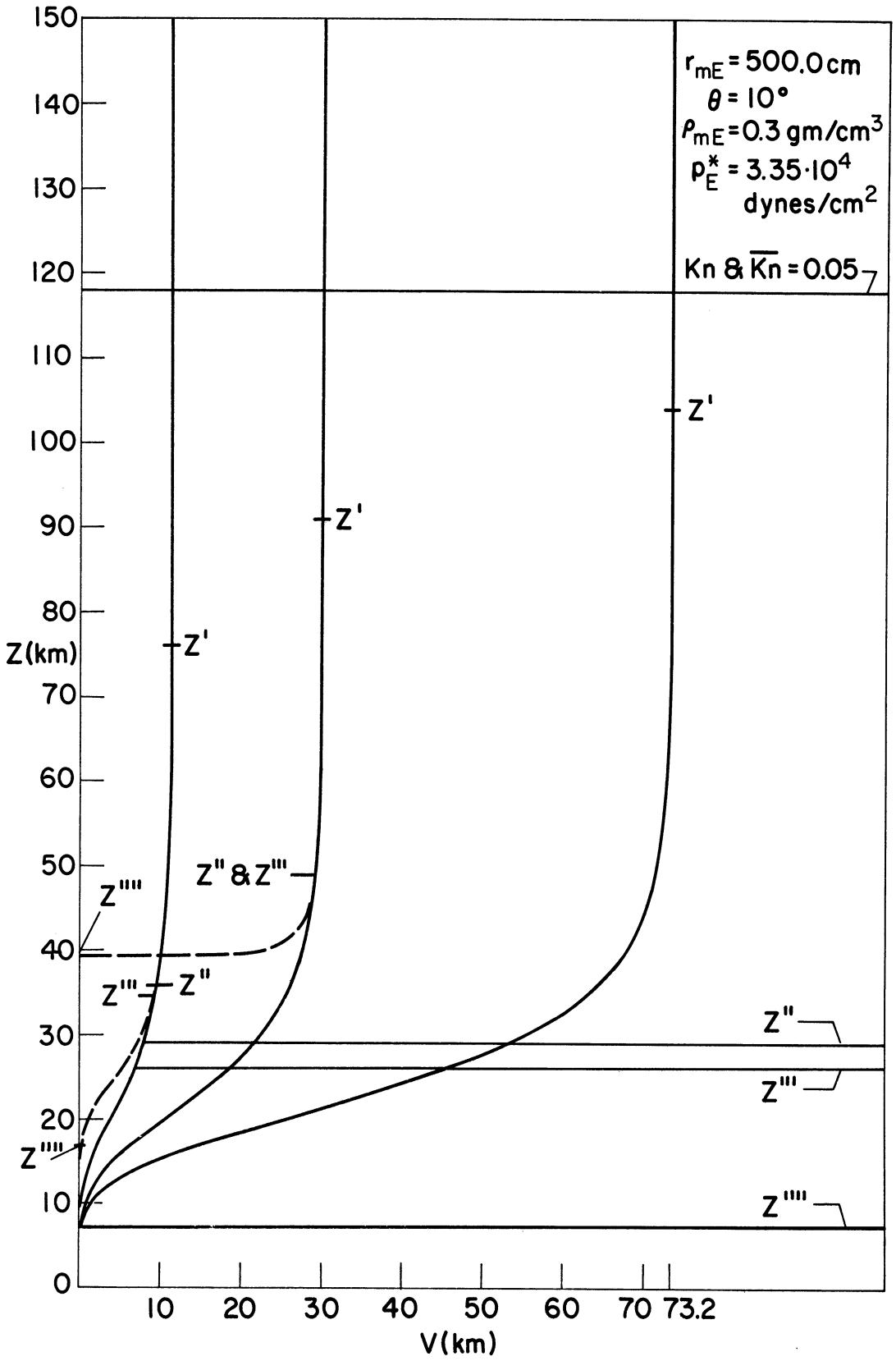

Figure 43. Meteor velocity as a function of altitude (σ = 0, solid curve; $\sigma = 5 \cdot 10^{-12}$ sec²/cm², dashed curve), r_{mE} = 500.0 cm, θ = 10°, ρ_m = 0.3 g/cm³.

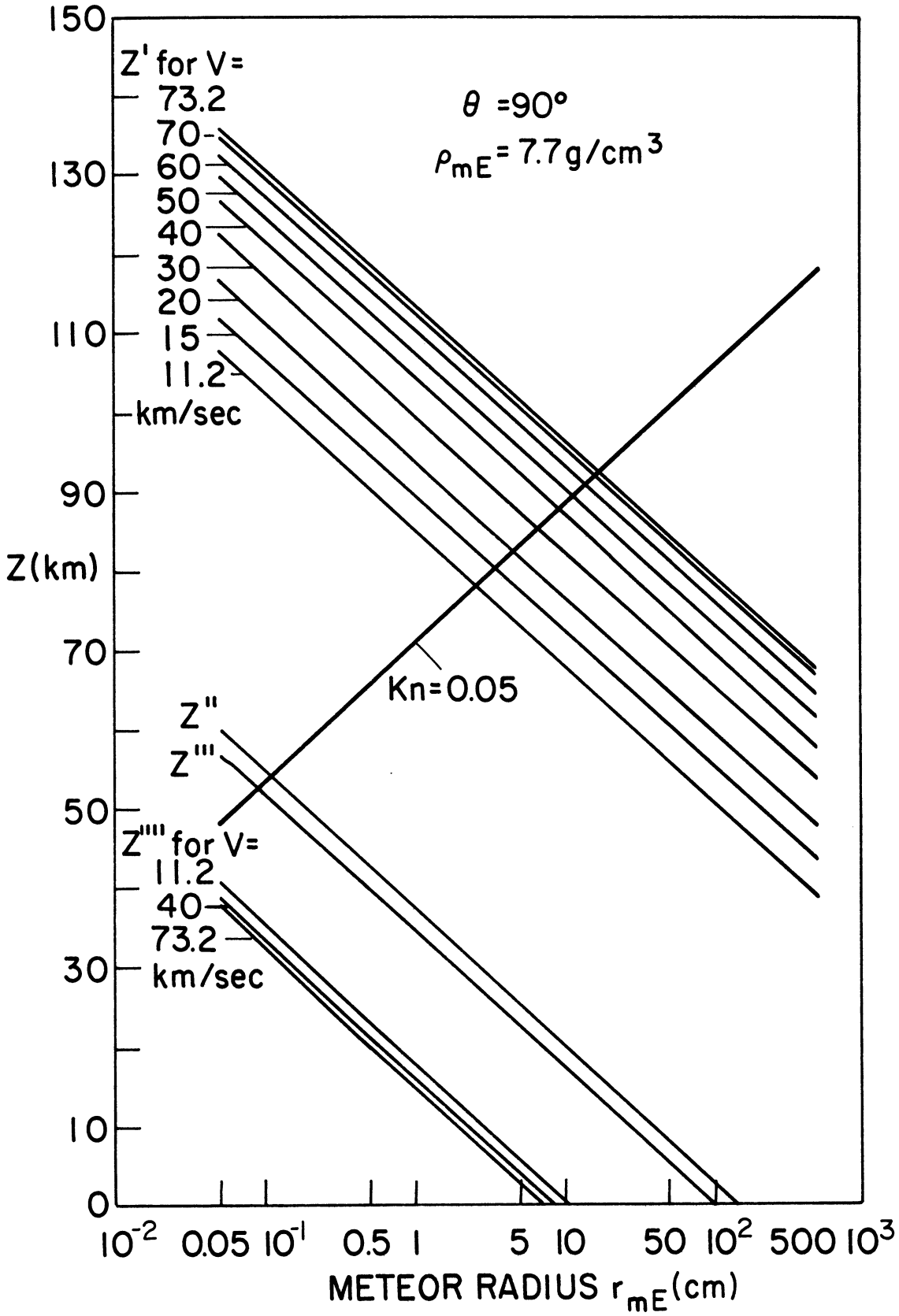

Figure 44. z', z'', z''', z'''', and Kn = 0.05 as a function of altitude and initial meteor radius with m/A constant ($\sigma = 0$), $\theta = 90°$, $\rho_m = 7.7$ g/cm^3.

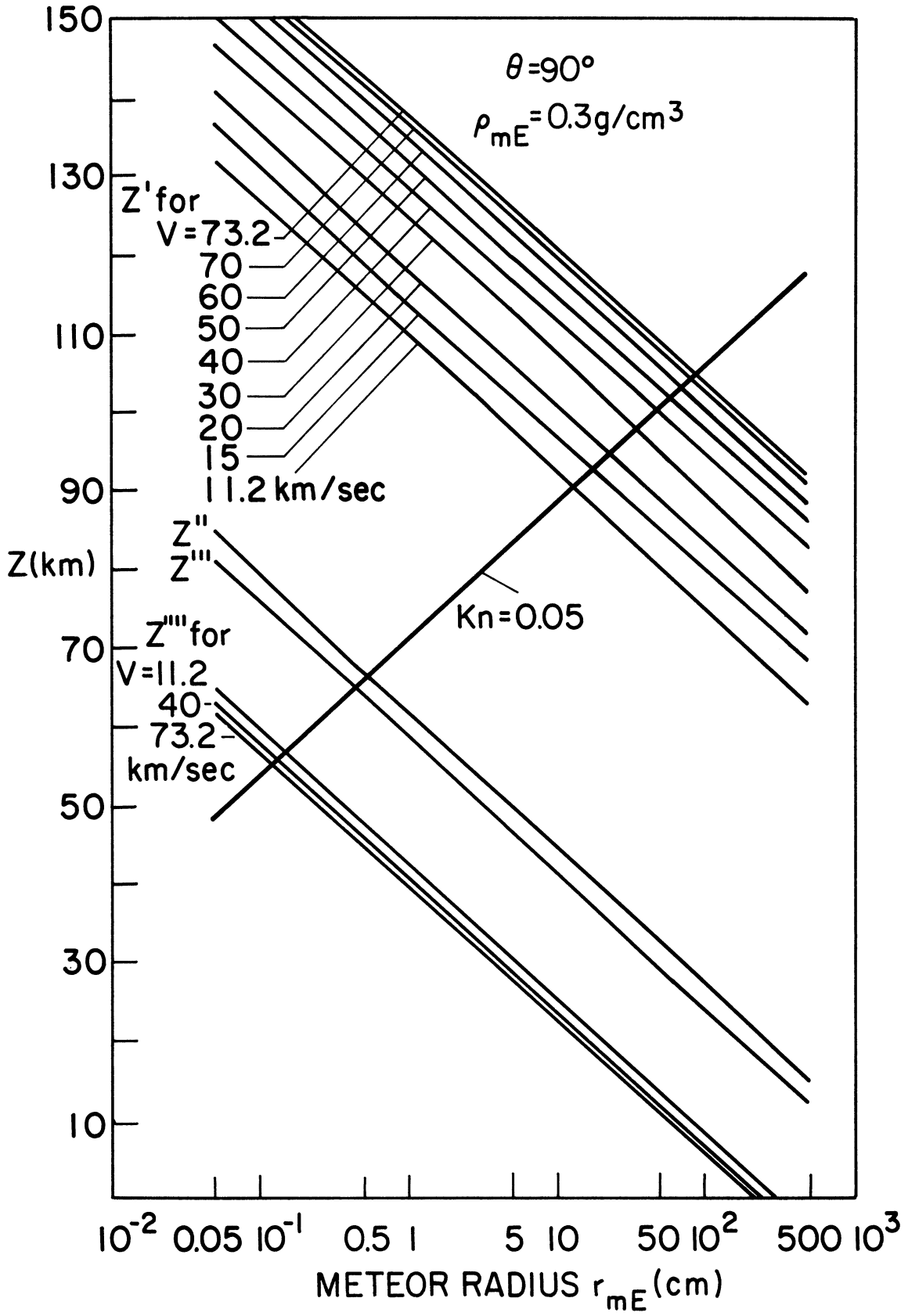

Figure 45. z', z'', z''', z'''', and Kn = 0.05 as a function of altitude and initial meteor radius with m/A constant ($\sigma = 0$), $\theta = 90°$, $\rho_m = 0.3$ g/cm^3.

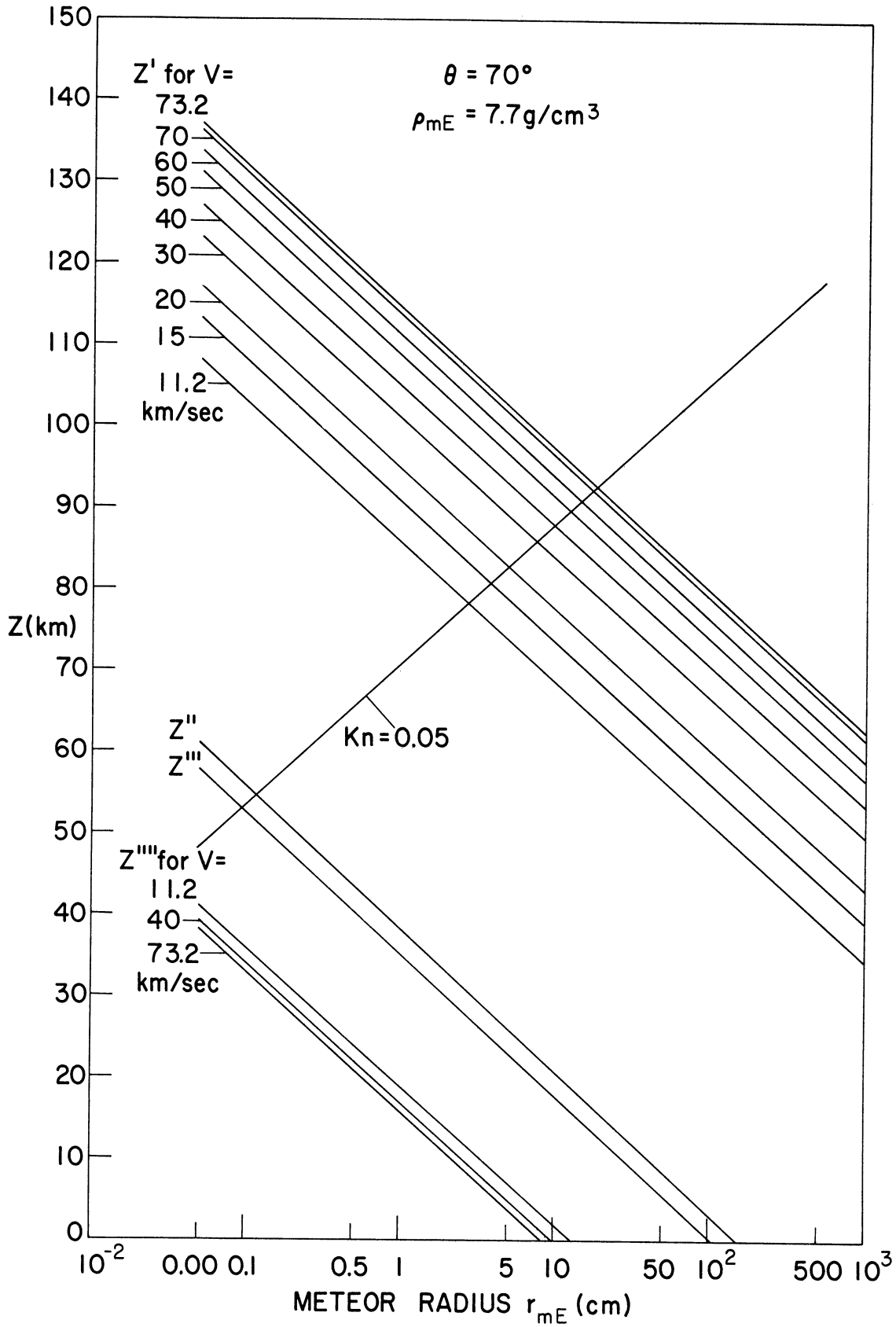

Figure 46. z', z'', z''', z'''', and Kn = 0.05 as a function of altitude and initial meteor radius with m/A constant ($\sigma = 0$), $\theta = 70°$, $\rho_m = 7.7$ g/cm^3.

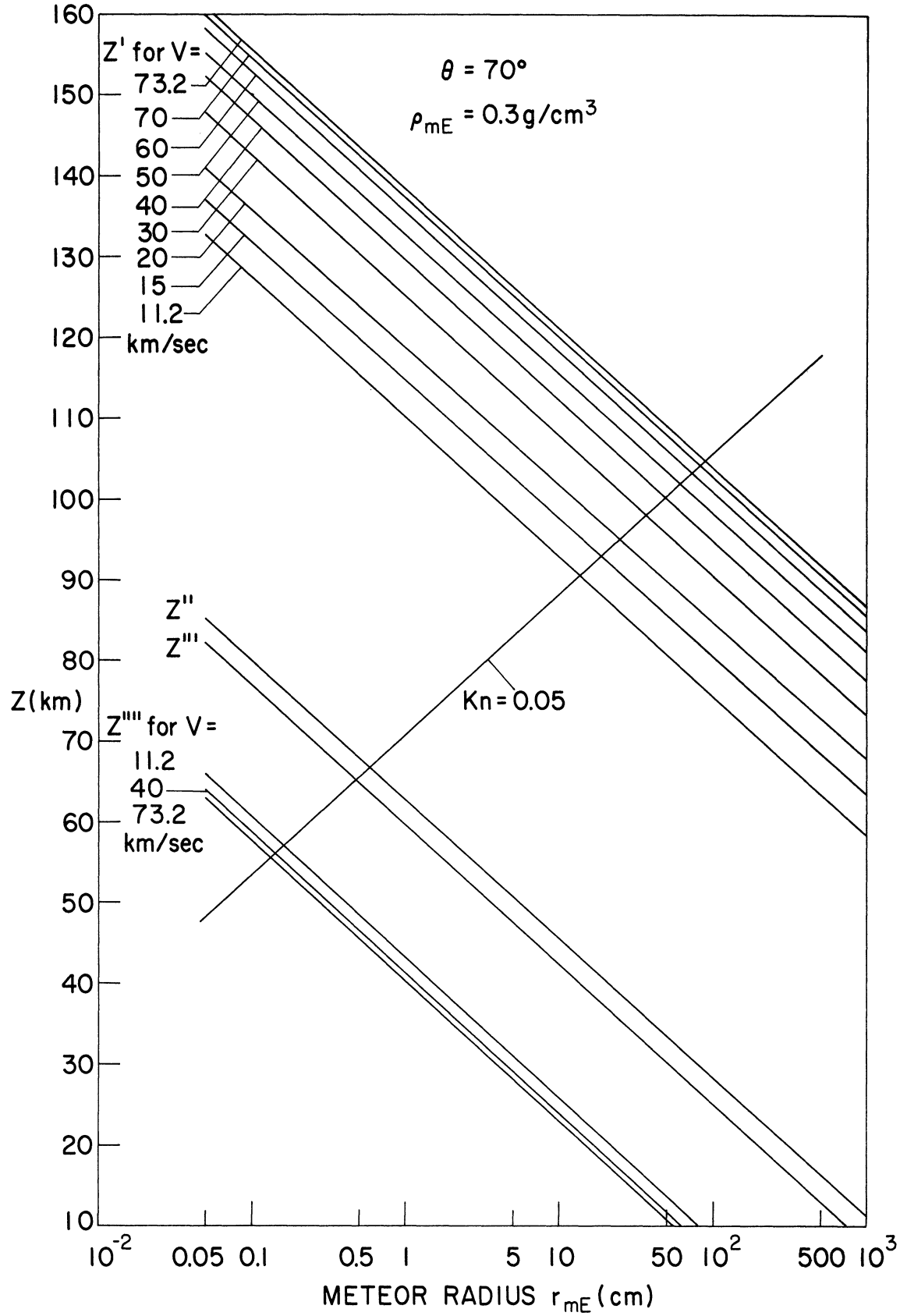

Figure 47. z', z'', z''', z'''', and Kn = 0.05 as a function of altitude and initial meteor radius with m/A constant ($\sigma = 0$), $\theta = 70°$, $\rho_m = 0.3$ g/cm^3.

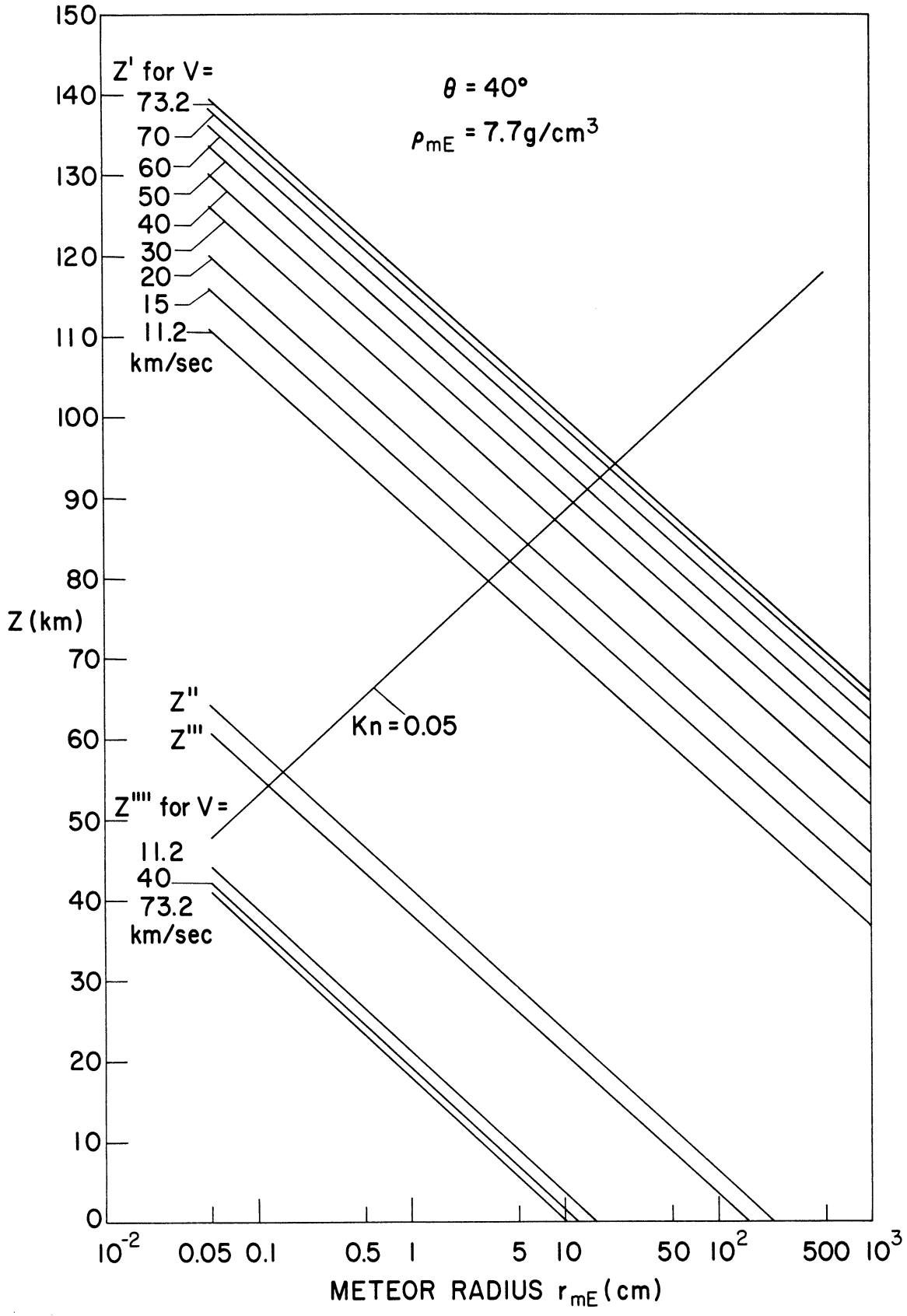

Figure 48. z', z'', z''', z'''', and Kn = 0.05 as a function of altitude and initial meteor radius with m/A constant ($\sigma = 0$), $\theta = 40°$, $\rho_m = 7.7$ g/cm^3.

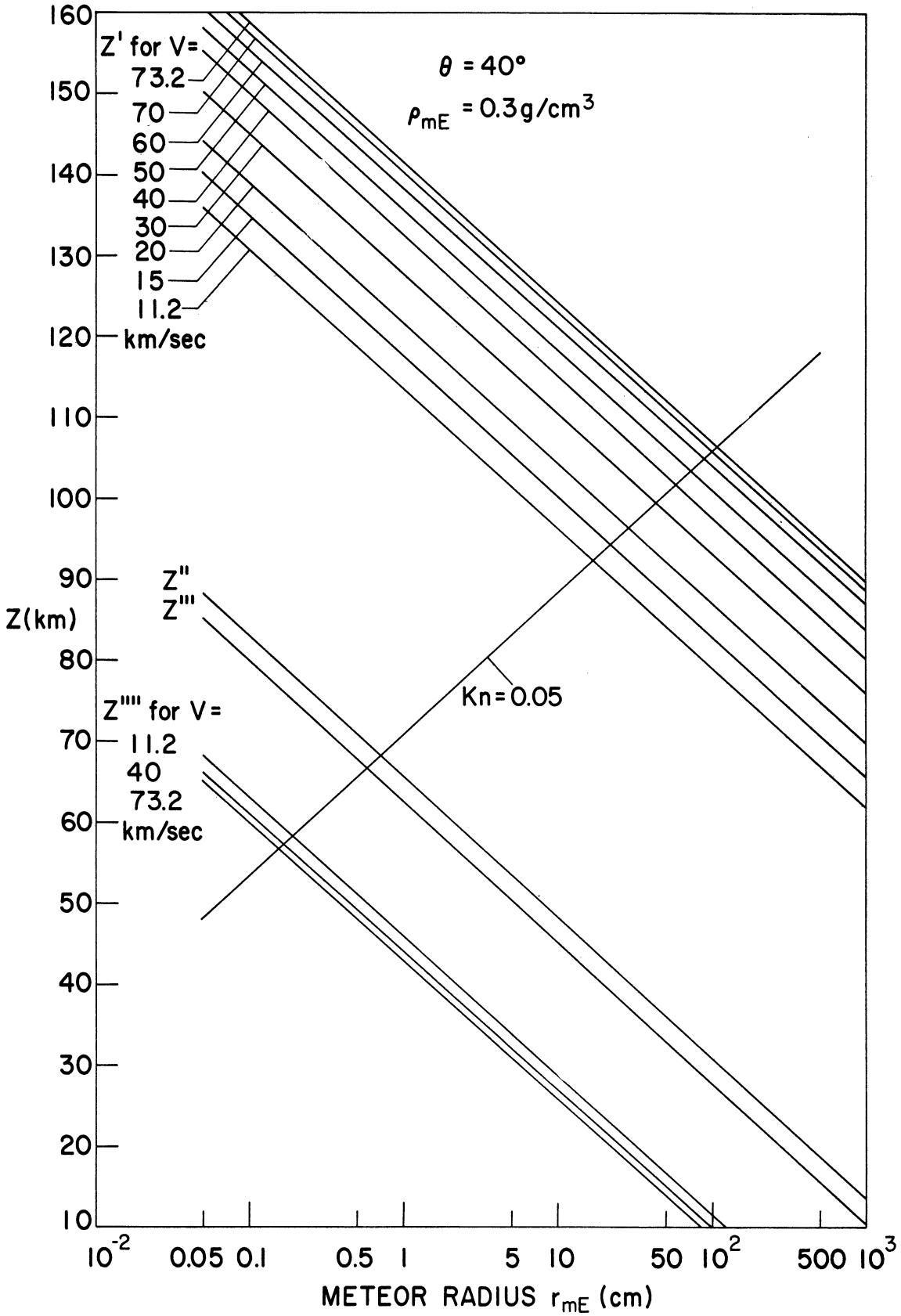

Figure 49. z', z'', z''', z'''', and Kn = 0.05 as a function of altitude and initial meteor radius with m/A constant ($\sigma = 0$), $\theta = 40°$, $\rho_m = 0.3$ g/cm^3.

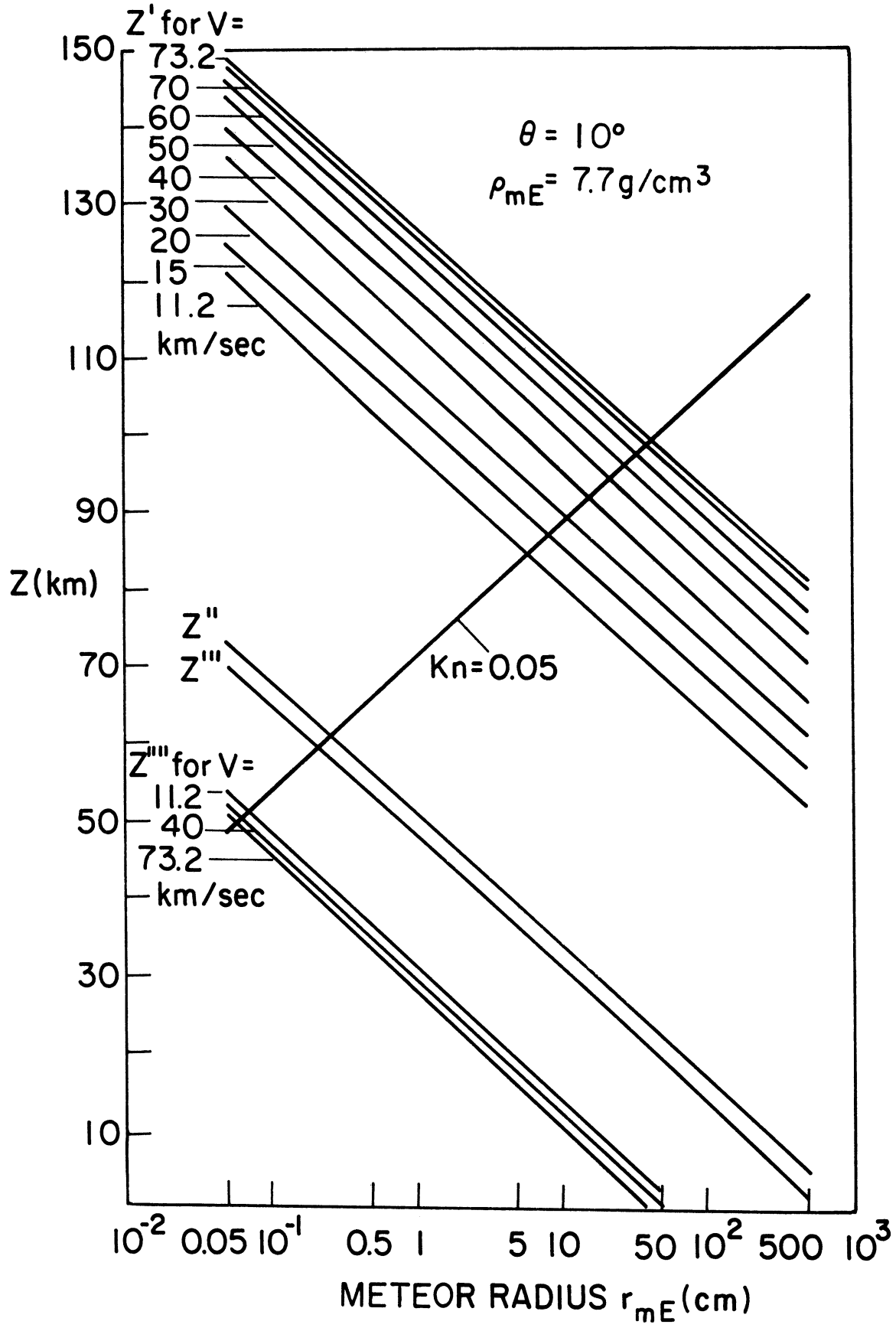

Figure 50. z', z'', z''', z'''', and Kn = 0.05 as a function of altitude and initial meteor radius with m/A constant ($\sigma = 0$), $\theta = 10°$, $\rho_m = 7.7$ g/cm^3.

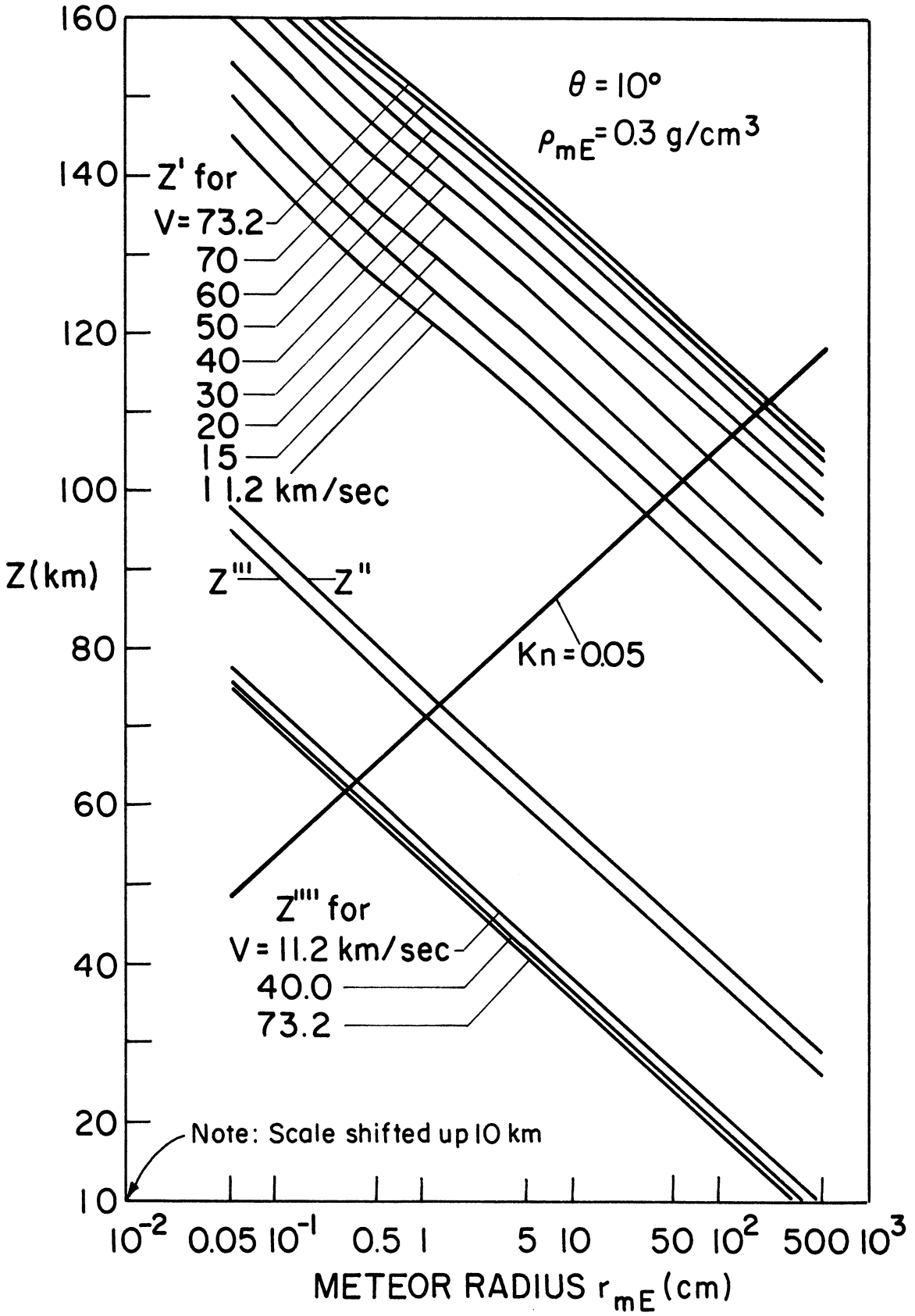

Figure 51. z', z'', z''', z'''', and Kn = 0.05 as a function of altitude and initial meteor radius with m/A constant ($\sigma = 0$), $\theta = 10°$, $\rho_m = 0.3$ g/cm^3.

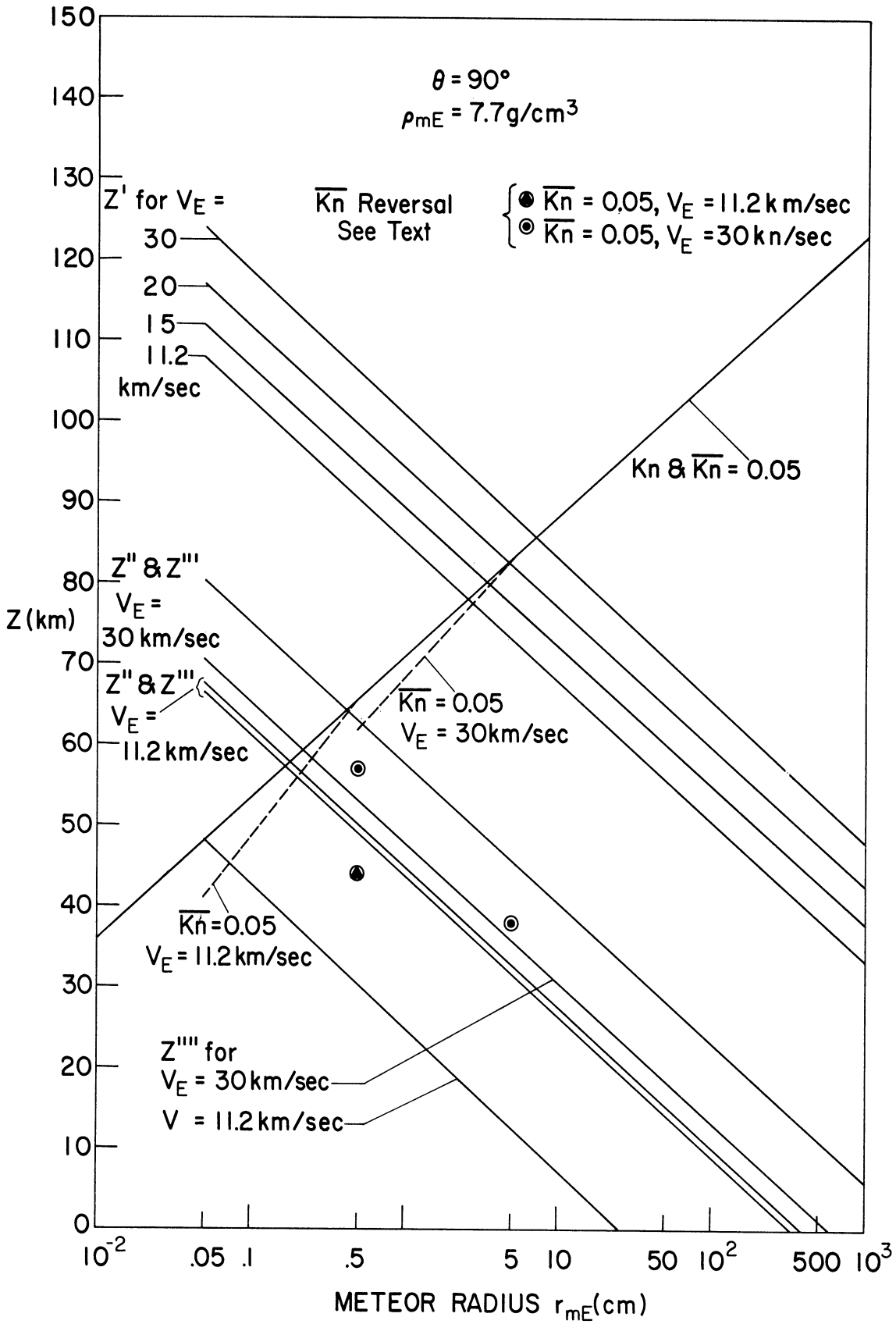

Figure 52. z', z'', z''', z'''', and $\overline{Kn}$ = 0.05 as a function of altitude and initial meteor radius with m/A decreasing exponentially ($\sigma = 5 \cdot 10^{-12}$ sec^2/cm^2), θ = 90°, ρ_m = 7.7 g/cm^3.

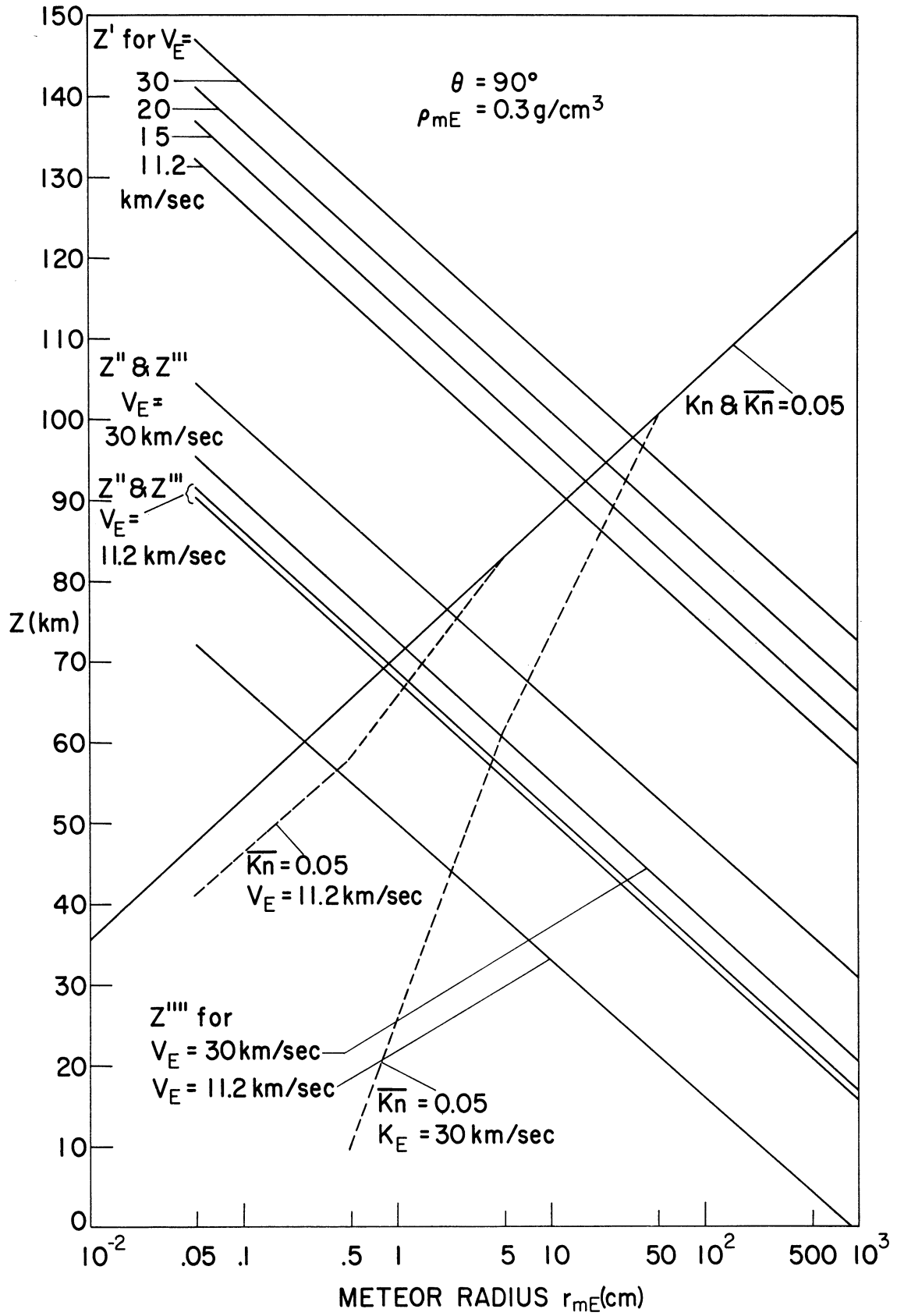

Figure 53. z', z'', z''', z'''', and $\overline{Kn}$ = 0.05 as a function of altitude and initial meteor radius with m/A decreasing exponentially ($\sigma = 5 \cdot 10^{-12}$ sec^2/cm^2), θ = 90°, ρ_m = 0.3 g/cm^3.

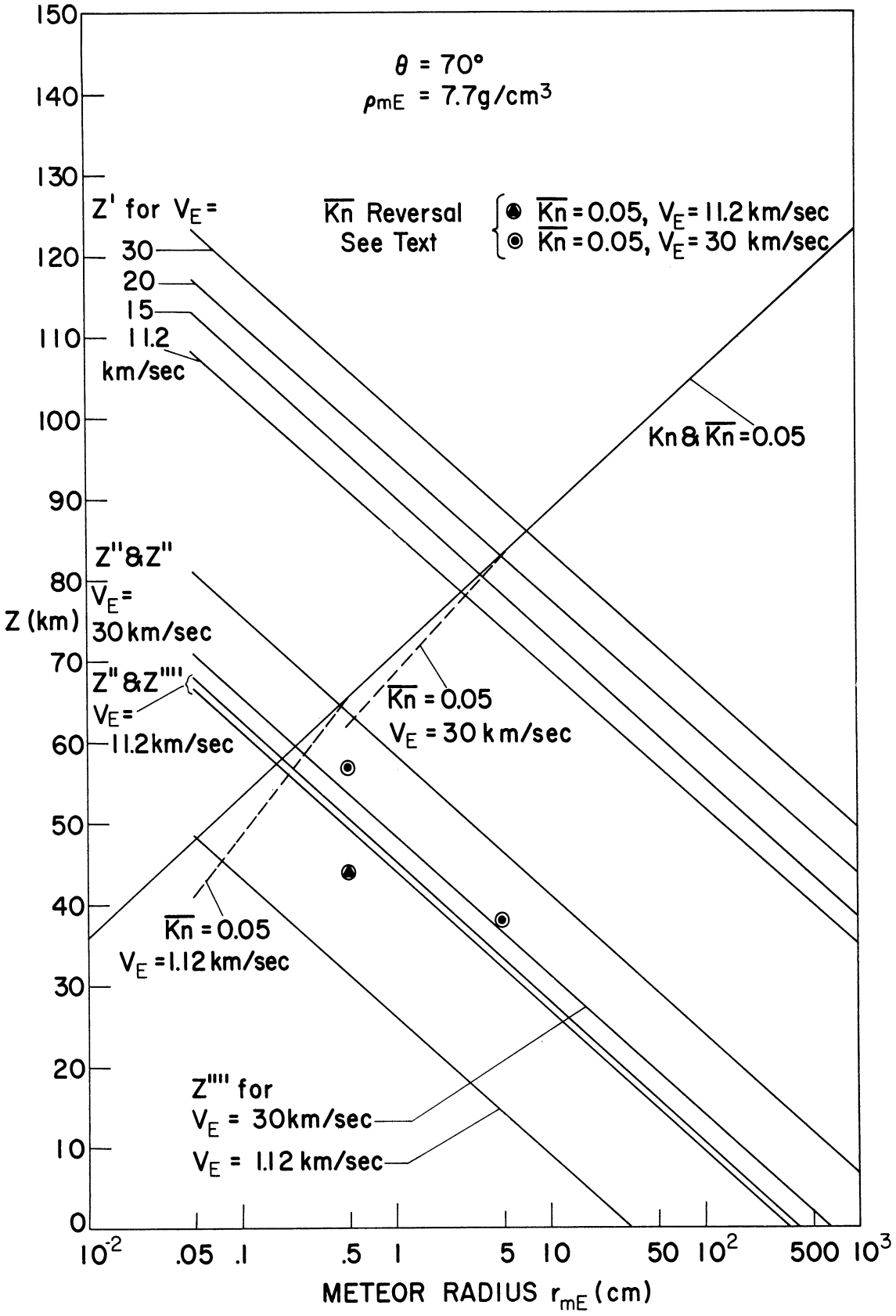

Figure 54. z', z'', z''', z'''', and $\overline{Kn}$ = 0.05 as a function of altitude and initial meteor radius with m/A decreasing exponentially ($\sigma = 5 \cdot 10^{-12}$ sec^2/cm^2), $\theta = 70°$, $\rho_m = 7.7$ g/cm^3.

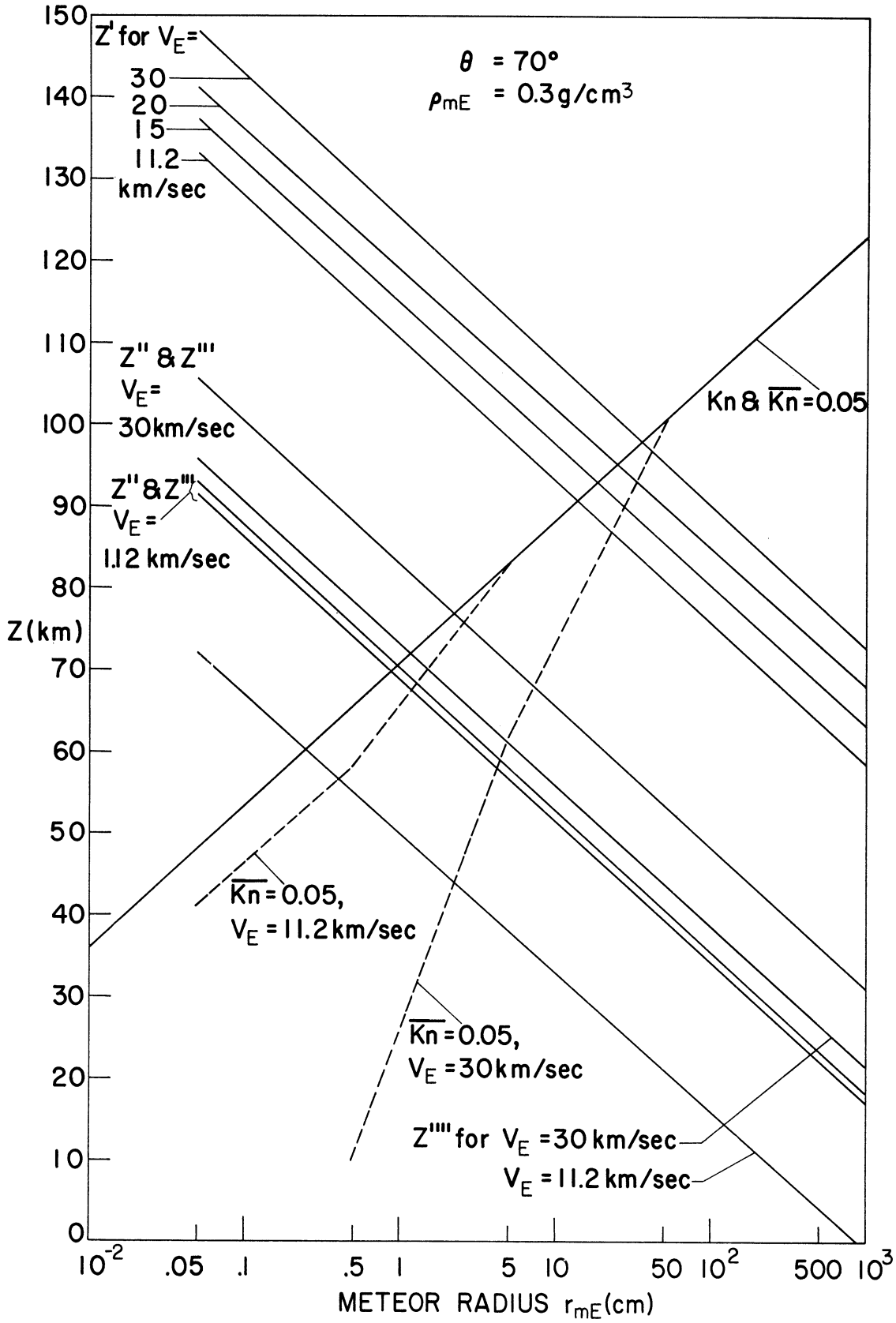

Figure 55. z', z'', z''', z'''', and $\overline{Kn}$ = 0.05 as a function of altitude and initial meteor radius with m/A decreasing exponentially ($\sigma = 5 \cdot 10^{-12}$ sec^2/cm^2), $\theta = 70°$, $\rho_m = 0.3$ g/cm^3.

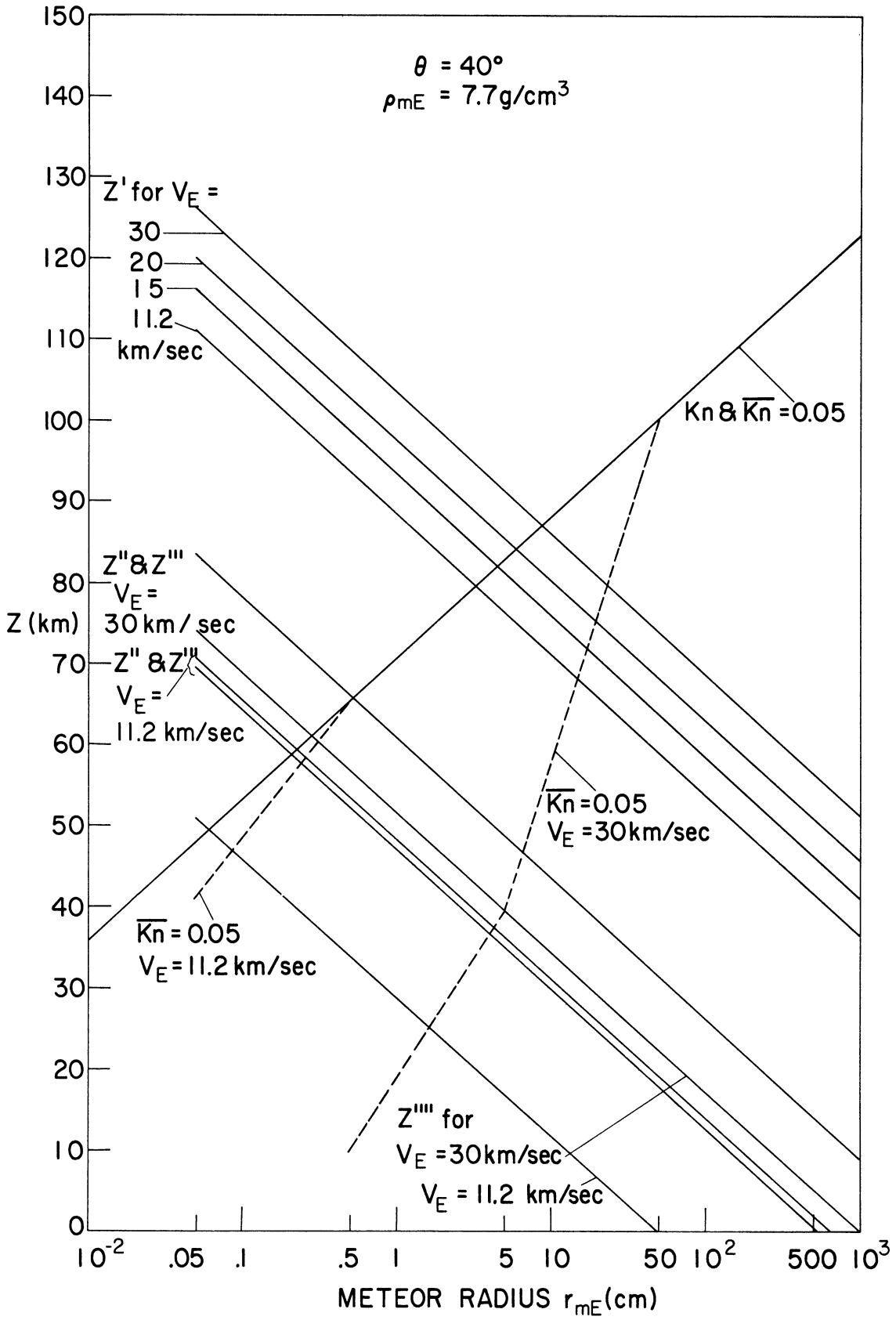

Figure 56. z', z'', z''', z'''', and Kn = 0.05 as a function of altitude and initial meteor radius with m/A decreasing exponentially ($\sigma = 5 \cdot 10^{-12}$ sec^2/cm^2), $\theta = 40°$, $\rho_m = 7.7$ g/cm^3.

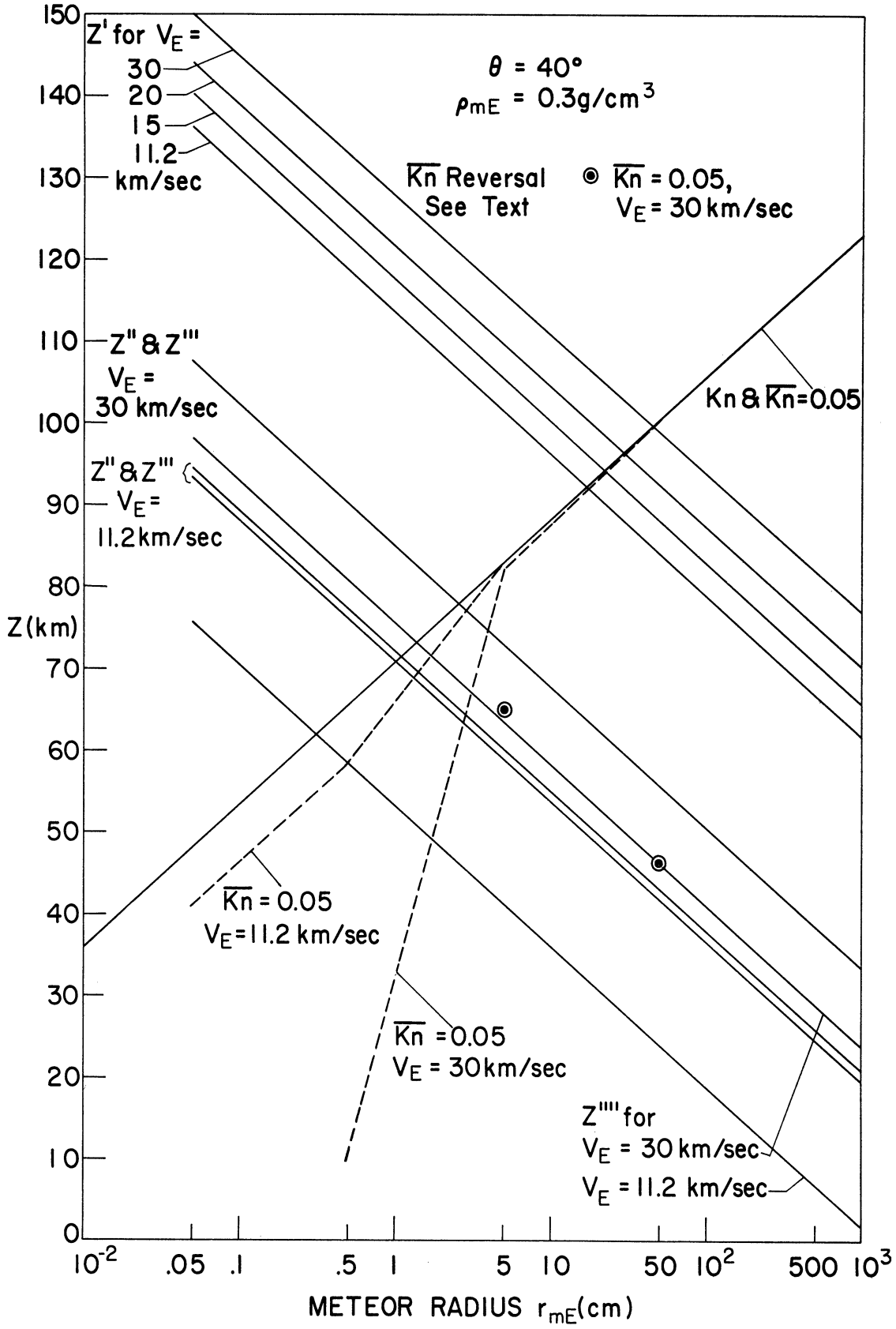

Figure 57. z', z'', z''', z'''', and $\overline{Kn}$ = 0.05 as a function of altitude and initial meteor radius with m/A decreasing exponentially ($\sigma = 5 \cdot 10^{-12}$ sec^2/cm^2), θ = 40°, ρ_m = 0.3 g/cm^3.

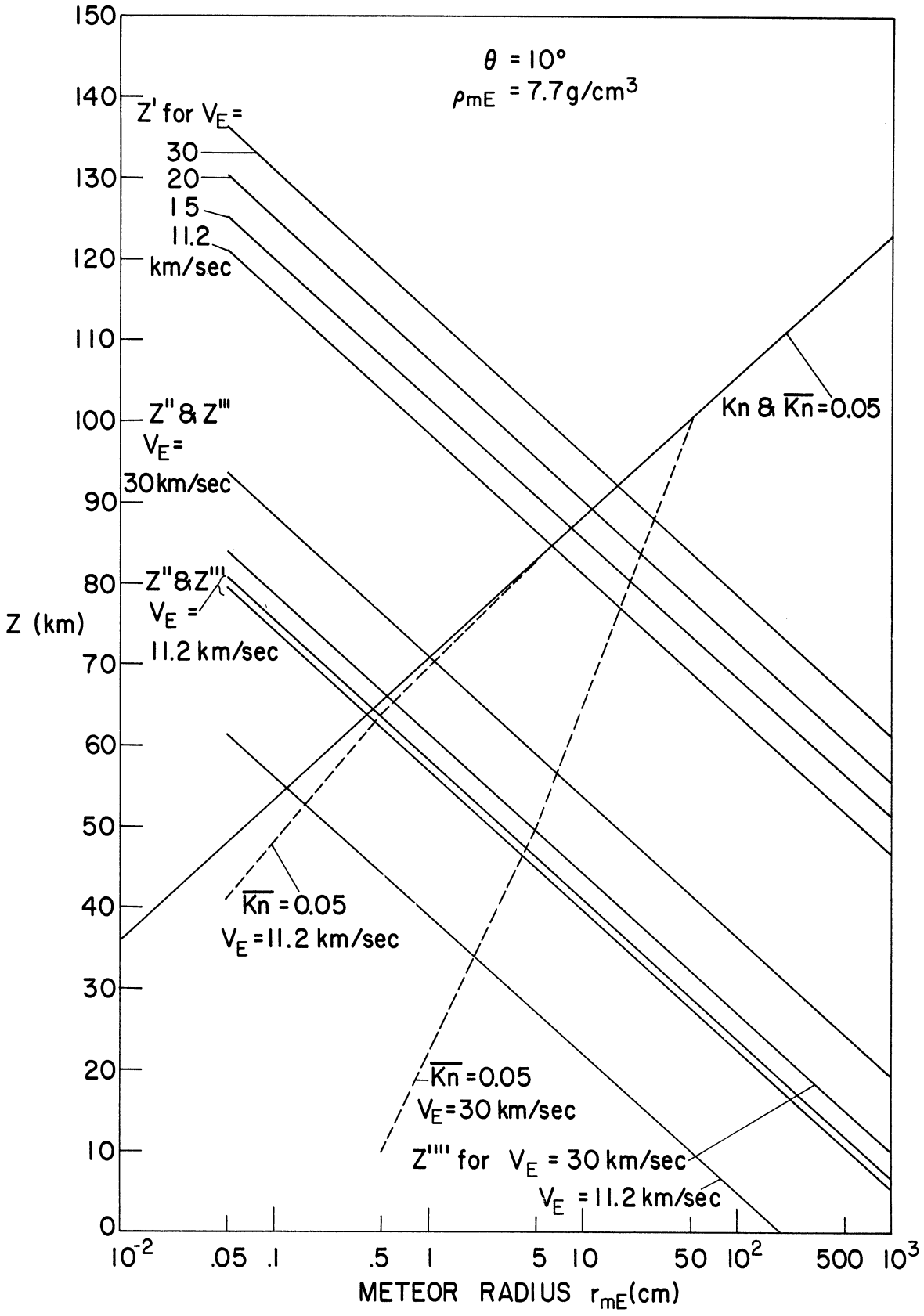

Figure 58. z', z'', z''', z'''', and $\overline{Kn}$ = 0.05 as a function of altitude and initial meteor radius with m/A decreasing exponentially ($\sigma = 5 \cdot 10^{-12}$ sec^2/cm^2), $\theta = 10°$, $\rho_m = 7.7$ g/cm^3.

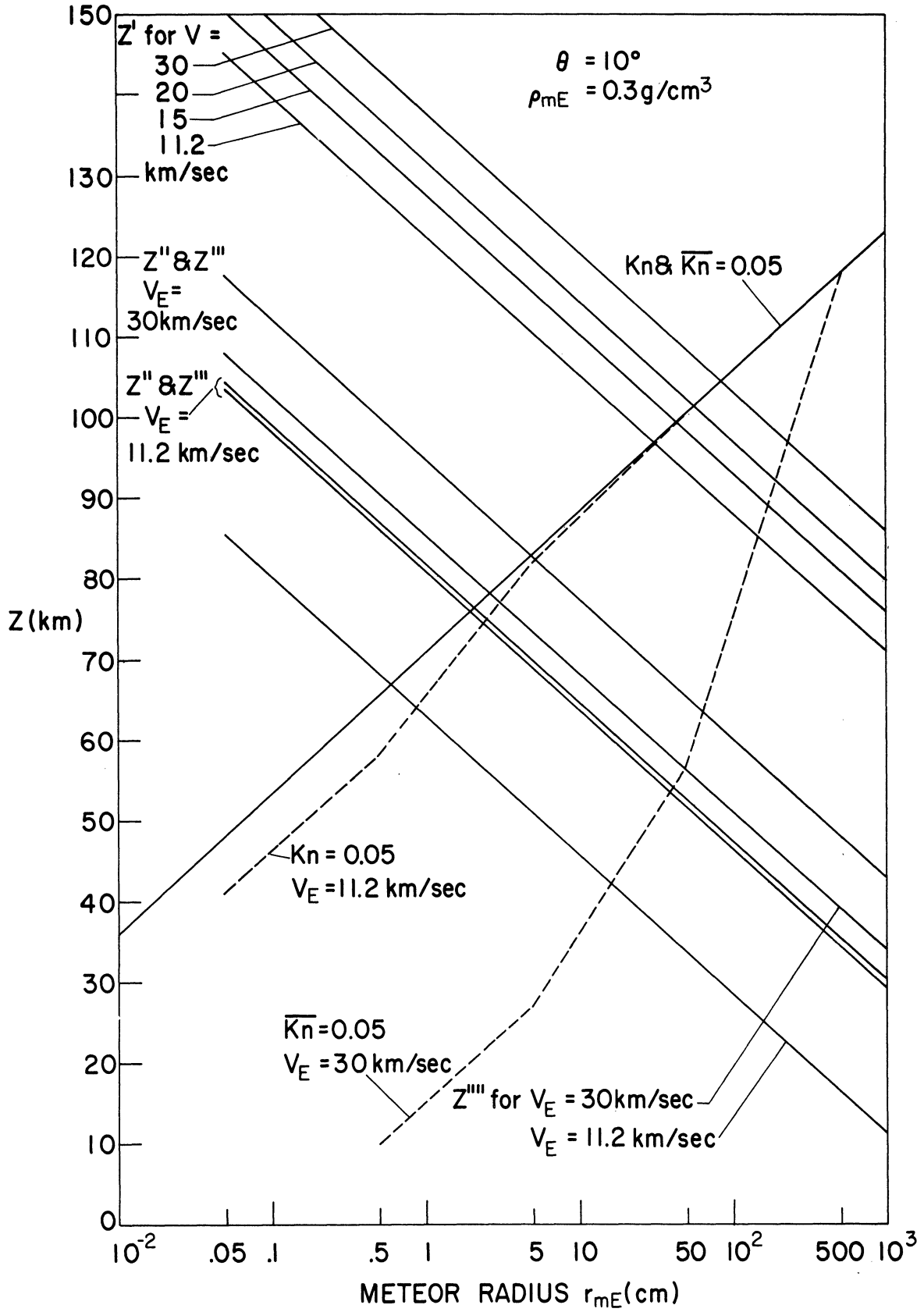

Figure 59. z', z'', z''', z'''', and $\overline{Kn}$ = 0.05 as a function of altitude and initial meteor radius with m/A decreasing exponentially ($\sigma = 5 \cdot 10^{-12}$ sec^2/cm^2), $\theta = 10°$, $\rho_m = 0.3$ g/cm^3.

TABLE 1

Isothermal Model Atmosphere Data

Altitude (km)	Pressure (dynes/cm^2)	Density (g/cm^3)	Mean Free Path (cm)
0.000E 00	0.101E 07	0.140E-02	0.781E-05
0.100E 01	0.887E 06	0.122E-02	0.892E-05
0.200E 01	0.776E 06	0.107E-02	0.102E-04
0.300E 01	0.679E 06	0.938E-03	0.117E-04
0.400E 01	0.594E 06	0.821E-03	0.133E-04
0.500E 01	0.520E 06	0.719E-03	0.152E-04
0.600E 01	0.455E 06	0.629E-03	0.174E-04
0.700E 01	0.398E 06	0.550E-03	0.199E-04
0.800E 01	0.349E 06	0.482E-03	0.227E-04
0.900E 01	0.305E 06	0.422E-03	0.259E-04
0.100E 02	0.267E 06	0.369E-03	0.296E-04
0.110E 02	0.234E 06	0.323E-03	0.339E-04
0.120E 02	0.205E 06	0.283E-03	0.387E-04
0.130E 02	0.179E 06	0.247E-03	0.442E-04
0.140E 02	0.157E 06	0.216E-03	0.505E-04
0.150E 02	0.137E 06	0.189E-03	0.577E-04
0.160E 02	0.120E 06	0.166E-03	0.659E-04
0.170E 02	0.105E 06	0.145E-03	0.753E-04
0.180E 02	0.919E 05	0.127E-03	0.861E-04
0.190E 02	0.804E 05	0.111E-03	0.984E-04
0.200E 02	0.704E 05	0.973E-04	0.112E-03
0.210E 02	0.616E 05	0.851E-04	0.128E-03
0.220E 02	0.539E 05	0.745E-04	0.147E-03
0.230E 02	0.472E 05	0.652E-04	0.168E-03
0.240E 02	0.413E 05	0.571E-04	0.192E-03
0.250E 02	0.361E 05	0.499E-04	0.219E-03
0.260E 02	0.316E 05	0.437E-04	0.250E-03
0.270E 02	0.277E 05	0.382E-04	0.286E-03
0.280E 02	0.242E 05	0.335E-04	0.327E-03
0.290E 02	0.212E 05	0.293E-04	0.373E-03
0.300E 02	0.186E 05	0.256E-04	0.426E-03
0.310E 02	0.162E 05	0.224E-04	0.487E-03
0.320E 02	0.142E 05	0.196E-04	0.557E-03
0.330E 02	0.124E 05	0.172E-04	0.636E-03
0.340E 02	0.109E 05	0.150E-04	0.727E-03
0.350E 02	0.953E 04	0.132E-04	0.831E-03
0.360E 02	0.834E 04	0.115E-04	0.949E-03
0.370E 02	0.730E 04	0.101E-04	0.108E-02
0.380E 02	0.639E 04	0.882E-05	0.124E-02
0.390E 02	0.559E 04	0.772E-05	0.142E-02
0.400E 02	0.489E 04	0.676E-05	0.162E-02
0.410E 02	0.428E 04	0.591E-05	0.185E-02
0.420E 02	0.375E 04	0.518E-05	0.211E-02
0.430E 02	0.328E 04	0.591E-05	0.241E-02
0.440E 02	0.287E 04	0.453E-05	0.276E-02
0.450E 02	0.251E 04	0.347E-05	0.315E-02

TABLE 1
(con't.)

0.460E 02	0.220E 04	0.304E-05	0.315E-02
0.470E 02	0.192E 04	0.266E-05	0.411E-02
0.480E 02	0.168E 04	0.233E-05	0.470E-02
0.490E 02	0.147E 04	0.204E-05	0.537E-02
0.500E 02	0.129E 04	0.178E-05	0.614E-02
0.510E 02	0.113E 04	0.156E-05	0.701E-02
0.520E 02	0.987E 03	0.136E-05	0.801E-02
0.530E 02	0.864E 03	0.119E-05	0.916E-02
0.540E 02	0.756E 03	0.104E-05	0.105E-01
0.550E 02	0.662E 03	0.915E-06	0.120E-01
0.560E 02	0.579E 03	0.800E-06	0.137E-01
0.570E 02	0.507E 03	0.700E-06	0.156E-01
0.580E 02	0.444E 03	0.613E-06	0.178E-01
0.590E 02	0.388E 03	0.537E-06	0.204E-01
0.600E 02	0.340E 03	0.470E-06	0.233E-01
0.610E 02	0.297E 03	0.411E-06	0.266E-01
0.620E 02	0.260E 03	0.360E-06	0.304E-01
0.630E 02	0.228E 03	0.315E-06	0.347E-01
0.640E 02	0.199E 03	0.275E-06	0.397E-01
0.650E 02	0.174E 03	0.241E-06	0.453E-01
0.660E 02	0.153E 03	0.211E-06	0.518E-01
0.670E 02	0.134E 03	0.185E-06	0.592E-01
0.680E 02	0.117E 03	0.162E-06	0.676E-01
0.690E 02	0.102E 03	0.141E-06	0.773E-01
0.700E 02	0.896E 02	0.124E-06	0.883E-01
0.710E 02	0.784E 02	0.108E-06	0.101E 00
0.720E 02	0.686E 02	0.948E-07	0.115E 00
0.730E 02	0.600E 02	0.830E-07	0.132E 00
0.740E 02	0.525E 02	0.726E-07	0.151E 00
0.750E 02	0.460E 02	0.635E-07	0.172E 00
0.760E 02	0.402E 02	0.556E-07	0.197E 00
0.770E 02	0.352E 02	0.487E-07	0.225E 00
0.780E 02	0.308E 02	0.426E-07	0.257E 00
0.790E 02	0.270E 02	0.373E-07	0.293E 00
0.800E 02	0.236E 02	0.326E-07	0.335E 00
0.810E 02	0.207E 02	0.286E-07	0.383E 00
0.820E 02	0.181E 02	0.250E-07	0.437E 00
0.830E 02	0.158E 02	0.219E-07	0.500E 00
0.840E 02	0.139E 02	0.191E-07	0.571E 00
0.850E 02	0.121E 02	0.168E-07	0.653E 00
0.860E 02	0.106E 02	0.147E-07	0.746E 00
0.870E 02	0.929E 01	0.128E-07	0.852E 00
0.880E 02	0.813E 01	0.112E-07	0.974E 00
0.890E 02	0.711E 01	0.983E-08	0.111E 00
0.900E 02	0.622E 01	0.860E-08	0.127E 01
0.910E 02	0.545E 01	0.753E-08	0.145E 01
0.920E 02	0.477E 01	0.659E-08	0.166E 01
0.930E 02	0.417E 01	0.576E-08	0.190E 01
0.940E 02	0.365E 01	0.505E-08	0.217E 01

TABLE 1
(con't.)

0.950E 02	0.320E 01	0.442E-08	0.248E 01
0.960E 02	0.280E 01	0.386E-08	0.283E 01
0.970E 02	0.245E 01	0.338E-08	0.323E 01
0.980E 02	0.214E 01	0.296E-08	0.369E 01
0.990E 02	0.187E 01	0.259E-08	0.422E 01
0.100E 03	0.164E 01	0.227E-08	0.482E 01
0.101E 03	0.144E 01	0.198E-08	0.551E 01
0.102E 03	0.126E 01	0.174E-08	0.630E 01
0.103E 03	0.110E 01	0.152E-08	0.719E 01
0.104E 03	0.962E 00	0.133E-08	0.822E 01
0.105E 03	0.842E 00	0.116E-08	0.939E 01
0.106E 03	0.737E 00	0.102E-08	0.107E 02
0.107E 03	0.645E 00	0.891E-09	0.123E 02
0.108E 03	0.565E 00	0.780E-09	0.140E 02
0.109E 03	0.494E 00	0.683E-09	0.160E 02
0.110E 03	0.432E 00	0.598E-09	0.183E 02
0.111E 03	0.378E 00	0.523E-09	0.209E 02
0.112E 03	0.331E 00	0.458E-09	0.239E 02
0.113E 03	0.290E 00	0.401E-09	0.273E 02
0.114E 03	0.254E 00	0.351E-09	0.312E 02
0.115E 03	0.222E 00	0.307E-09	0.356E 02
0.116E 03	0.194E 00	0.268E-09	0.407E 02
0.117E 03	0.170E 00	0.235E-09	0.465E 02
0.118E 03	0.149E 00	0.206E-09	0.532E 02
0.119E 03	0.130E 00	0.180E-09	0.607E 02
0.120E 03	0.114E 00	0.158E-09	0.694E 02

Note: For the above values, E, with its associated sign and two digits, refers to the positive or negative power of ten which each value is to be multiplied by.

TABLE 2

RESULTS OF ENTRY DYNAMICS CALCULATIONS

Case	r_{mE} (cm)	ρ_{mE} (g/cm^3)	θ (°)	$\sigma = 0$ V_E = 11.2 - 73.2 (km/sec)	$\sigma = 5 \cdot 10^{-12}$ sec^2/cm^2 V_E = 11.2 (km/sec)	V_E = 30 (km/sec)	Initial Kinetic Energy (ergs)	Comments
1	0.05	7.70	90.0	X	--	--	$2.5 \cdot 10^9$ - $1.1 \cdot 10^{11}$	A
2	0.05	7.70	90.0	--	X	--	$2.5 \cdot 10^9$	B
3	0.05	7.70	90.0	--	--	X	$1.8 \cdot 10^{10}$	B
4	0.05	0.30	90.0	X	--	--	$9.9 \cdot 10^7$ - $4.2 \cdot 10^9$	C
5	0.05	0.30	90.0	--	X	--	$9.9 \cdot 10^7$	B
6	0.05	0.30	90.0	--	--	X	$7.3 \cdot 10^8$	B
7	0.05	7.70	70.0	X	--	--	$2.5 \cdot 10^9$ - $1.1 \cdot 10^{11}$	A
8	0.05	7.70	70.0	--	X	--	$2.5 \cdot 10^9$	B
9	0.05	7.70	70.0	--	--	X	$1.8 \cdot 10^{10}$	B
10	0.05	0.30	70.0	X	--	--	$9.9 \cdot 10^7$ - $4.2 \cdot 10^9$	C
11	0.05	0.30	70.0	--	X	--	$9.9 \cdot 10^7$	B
12	0.05	0.30	70.0	--	--	X	$7.3 \cdot 10^8$	B
13	0.05	7.70	40.0	X	--	--	$2.5 \cdot 10^9$ - $1.1 \cdot 10^{11}$	D
14	0.05	7.70	40.0	--	X	--	$2.5 \cdot 10^9$	B
15	0.05	7.70	40.0	--	--	X	$1.8 \cdot 10^{10}$	B
16	0.05	0.30	40.0	X	--	--	$9.9 \cdot 10^7$ - $4.2 \cdot 10^9$	C
17	0.05	0.30	40.0	--	X	--	$9.9 \cdot 10^7$	B
18	0.05	0.30	40.0	--	--	X	$7.3 \cdot 10^8$	B
19	0.05	7.70	10.0	X	--	--	$2.5 \cdot 10^9$ - $1.1 \cdot 10^{11}$	C
20	0.05	7.70	10.0	--	X	--	$2.5 \cdot 10^9$	B
21	0.05	7.70	10.0	--	--	X	$1.8 \cdot 10^{10}$	B
22	0.05	0.30	10.0	X	--	--	$9.9 \cdot 10^7$ - $4.2 \cdot 10^9$	C

TABLE 2 (Continued)

Case	r_{mE} (cm)	ρ_{mE} (g/cm^3)	θ (°)	$\sigma = 0$ V_E = 11.2 - 73.2 (km/sec)	$\sigma = 5 \cdot 10^{-12}$ sec^2/cm^2 V_E = 11.2 (km/sec)	$\sigma = 5 \cdot 10^{-12}$ sec^2/cm^2 V_E = 30 (km/sec)	Initial Kinetic Energy (ergs)	Comments
23	0.05	0.30	10.0	--	X	--	$9.9 \cdot 10^{7}$	B
24	0.05	0.30	10.0	--	--	X	$7.3 \cdot 10^{8}$	B
25	0.50	7.70	90.0	X	--	--	$2.5 \cdot 10^{12}$ - $1.1 \cdot 10^{14}$	E
26	0.50	7.70	90.0	--	X	--	$2.5 \cdot 10^{12}$	F
27	0.50	7.70	90.0	--	--	X	$1.8 \cdot 10^{13}$	G
28	0.50	0.30	90.0	X	--	--	$9.9 \cdot 10^{10}$ - $4.2 \cdot 10^{12}$	E
29	0.50	0.30	90.0	--	X	--	$9.9 \cdot 10^{10}$	H
30	0.50	0.30	90.0	--	--	X	$7.3 \cdot 10^{11}$	B
31	0.50	7.70	70.0	X	--	--	$2.5 \cdot 10^{12}$ - $1.1 \cdot 10^{14}$	E
32	0.50	7.70	70.0	--	X	--	$2.5 \cdot 10^{12}$	F
33	0.50	7.70	70.0	--	--	X	$1.8 \cdot 10^{13}$	G
34	0.50	0.30	70.0	X	--	--	$9.9 \cdot 10^{10}$ - $4.2 \cdot 10^{12}$	E
35	0.50	0.30	70.0	--	X	--	$9.9 \cdot 10^{10}$	I
36	0.50	0.30	70.0	--	--	X	$7.3 \cdot 10^{11}$	B
37	0.50	7.70	40.0	X	--	--	$2.5 \cdot 10^{12}$ - $1.1 \cdot 10^{14}$	E
38	0.50	7.70	40.0	--	X	--	$2.5 \cdot 10^{12}$	J
39	0.50	7.70	40.0	--	--	X	$1.8 \cdot 10^{13}$	B
40	0.50	0.30	40.0	X	--	--	$9.9 \cdot 10^{10}$ - $4.2 \cdot 10^{12}$	E
41	0.50	0.30	40.0	--	X	--	$9.9 \cdot 10^{10}$	B
42	0.50	0.30	40.0	--	--	X	$7.3 \cdot 10^{11}$	B
43	0.50	7.70	10.0	X	--	--	$2.5 \cdot 10^{12}$ - $1.1 \cdot 10^{14}$	E
44	0.50	7.70	10.0	--	X	--	$2.5 \cdot 10^{12}$	K
45	0.50	7.70	10.0	--	--	X	$1.8 \cdot 10^{13}$	B

TABLE 2 (Continued)

Case	r_{mE} (cm)	ρ_{mE} (g/cm^3)	θ (°)	$\sigma = 0$ V_E = 11.2 - 73.2 (km/sec)	$\sigma = 5 \cdot 10^{-12}$ sec^2/cm^2 V_E = 11.2 (km/sec)	$\sigma = 5 \cdot 10^{-12}$ sec^2/cm^2 V_E = 30 (km/sec)	Initial Kinetic Energy (ergs)	Comments
46	0.50	0.30	10.0	X	--	--	$9.9 \cdot 10^{10}$ - $4.2 \cdot 10^{12}$	A
47	0.50	0.30	10.0	--	X	--	$9.9 \cdot 10^{10}$	B
48	0.50	0.30	10.0	--	--	X	$7.3 \cdot 10^{11}$	B
49	5.0	7.70	90.0	X	--	--	$2.5 \cdot 10^{15}$ - $1.1 \cdot 10^{17}$	E
50	5.0	7.70	90.0	--	X	--	$2.5 \cdot 10^{15}$	L
51	5.0	7.70	90.0	--	--	X	$1.8 \cdot 10^{16}$	M
52	5.0	0.30	90.0	X	--	--	$9.9 \cdot 10^{13}$ - $4.2 \cdot 10^{15}$	E
53	5.0	0.30	90.0	--	X	--	$9.9 \cdot 10^{13}$	N
54	5.0	0.30	90.0	--	--	X	$7.3 \cdot 10^{14}$	O
55	5.0	7.70	70.0	X	--	--	$2.5 \cdot 10^{15}$ - $1.1 \cdot 10^{17}$	E
56	5.0	7.70	70.0	--	X	--	$2.5 \cdot 10^{15}$	L
57	5.0	7.70	70.0	--	--	X	$1.8 \cdot 10^{16}$	M
58	5.0	0.30	70.0	X	--	--	$9.9 \cdot 10^{13}$ - $4.2 \cdot 10^{15}$	E
59	5.0	0.30	70.0	--	X	--	$9.9 \cdot 10^{13}$	N
60	5.0	0.30	70.0	--	--	X	$7.3 \cdot 10^{14}$	O
61	5.0	7.70	40.0	X	--	--	$2.5 \cdot 10^{15}$ - $1.1 \cdot 10^{17}$	E
62	5.0	7.70	40.0	--	X	--	$2.5 \cdot 10^{15}$	P
63	5.0	7.70	40.0	--	--	X	$1.8 \cdot 10^{16}$	QQ
64	5.0	0.30	40.0	X	--	--	$9.9 \cdot 10^{13}$ - $4.2 \cdot 10^{15}$	E
65	5.0	0.30	40.0	--	X	--	$9.9 \cdot 10^{13}$	Q
66	5.0	0.30	40.0	--	--	X	$7.3 \cdot 10^{14}$	R
67	5.0	7.70	10.0	X	--	--	$2.5 \cdot 10^{15}$ - $1.1 \cdot 10^{17}$	E
68	5.0	7.70	10.0	--	X	--	$2.5 \cdot 10^{15}$	S

TABLE 2 (Continued)

Case	r_{mE} (cm)	ρ_{mE} (g/cm^3)	θ (°)	$\sigma = 0$ V_E = 11.2 - 73.2 (km/sec)	$\sigma = 5 \cdot 10^{-12}$ sec^2/cm^2 V_E = 11.2 (km/sec)	$\sigma = 5 \cdot 10^{-12}$ sec^2/cm^2 V_E = 30 (km/sec)	Initial Kinetic Energy (ergs)	Comments
69	5.0	7.70	10.0	--	--	X	$1.8 \cdot 10^{16}$	T
70	5.0	0.30	10.0	X	--	--	$9.9 \cdot 10^{13}$ - $4.2 \cdot 10^{15}$	E
71	5.0	0.30	10.0	--	X	--	$9.9 \cdot 10^{13}$	U
72	5.0	0.30	10.0	--	--	X	$7.3 \cdot 10^{14}$	B
73	50.0	7.70	90.0	X	--	--	$2.5 \cdot 10^{18}$ - $1.1 \cdot 10^{20}$	E
74	50.0	7.70	90.0	--	X	--	$2.5 \cdot 10^{18}$	V
75	50.0	7.70	90.0	--	--	X	$1.8 \cdot 10^{19}$	W
76	50.0	0.30	90.0	X	--	--	$9.9 \cdot 10^{16}$ - $4.2 \cdot 10^{18}$	E
77	50.0	0.30	90.0	--	X	--	$9.9 \cdot 10^{16}$	X
78	50.0	0.30	90.0	--	--	X	$7.3 \cdot 10^{17}$	Y
79	50.0	7.70	70.0	X	--	--	$2.5 \cdot 10^{18}$ - $1.1 \cdot 10^{20}$	E
80	50.0	7.70	70.0	--	X	--	$2.5 \cdot 10^{18}$	V
81	50.0	7.70	70.0	--	--	X	$1.8 \cdot 10^{19}$	W
82	50.0	0.30	70.0	X	--	--	$9.9 \cdot 10^{16}$ - $4.2 \cdot 10^{18}$	E
83	50.0	0.30	70.0	--	X	--	$9.9 \cdot 10^{16}$	X
84	50.0	0.30	70.0	--	--	X	$7.3 \cdot 10^{17}$	Z
85	50.0	7.70	40.0	X	--	--	$2.5 \cdot 10^{18}$ - $1.1 \cdot 10^{20}$	E
86	50.0	7.70	40.0	--	X	--	$2.5 \cdot 10^{18}$	AA
87	50.0	7.70	40.0	--	--	X	$1.8 \cdot 10^{19}$	BB
88	50.0	0.30	40.0	X	--	--	$9.9 \cdot 10^{16}$ - $4.2 \cdot 10^{18}$	E
89	50.0	0.30	40.0	--	X	--	$9.9 \cdot 10^{16}$	CC
90	50.0	0.30	40.0	--	--	X	$7.3 \cdot 10^{17}$	DD
91	50.0	7.70	10.0	X	--	--	$2.5 \cdot 10^{18}$ - $1.1 \cdot 10^{20}$	E

TABLE 2 (Concluded)

Case	r_{mE} (cm)	ρ_{mE} (g/cm^3)	θ (°)	$\sigma = 0$ V_E = 11.2 - 73.2 (km/sec)	$\sigma = 5 \cdot 10^{-12}$ sec^2/cm^2 V_E = 11.2 (km/sec)	$\sigma = 5 \cdot 10^{-12}$ sec^2/cm^2 V_E = 30 (km/sec)	Initial Kinetic Energy (ergs)	Comments
92	50.0	7.70	10.0	--	X	--	$2.5 \cdot 10^{18}$	EE
93	50.0	7.70	10.0	--	--	X	$1.8 \cdot 10^{19}$	FF
94	50.0	0.30	10.0	X	--	--	$9.9 \cdot 10^{16}$ - $4.2 \cdot 10^{18}$	E
95	50.0	0.30	10.0	--	X	--	$9.9 \cdot 10^{16}$	GG
96	50.0	0.30	10.0	--	--	X	$7.3 \cdot 10^{17}$	HH

Note: For all additional cases comment E applies except where $\sigma \neq 0$, V_E has a maximum upper limit of 30 km/sec, i.e., for r_{mE} = 500.0 cm, regardless of ρ_{mE} or θ, supersonic velocities are always dynamically possible over certain altitude ranges. Ten-meter diameter meteors are rare enough so that listing of their specific altitude ranges of interest does not seem appropriate. For more details on their rarity see Section VI (Part 3). For more details on their specific altitude ranges of interest, see Figures 36-43.

Comment Code for Table 2

A Dynamically possible for $11.2 \leq V_E \leq 73.2$ km/sec; for drag coefficient, C_D, of 2.0, only possible for $V_E > 20$ km/sec

B Supersonic velocities do not exist in an altitude region where $\overline{Kn} \leq 0.05$

C There is no value of V_E for which supersonic velocities remain to an altitude region where $Kn \leq 0.05$

D Dynamically possible for $11.2 \leq V_E \leq 73.2$ km/sec; for $C_D = 2.0$, only possible for $V_E > 60$ km/sec

E Dynamically possible for $11.2 \leq V_E \leq 73.2$ km/sec

F Dynamically possible from 66-44 km altitude

G Dynamically possible from 62-57 km altitude

H Dynamically possible from 58-56 km altitude; for $C_D = 2.0$, it is not dynamically possible

I Dynamically possible from 58-56.5 km altitude; for $C_D = 2.0$, it is not dynamically possible

J Dynamically possible from 66-35 km altitude

K Dynamically possible from 64-45 km altitude

L Dynamically possible from 83-15 km altitude

M Dynamically possible from 83-38 km altitude

N Dynamically possible from 83-39 km altitude

O Dynamically possible from 62-60.5 km altitude

P Dynamically possible from 83-18 km altitude

Q Dynamically possible from 83-42.5 km altitude

R Dynamically possible from 82.5-65 km altitude

S Dynamically possible from 83-28.5 km altitude

T	Dynamically possible from 50-49.5 km altitude
U	Dynamically possible from 82.5-52 km altitude
V	Dynamically possible from 100 km-ground level
W	Dynamically possible from 100-19 km altitude
X	Dynamically possible from 100-22.5 km altitude
Y	Dynamically possible from 100-43 km altitude
Z	Dynamically possible from 100-43.5 km altitude
AA	Dynamically possible from 100-2 km altitude
BB	Dynamically possible from 100-22.5 km altitude
CC	Dynamically possible from 100-25.5 km altitude
DD	Dynamically possible from 100-46.5 km altitude
EE	Dynamically possible from 100-12 km altitude
FF	Dynamically possible from 100-32 km altitude
GG	Dynamically possible from 100-35 km altitude
HH	Dynamically possible from 57-56.5 km altitude
QQ	Dynamically possible from 40-39.5 km altitude

TABLE 3

SUMMARY OF TABLE 2 RESULTS

Case	Meteor Kinetic Energy at Entry (ergs)	r_{mE}				ρ_{mE}		θ				σ			
	10^8 10^9 10^{10} 10^{11} 10^{12} 10^{13} 10^{14} 10^{15} 10^{16} 10^{17} 10^{18} 10^{19} 10^{20}	0.05	0.5	5.0	50.0	0.30	7.70	90	70	40	10	$5\cdot10^{-12}$ V_E 11.2	$5\cdot10^{-12}$ V_E 30	0 V_E 11.2 to 73.2
1, 7, 13	⟷	X					X	X	X	X				X
29, 35	⟷		X			X		X	X			X		
28, 34, 40, 46	⟷		X			X								X
26, 32, 38, 44	⟷		X				X	X	X	X	X	X		
25, 31, 37, 43	⟷		X				X	X	X	X	X			X
27, 33	|		X				X	X	X				X	
53, 59, 65, 71	⟷			X		X		X	X	X	X	X		
52, 58, 64, 70	⟷			X		X		X	X	X	X			X
54, 60, 66	|			X		X		X	X	X			X	
50, 56, 62, 68	⟷			X			X	X	X	X	X	X		
49, 55, 61, 67	⟷			X			X	X	X	X	X			X
51, 57, 63	|			X			X	X	X	X			X	
77, 83, 89, 95	⟷				X	X		X	X	X	X	X		
76, 82, 88, 94	⟷				X	X		X	X	X	X			X
78, 84, 90, 96	⟷				X		X	X	X	X	X	X		
74, 80, 86, 92	⟷				X		X	X	X	X	X			X
73, 79, 85, 91	⟷				X		X	X	X	X	X		X	
75, 81, 87, 93	|												

Note: X's indicate dynamically possible cases.